ISSN 1028-8546

Azərbaycan Milli Elmlər Akademiyası
Fizika-Riyaziyyat və Texnika Elmləri Bölməsi
Fizika İnstitutu

4

Fizika

Cild

VIII

2002

Bakı ✵ Elm

SL(3,C)-GROUP ELEMENT SOLUTION OF THE PRINCIPAL CHIRAL FIELD PROBLEM

M.A. MUKHTAROV
Institute of Mathematics and Mechanics
370602 Baku, F. Agaev str.9, A erbaijan

The group element solutions of the principal chiral field problem are constructed by means of discrete symmetry transformations for the algebra SL(3,C).

1. The problem of constructing the exact solutions of nonlinear evolution equations in the explicit form remains important for the present time. Among these so called integrable system the four dimensional self-dual Yang Mills (SDYM) equations plays the central role being the universal integrable system from which the systems in lower than four dimensions can be obtained by symmetry reduction or by imposing constrains on Yang Mills potentials. The problem of integration of SDYM has successfully solved only for the case of SL(2,C) algebra and for instanton number not greater than two. The famous ADHM ansatz [1] gives the qualitative description of instanton solution but not its explicit form. Two effective methods of integration of SDYM for arbitrary semisimple algebra have been proposed in series of papers [2]. Another, the discrete symmetry transformation approach has been suggested [3] that allows to generate new solutions from the old ones. This method has been applied to many cases, for instance, the exact solutions of principal chiral field problem were obtained in [4] for the case of SL(2,C) algebra and in [5] for SL(3,C) and the rest semisimple algebras of the rank greater than two.

This work must be considered as a continuation of the paper [5]. The purpose of the present paper is to do the same for the group-valued element what is important for applications.

2. Let us remind the basic statements from [5].

Equations of the principal chiral field problem are the systems of equations for the element f, taking values in the semisimple algebra,

$$\left(\theta_i - \theta_j\right)\frac{\partial^2 f}{\partial x_i \partial x_j} = \left[\frac{\partial f}{\partial x_i}, \frac{\partial f}{\partial x_j}\right], \tag{1}$$

In the case of two-dimensional space: $\theta_1 = 1$, $\theta_2 = -1$, $x_1 = \xi$, $x_2 = \nu$.

For the case of a semisimple Lie algebra and for an element f being a solution of (1), the following statement takes place:

There exists such an element S taking values in a gauge group that

$$S^{-1}\frac{\partial S}{\partial x_i} = \frac{1}{\tilde{f}_-}\left[\frac{\partial \tilde{f}}{\partial x_i}, X_M^+\right] - \theta_i \frac{\partial}{\partial x_i}\frac{1}{\tilde{f}_-}X_M^+ \tag{2}$$

Here X_M^+ is the element of the algebra corresponding to its maximal root divided by its norm, i.e.,

$$\left[X_M^+, X^-\right] = H, \left[H, X^\pm\right] = \pm 2X^\pm \quad ,$$

$\tilde{f}_-$ - is the coefficient function in the decomposition of $\tilde{f}$ of the element corresponding to the minimal root of the algebra, $\tilde{f} = \sigma f \sigma^{-1}$ and where σ is an automorfism of the algebra, changing the positive and negative roots.

In the case of algebra SL(3,C) we'll consider the case of three dimensional representation of algebra and the following form of $\sigma = \begin{pmatrix} 0 & 0 & 1 \\ 0 & 1 & 0 \\ -1 & 0 & 0 \end{pmatrix}$.

The discrete symmetry transformation, producing new solutions from the known ones, is as follows:

$$\frac{\partial F}{\partial x_i} = S\frac{\partial \tilde{f}}{\partial x_i}S^{-1} + \theta_i \frac{\partial S}{\partial x_i}S^{-1} \tag{3}$$

Using the equations of the principal chiral field problem for the group-valued element

$$\theta_i(g)_{x_i}\, g^{-1} = (f)_{x_i}$$

the relations (3) can be rewritten as

$$\theta_i(S_n \sigma g_n)_{x_i} (S_n \sigma g_n)^{-1} = (f_{n+1})_{x_i} \quad ,$$

So we see that the group valued elements g_{n+1} and g_n are connected by the relation

$$g_{n+1} = S_n \sigma g_n \tag{6}$$

3. Let's represent the explicit formulae of the recurrent procedure of obtaining the group-valued element solutions of the self-duality equations in the case of SL(3,C) algebra .

At every step, as it shown in [5], S is upper triangular matrix and can be represented in the following form:

$$S_n = exp(\beta_1)_n X_1^+ \; exp(\beta_{1,2})_n X_{1,2}^+ \; exp(\beta_2)_n X_2^+ \; exp(\beta_0)_n H \quad , \tag{7}$$

where $H=h_1+h_2$ and for g_n we use the following parameterization:

$$\begin{aligned} g_n = {} & exp(\eta_1^+)_n X_1^+ \; exp(\eta_{1,2}^+)_n X_{1,2}^+ \; exp(\eta_2^+)_n X_2^+ \; exp((t_1)_n h_1 + (t_2)_n h_2) \times \\ & \times exp(\eta_2^-)_n X_2^- \; exp(\eta_{1,2}^-)_n X_{1,2}^- \; exp(\eta_1^-)_n X_1^- \end{aligned} \tag{8}$$

with

$$g_0 = exp(\eta_1^+)_0 X_1^+ \; exp(\eta_{1,2}^+)_0 X_{1,2}^+ \; exp(\eta_2^+)_0 X_2^+ \; exp((t_1)_0 h_1 + (t_2)_0 h_2)$$

as an initial solution.

Hereafter, $X_1^{\pm}$, $X_2^{\pm}$, $X_{1,2}^{\pm}$, h_1, h_2 are the generators of SL(3,C) algebra.

Following the general scheme from [5] and using (2) we have at
(0)-step:

$$(t_i)_0 = \tau_i^{-1} \equiv \nu_i \,, (\eta_i^+)_0 = \alpha_i^{-1}, i = 1,2 \,, (\eta_{1,2}^+)_0 = \alpha_{1,2}^{-1,0} \quad ;$$

(1)-step:

$$(t_1)_1 = -\nu_1 + ln\left(-\frac{\alpha_{1,2}^{-1,0}}{\alpha_{1,2}^{0,0}}\right) \,, \; (t_2)_1 = -\nu_2 + ln\left(-\frac{\alpha_{1,2}^{0,-1}}{\alpha_{1,2}^{0,0}}\right) \,,$$

$$(\eta_1^-)_1 = -\frac{\alpha_2^{-1}}{\alpha_{1,2}^{-1,0}} exp\,\delta_1 \,, \; (\eta_2^-)_1 = \frac{\alpha_1^{-1}}{\alpha_{1,2}^{0,-1}} exp\,\delta_2 \,, (\eta_{1,2}^-)_1 = \frac{1}{\alpha_{1,2}^{-1,0}} exp(\delta_1 + \delta_2),$$

$$(\eta_1^+)_1 = -\frac{det\begin{pmatrix} \alpha_1^{-1} & \alpha_1^{0} \\ \alpha_{1,2}^{-1,0} & \alpha_{1,2}^{0,0} \end{pmatrix}}{\alpha_{1,2}^{-1,0}} \,, (\eta_2^+)_1 = -\frac{det\begin{pmatrix} \alpha_2^{-1} & \alpha_2^{0} \\ \alpha_{1,2}^{0,-1} & \alpha_{1,2}^{0,0} \end{pmatrix}}{\alpha_{1,2}^{0,-1}} \,, (\eta_{1,2}^+)_1 = \frac{det\begin{pmatrix} \alpha_{1,2}^{-1,0} & \alpha_{1,2}^{-1,1} \\ \alpha_{1,2}^{0,0} & \alpha_{1,2}^{0,1} \end{pmatrix}}{\alpha_{1,2}^{-1,0}} \,,$$

$$\delta_i = 2\nu_i - \nu_j \,, i \neq j \quad ;$$

(2)-step:

$$\left(\eta_1^-\right)_2 = -\frac{det\begin{pmatrix}\alpha_2^{-1} & \alpha_2^{0}\\ \alpha_{1,2}^{1,-1} & \alpha_{1,2}^{1,0}\end{pmatrix}}{det\begin{pmatrix}\alpha_{1,2}^{-1,0} & \alpha_{1,2}^{-1,1}\\ \alpha_{1,2}^{0,0} & \alpha_{1,2}^{0,1}\end{pmatrix}} exp\,\delta_1 \quad , \quad \left(\eta_2^-\right)_2 = \frac{det\begin{pmatrix}\alpha_1^{-1} & \alpha_1^{0}\\ \alpha_{1,2}^{0,0} & \alpha_{1,2}^{1,0}\end{pmatrix}}{det\begin{pmatrix}\alpha_{1,2}^{0,-1} & \alpha_{1,2}^{0,0}\\ \alpha_{1,2}^{1,-1} & \alpha_{1,2}^{1,0}\end{pmatrix}} exp\,\delta_2 \quad ,$$

$$\left(\eta_{1,2}^-\right)_2 = \frac{1}{det\begin{pmatrix}\alpha_{1,2}^{-1,0} & \alpha_{1,2}^{-1,1}\\ \alpha_{1,2}^{0,0} & \alpha_{1,2}^{0,1}\end{pmatrix}} exp(\delta_1 + \delta_2),$$

$$\left(\eta_1^+\right)_2 = \frac{det\begin{pmatrix}\alpha_1^{-1} & \alpha_1^{0} & \alpha_1^{1}\\ \alpha_{1,2}^{-1,0} & \alpha_{1,2}^{0,0} & \alpha_{1,2}^{1,0}\\ \alpha_{1,2}^{-1,1} & \alpha_{1,2}^{0,1} & \alpha_{1,2}^{1,1}\end{pmatrix}}{det\begin{pmatrix}\alpha_{1,2}^{-1,0} & \alpha_{1,2}^{-1,1}\\ \alpha_{1,2}^{0,0} & \alpha_{1,2}^{0,1}\end{pmatrix}}_1 \quad , \quad \left(\eta_2^+\right)_2 = \frac{det\begin{pmatrix}\alpha_2^{-1} & \alpha_2^{0} & \alpha_2^{1}\\ \alpha_{1,2}^{0,-1} & \alpha_{1,2}^{0,0} & \alpha_{1,2}^{0,1}\\ \alpha_{1,2}^{1,-1} & \alpha_{1,2}^{1,0} & \alpha_{1,2}^{1,1}\end{pmatrix}}{det\begin{pmatrix}\alpha_{1,2}^{0,-1} & \alpha_{1,2}^{0,0}\\ \alpha_{1,2}^{1,-1} & \alpha_{1,2}^{1,0}\end{pmatrix}}_2 \quad ,$$

$$\left(\eta_{1,2}^+\right)_2 = \frac{det\begin{pmatrix}\alpha_{1,2}^{-1,0} & \alpha_{1,2}^{-1,1} & \alpha_{1,2}^{-1,2}\\ \alpha_{1,2}^{0,0} & \alpha_{1,2}^{0,1} & \alpha_{1,2}^{0,2}\\ \alpha_{1,2}^{1,0} & \alpha_{1,2}^{1,1} & \alpha_{1,2}^{1,2}\end{pmatrix}}{det\begin{pmatrix}\alpha_{1,2}^{-1,0} & \alpha_{1,2}^{-1,1}\\ \alpha_{1,2}^{0,0} & \alpha_{1,2}^{0,1}\end{pmatrix}}$$

Here, α_1^i, α_2^j, $\alpha_{1,2}^{i,j}$ - chains of solutions of principle chiral field problem determined by formulae (9-12) from [5].

[1] *M.F.Atiyah,N.J.Hitchin,V.G. Drinfeld and Yu.I. Manin*. Phys. Lett. A65, 1978, 2.

[2] *A.N.Le nov and M.A.Mukhtarov.* J.Math. Phys. 28 (11), 1987, 2574; Prepr.IHEP 87-90, 1987; Prepr. ICTP 163, Trieste, Italy,1990; J.Sov. Lazer Research, 13 (4), 1992, 284

[3] *A.N. Le nov.* IHEP preprint-92/87,1990.

[4] *A.N.Le nov,M.A.Mukhtarov and W.J.Zakr ewski.* Tr.J.of Physics 19, 1995, 416

[5] *M.A. Mukhtarov.* Fizika 5, 2002, 38

M.A. Mıxtarov

SL(3,C)-QRUP ELEMENTİ ÜÇÜN ƏSAS KİRAL SAHƏNİN MƏSƏLƏSİNİN HƏLLİ

SL(3,C)- cəbri halında diskret spektr metodu vəsitəsilə əsas kiral sahənin məsələsinin həlli tapılmışdır.

M.A. Мухтаров

РЕШЕНИЕ ЗАДАЧИ ГЛАВНОГО КИРАЛЬНОГО ПОЛЯ ДЛЯ SL(3,C)-ГРУППОВОГО ЭЛЕМЕНТА

Построены решения для группового элемента уравнений главного кирального поля методом дискретных симметрий в случае алгебры SL(3,C).

Received: 21.08.02

ROLES OF SUBSTRATE INHIBITION AND ENZYME ISOMERIZATION IN KINETICS OF BIOCHEMICAL OSCILLATIONS

SH.K. BAYRAMOV

Azerbaijan Medical University, 370022, Bakikhanov str.23, Baku, Azerbaijan.
E-mail: shahinru@yahoo.com

The chemical kinetic model is investigated to determine the condition under which a substrate inhibition and enzyme isomerization can lead to biochemical oscillation. A kinetic model for the two-center enzyme which under certain conditions allows the existence of oscillatory behavior is suggested. The main kinetic requirements for the existence of oscillatory regimes in biochemical reaction systems are distinguished.

Key words: enzyme oscillations

INTRODUCTION

Oscillatory behavior has been observed in many enzyme reaction systems [1]. Many investigators of biochemical oscillations believe that its chemical kinetic source has been generally attributed to an autocatalytic reaction mechanism. Even there is an opinion of necessity of autocatalysis for the oscillatory phenomena in enzyme reaction systems [2]. On the other hand, in number of studies it is suggested that substrate inhibition kinetics can also be a source of oscillatory behavior in chemical systems, particularly enzyme reactions. Spangler and Snell [3,4] studied a two-enzyme model system in which the product of one enzyme-catalyzed reaction acts as inhibitor for the other enzyme. This two-enzyme model was shown to exhibit bistability and sustained oscillations. Sel'kov [5] investigated a single enzyme model involving both substrate inhibition and product activation and observed oscillatory phenomena. The oscillations observed were attributed to the substrate inhibition kinetics, but no proof of this assertion was given. Seelig [6] investigated a model involving a single enzyme with substrate inhibition kinetics only (no product activation) and observed oscillations. However, this model involves two substrates, only one of which is an inhibitor. It is not clear whether the existence of multiple substrates is the necessary condition for oscillatory behavior in a system governed by substrate inhibition. Goldstein and Ivanova [7] considered a model of enzyme reaction system with both substrate inhibition and the enzyme isomerization and observed oscillatory phenomena. This model involves the double substrate inhibition, i.e. the substrate inhibits two conformational changed (isomerized) enzyme forms. Shen and Larter [8] investigated a model involving substrate inhibition and autocatalysis. Their investigation shows that though oscillatory behavior is observed in this system, it is caused by either autocatalytic properties of the mechanism or substrate inhibition coupled with product inhibition. They concluded that only substrate inhibition is insufficient for oscillatory phenomena in this mechanism. Several examples exit in the literature [9,10,11], but they comprise only evidence of sufficient conditions for oscillatory behavior, but which are not necessary. As it is obvious from the mentioned above, the autocatalysis mechanism is not necessary condition for the oscillatory phenomena in biochemical reaction networks, as well. Then the principle question arises about necessity of additional conditions for oscillations in chemical reaction systems, particularly enzyme reactions. In this paper we show that (1) neither autocatalysis, nor any other concrete reaction mechanism or its combinations (such as, substrate inhibition, product inhibition etc.) is not necessary condition for the oscillations; (2) for the oscillation phenomena it is necessary the existence of so called "critical reaction fragments".

THE METHOD OF ANALYSIS

Our analysis of non-linear kinetics of chemical reaction networks was carried out on the base of double-barrel graph theory [12,13,14]. The method connects structure of the kinetic schemes with the critical phenomena arising in it (multiplicity of stationary states, self-oscillations). It is known, that the kinetic behavior of system is determined by a characteristic polynomial of linearized systems of the kinetic equations:

$$P = \lambda^n + a_1\lambda^{n-1} + a_2\lambda^{n-2} + \ldots + a_m \qquad (1)$$

If in a stationary state even one of the coefficients in (1) has a negative sign this state becomes unstable and in the system there can be multiple steady states or self-oscillations. Ivanova [12] proved, that if the lower non-zero coefficient (a_m) was negative and there were no steady-state points at the border of the polyhedron of invariance determined by the material balance equations in the phase space, then there should be several steady-state points inside the polyhedron (multiple steady-states).

If $a_m>0$ at any concentration, then there is a single steady-state point (if the boundary conditions are fulfilled). In this case, if another coefficient $a_{m-k}<0$, then a single steady-state point can be unstable. A stable limited cycle i.e. self-oscillations occurs in the vicinity of this single unstable steady-state point.

This means that oscillations can arise if in the graph of common reaction network there is a critical fragment of lower order. This allows searching for the reason of oscillations in critical fragments of the lowered order. Such fragments in various reaction mechanisms can arise. They may be both autocatalytic and non-autocatalytic mechanisms, although, the number of such reaction mechanism is not large [15]. Therefore this shows, that neither autocatalysis, nor any other concrete reaction mechanism or its combinations is not the necessary condition for the oscillation phenomena.

The existence of lowered order of critical subgraph (reaction fragment) is the necessary condition, but un-sufficient for the arising of oscillatory behavior. Our structural-kinetic analysis allows us to support some additional requirements, which can lead to sustained oscillations. (1) From our careful study of the oscillatory kinetic models we have shown that the presence of the flow terms for the substrate (and/or other non-balanced compounds) is crucial for oscillatory behavior. (2) The rates of reaction stages, which consist of the critical fragment, could be sufficiently larger than the other reaction rates. In this case, if the sum of contributions of high-ordered subgrpahs remains positively, then oscillatory behavior is possible.

THE ROLE OF THE ENZYME ISOMERIZATION IN BIOCHEMICAL OSCILLATIONS

It is well-known, that enzymes in a solution exist in several (usually in two) isomerized forms [16]. Transitions between the conformers have essential significance for the oscillation behavior. Conformers of the enzyme, as a rule, have various affinities to substrate. In solutions these enzyme conformers interact with one substrate and thus create competition between these two forms of enzyme. It leads to the occurrence in the graph of two negative ways sequence, which enters into an even cycle and together with catalytic cycle forms the critical fragment. Thus there is an opportunity for existence of an oscillatory mode. To illustrate the role of enzyme isomerization in oscillation phenomena we had chosen the Guinoprotein Glucose Dehydrogenase enzyme (GDH), as an example. Experimental data show the biphasic cooperativity containing two sets of apparent kinetic parameters. The data allow to suggest, that GDH have two subunits in the two states of mutual interactions and the two catalytic cycles of GDH have different rate limiting steps [17]. Summarizing the literary data it is possible to present the basic scheme of reactions, catalyzed by the GDH, as follows:

1. $E + A \rightarrow EA;\ EA + S \rightarrow EAS;\ EAS \rightarrow EBP;$
   $EBP \rightarrow E^*B+P;\ E^*B \rightarrow E^* + B;$
2. $E + S \leftrightarrow ES$
3. $E^* \rightarrow E$
4. $E^* + A \rightarrow E^*A;\ E^*A + S \rightarrow E^*AS;\ E^*AS \rightarrow E^*BP;$
   $E^*BP \rightarrow E^*B+P;\ E^*B \rightarrow E^*+B.$

Here E and E^* are the different isomerized forms of free enzyme, A is the coenzyme, S is the substrate, B is the oxidized coenzyme and P is the product. As in other dehydrogenase reactions, in this scheme the linkage stage of a substrate to enzyme-coenzyme complex and the stage of isomerization of enzyme are rate limiting stages [16,17]. Stopping at slow stages of the reaction catalyzed by GDH, it is possible to present reaction in the following sequence: the substrate (S) contacts with the first catalytic center of enzyme (E). The first catalytic act occurs and enzyme passes to another isomerized form (E*) at which catalytic center of the second subunits becomes accessible for the substrate. It is a new isomerized form of enzyme, which has other affinity to a substrate, and is catalytic active, too. It can form active enzyme - substrate complex (E^*AS) and create a product (P). As well the conformation transition of the second isomerized form of enzyme into the first can be occurred ($E^* \rightarrow E$). Thus, as a result of two catalytic acts in the system there will be a biphase accumulation of a product with different parameters. Besides, this scheme permits the substrate inhibition: one can assume, that it occurs at linkage of the substrate to the second active center in the first conformation of enzyme and forms the inactive enzyme-substrate complex (ES), which is in a good agreement with experimental data [16]. Thus, stopping at slowly-stages, it can be written:

1. $E + A + S \xrightarrow{1} E^* + B + P;$
2. $E^* \xrightarrow{2} E;$
3. $E^* + A + S \xrightarrow{3} E^*AS$
4. $E + S \xrightarrow{4} ES$
5. $E^*AS \xrightarrow{5} E^* + B + P$
6. $ES \xrightarrow{6} E + S$

Consider a possibility of the arising of oscillation behavior in the suggested scheme of reaction. Five variable concentrations participate in the system. We shall denote their dimensionless quantities as:

$$c_1=S/S_0,\ c_2=E^*/E_0,\ c_3=E/E_0,\ c_4=ES/E_0,\ c_5=E^*S/E_0,$$

there, S_0 is the stationary concentration of the substrate, E_0 is the total concentration of enzyme (the sum of all enzyme and enzyme complexes). These variables are connected with a balance ratio:

$$c_2 + c_3 + c_4 + c_5 = 1$$

Hence, only four variables are independent and therefore, the characteristic polynomial of system will be of the 4-th order:

$$P = \lambda^4 + a_1\lambda^3 + a_2\lambda^2 + a_3\lambda + a_4 \qquad (2)$$

The sign of smallest nonzero coefficient a_4 of the characteristic polynomial for the given system is determined by the critical fragment of the 4-th order. If $a_4 > 0$ for any c_i in invariant area, i.e. in area where

$$c_i > 0,\ c_2 + c_3 + c_4 + c_5 = 1,\ c_1 \le c_{max},$$

then the stationary point is unique. Thus it is taken into account, that on a border of invariant polyhedron there are no stationary points. If, besides the inequality $a_3 < 0$ in a unique point, then this unique stationary point is unstable and is carried out around this point there is a steady limited cycle.

Stationary rates of reactions are connected by means of the following equality:

$$\upsilon_1=\upsilon_2,\ \upsilon_3=\upsilon_5,\ \upsilon_4=\upsilon_6,\ \upsilon_0=\upsilon_1+\upsilon_3.$$

Thus, from 12 stationary rates and concentrations seven are independent. Using a method of calculation of the characteristic polynomial coefficients [13,14] we obtain the expressions for the coefficients of characteristic polynomial

a_1, a_2, a_3 and a_4. The coefficients a_1 and a_2 are positive for any positive values of independent variables. An analysis of expression for a_3 shows, that in the field of self-oscillations the quantities $\upsilon_4=\upsilon_6$ should be small enough. Therefore neglecting the members containing υ_4 and υ_6 in the expression for a_3 one obtains more simple expression for a_3 as:

$$a_3 = \frac{\upsilon_2\upsilon_5}{c_1c_2c_3c_5}\{\upsilon_2(c_3 - c_5) + \upsilon_5(c_2 + 2c_3)\}$$

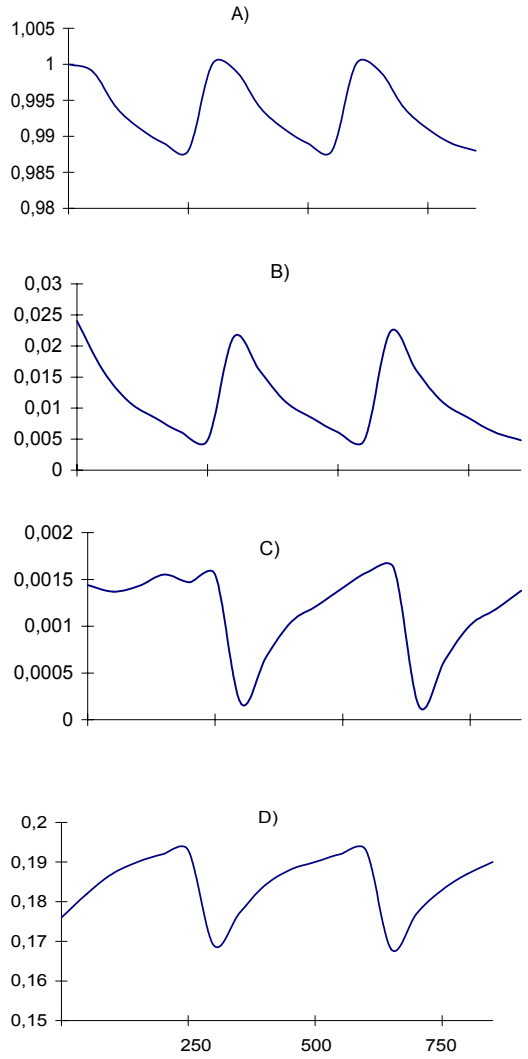

Fig.1. A time dependence of relative concentrations of the reaction scheme, considered above: A) substrate concentration (c_1); B) Free enzyme concentration (c_2); C) concentration of isomerized enzyme (c_3); D) concentration of E^*AS (c_5). Curves are obtained for the following values of relative concentrations and rate constants: $c_1=1$, $c_2=0.024$, $c_3=0.002$, $c_5=0.15$, $k_1=200$, $k_2=200$, $k_3=40$, $k_4=0.001$, $k_5=300$, $k_6=0.4$.

From this expression it is seen, that for occurrence of oscillations it is necessary, that $c_3 < c_5$. Therefore we shall consider below the area of concentration value, where this condition is satisfied. The expression for the coefficient a_4 has the form:

$$a_4 = \frac{\upsilon_2\upsilon_4\upsilon_5}{c_1c_2c_3c_4c_5}\{\upsilon_2(c_3 - c_5) + \upsilon_5(c_2 + 2c_3 + c_4)\}$$

For existence of self-oscillations, it is enough, that

$$\upsilon_5(c_2 + 2c_3) < \upsilon_2(c_5 - c_3)$$
$$\upsilon_5(c_2 + 2c_3 + c_4) > \upsilon_2(c_5 - c_3)$$

It is possible to combine these inequalities and as a result a sufficient condition for self-oscillations is obtained in a final form:

$$\frac{\upsilon_2}{\upsilon_5} < \frac{c_4}{c_5 - c_3}$$

If this condition is not fulfilled in the system there will be no self-oscillations, and there will be places of bistability in considered reaction system. Results of numerical calculations, which lead to non-damping self-oscillations, are shown in figure 1.

CONCLUSION

We have continued a study of substrate inhibition scheme originally done by Degn [19] to determine whether oscillatory behavior can be supported by it. Our calculation shows, that oscillatory behavior cannot be sustained only by such a mechanism. The application of double barrel graph theory allows us to support the main requirements, which lead to oscillation behavior: For the existence of oscillations in the system consisting of n reagents, at least m-order critical fragments must be: $m=n-f-1$. Here f is the number of the balance equations (i.e., the number of mass conservation laws). On the other hand we conclude, that the presence of the flow terms for the non-balanced reagents is necessary for the oscillation phenomena. Our third requirement is the existence of considerable difference of reaction rates between critical and non-critical fragments of common reaction networks. Obtained results also allow to predict from a general class of enzymes those that may be good candidates for the generation of oscillatory behavior. We find that soluble two-center dehydrogenases can lead to oscillations. Our model studies of oscillatory conditions for the two-center in the presence of substrate inhibition and the conformation transition may be a convenient basis for the investigation of more complex oscillatory events in biology. For example, in [20] it have been found that glucose stimulation of pancreatic β cells induces oscillations of the membrane potential, cytosolie Ca^{2+}, and insulin secretion. Each of those events depends on glucose metabolism. Both intrinsic oscillations of metabolism and repetitive activation of mitochondrial dehydrogenases by Ca^{2+} have been suggested by authors to decisive for this oscillatory behavior.

Acknowledgement. The author would like to acknowledge Prof. Dr. A.N.Ivanova (Institute of Problems of Chemical Physics, Russian AS) for the useful consultations.

[1] *R.J.Field, and L. Gyorgyi.* Chaos in Chemistry and Biochemistry. World Scientific Publishers, Singapore, 1993, 289 pp.
[2] *A.M.Jabotinskiy.* Concentration self-oscillations [in Russian], (Nauka, Moscow, 1974, 300 pp.
[3] *R.A.Spangler, F.M.Snell.* Sustained oscillations in a catalytic chemical system. Nature.1961, 191,457-458
[4] R.A.Spangler, and F.M.Snell. Transfer function analysis of an oscillatory model chemical system. J.Theor.Biol.1967, 16,381-405.
[5] *E.E. Sel'kov.* Self-oscillations in glycolysis. 1. A simple kinetic model. Eur.J.Biochem. 1968, 4, 79-86.
[6] *F.F. Seelig.* Chemical oscillations by substrate inhibition. Z.Naturforsch, 1976, 31A, 731-738.
[7] *B.N.Goldsteyn, A.N.Ivanova.* Simple kinetic models interpreting the critical Phenomena in the enzyme reactions with enzyme and substrate isomerization. Molekulyarnaya biol., 1988, 22, 1381-1391.
[8] *P.Shen, and R.Larter*. Role of substrate inhibition Kinetics in Enzymatic Chemical Oscillations. Biophys.J. 1994, 67,p. 1414-1417.
[9] *H.Degn, D.E.Harrison*. Theory of oscillations of respiration rate in continues culture of klebsiella aerogenes. 1969, J.Theor.Biol. 22, 238-248.
[10] D.Thomas. Artifical enzyme membranes,transport, Memory and oscillatory phenomena. *In*: Analysis and control of immobilized enzyme systems. (D.Thomas and J.-P. Kernevez, eds), 1976, pp.115-150.Springer Verlag, New York.
[11] *I.Lengyel, G.Rabai and I.R.Epsteyn*. Batsh oscillations in the reaction of chlorine dioxide with iodine and malonic acid, J.Am.Chem. Soc. 1990, 112, 4606-4607.
[12] *A.N.Ivanova*. A condition of steady state singularity of kinetic system, constrained with structure of reaction scheme, Kinetika i Kataliz. *20,*1541-1548.
[13] *Sh.K Bayramov* Algoritmic Rules for Determination of Subgraph Contribution Considering the Application of Bigraphs in the Kinetics of Biological processes, Biochemistry *(Moscow), 1999, 64,* 636-638.
[14] Sh.K.Bayramov (2001) Graph-theoretical method for the nonlinear kinetics of biochemical reactions, *Physics,2001, 7, 13-17.*
[15] Sh.K.Bayramov (2002) Simple critical schemes in non auto-catalytic Biochemical reactions, *Biochemistry Moscow), 67, 761-764.*
[16] C.Frieden (1979) Slow transitions and hysteretic behaviour in enzymes. *Ann.Rev.Biochem.48,*471-489.
[17] A.J.Olsthoorn, T. Otsuki and J.A.(1998) Duine Negative cooperativity in the steady-state kinetics of sugar oxidation by soluble quinoprotein glucose dehydrogenase from Acinetobacter calcoaceticus. *Eur. J.Biochem. 255,*255-261.
18. L.A.Basso, Engel P.C. and Walmsley A.R. (1995).The mechanism of substrate and coenzyme binding to clostridial glutamate dehydrogenase during reductive amination. *Eur. J. Biochem. 234,*603-615.
[18] 19. H.Degn (1968) Bistability caused by substrate inhibition of peroxidase in an open reaction systems. *Nature. 217,*1047-1050.
[19] M. A. Ravier, K. Eto, F. C. Jonkers, M. Nenquin, T. Kadowaki, and J.-C. Henquin. (2000)The Oscillatory Behavior of Pancreatic Islets from Mice with Mitochondrial Glycerol-3-phosphate Dehydrogenase Knockout *J. Biol. Chem 275,* 1587-1593

Ş.Q. Bayramov

SUBSTRAT İNHİBİRƏSİNİN VƏ FERMENT İZOMERİZASİYASININ BİOKİMYƏVİ RƏQSLƏRİN KİNETİKASINDA ROLU

Biokimyəvi rəqslərin yaranma şərtlərini təyin etmək üçün, substrat inhibirəsi və ferment izomerizasiyası olan fermentativ reaksiyaların kimyəvi modellərinin kinetikası tədqiq edilmişdir. Periodik axımın mövcudluğuna imkan verən, iki-mərkəzli ferment reaksiyası modeli təklif edilmişdir. Biokimyəvi reaksiya sistemlərində periodik rejimlərin mövcudluğu üçün əsas kinetik tələblər ayarlanmışdır.

Ш.К. Байрамов

РОЛИ СУБСТРАТНОГО ИНГИБИРОВАНИЯ И ИЗОМЕРИЗАЦИИ ФЕРМЕНТА В КИНЕТИКЕ БИОХИМИЧЕСКИХ КОЛЕБАНИЙ

Для определения условия возникновения биохимических колебаний исследована кинетика химической модели ферментативной реакции с изомеризацией фермента и субстратным ингибированием, Предложена кинетическая модель реакции двух-центрового фермента, которая позволяет существование колебательного поведения. Выделены основные кинетические требования для существования колебательных режимов в биохимических реакционных системах.

Received: 20.09.02

RELAXOR PROPERTIES OF $TlInS_2$ CRYSTALS DOPED BY Fe

R.M. SARDARLI, O.A. SAMEDOV, I.Sh. SADIGOV, I.I. ASLANOV, A.P. ABDULLAEV
Institute of Radiation Problems of Azerbaijan National Academy of Sciences
H.Javid ave., 31a, Baku, 370143

J.H. JABBAROV
Baku State University
Z.Khalilov St., 23, Baku, 370143

It is shown that $TlInS_2$ crystals doped by Fe show all peculiarities that are typical to the relaxor ferroelectrics. The temperature region of the microdomain (relaxor) state as well as the temperature of the transition to the macrodomain state have been determined.

The analysis of temperature dependences of the dielectric constant $\varepsilon(T)$ in the phase transitions region of $TlInS_2$ crystal showed that it has a different form for the samples that were taken from various technological batches. Authors of [1] determined that the different form of $\varepsilon(T)$ curves is connected with the fact that $TlInS_2$ crystal belongs to the class of compounds (berthollides) in which the rearrangement of composition occurs during the growth process. However this peculiarity does not lead to the smearing of the phase transitions and the dependence $\varepsilon^{-1}(T)$ obeys Curie-Weise law with the constant approximately equal to 10^{-3} beginning from the submillimetric spectral regions up to the measurements of $\varepsilon(T)$ in the kilohertz region [2, 3]. It was established by the neutron-diffraction research that $TlInS_2$ compound is an improper ferroelectric with an incommensurate phase [4].

The temperature region, in which instability of $TlInS_2$ crystal lattice is observed is a very sensitive to the trivalent cationic impurities that have different ionic radii and the coordination numbers. Moreover, the increase of phase transition temperatures is observed for some impurities while the decrease of phase transition temperatures is observed for others impurities (the results of this research are in preparation for publication). There is an interest to investigate the nature of these processes in $TlInS_2$ crystals. The transition metals of iron group being the multicharged impure ions can form the deep centers of strong localization that capable to the strong interaction with high-polarizable $TlInS_2$ crystal lattice.

The investigation results of dielectric, polarization and pyroelectric properties of $TlInS_2$<Fe> crystals are given in this paper.

EXPERIMENTAL TECHNIQUE.

$TlInS_2$ crystals have been grown by Bridgman-Stockbarger modified method. The anisotropy of dielectric properties in the plane of layer is not observed. The measurements have been carried out from the crystal faces cut out perpendicular to the polar axis. The crystal faces have been planished, polished and then covered by a silver paste. The dielectric constant ε and the dielectric loss tangent tgδ have been measured by the alternating current bridge E7-8 at the frequency 1 kHz and E7-12 at the frequency 1 MHz in the temperature region 150 - 250K. The velocity of temperature scanning was equal to 0.1 K/min. The dielectric-hysteresis loops were studied at the frequency 50 Hz by Soyer-Tauer modified scheme. The pyroeffect has been investigated by the quasistatic method using universal voltmeter V7-30.

RESULTS AND DISCUSSION.

The temperature dependence of the dielectric constant $\varepsilon(T)$ of both $TlInS_2$ (curves 1, 2) and $TlInS_2$<Fe> crystals (curves 3, 4, 5) in the cooling (curves 1, 3, 5) and heating regimes (curves 2, 4) are shown in figure 1. The measurement frequency to the curves 1, 2, 3 and 4 is equal to 1 kHz. The curve number 5 presents the results of measurement of ε(T) to $TlInS_2$<Fe> crystal at the frequency 1 MHz. As it is seen from figure 1, the known sequence of the phase transitions [3] is observed to $TlInS_2$ crystals (curves 1, 2). It is observed also the transitions from the paraelectric to the commensurate phase at 216K, as well as two transitions at 204 and 200K. The nature of these transitions was widely discussed in [5] and most likely it is connected with rearrangement of the modulated structure. The final transition to the polar phase occurs at 196K.

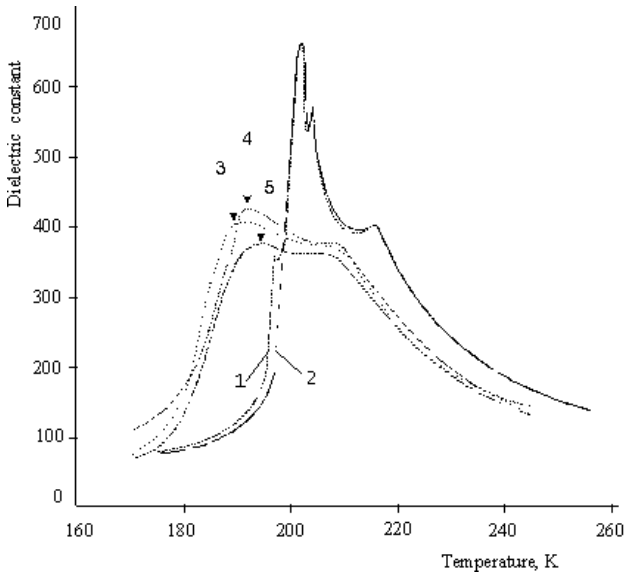

Fig.1. The temperature dependences of the dielectric constant $\varepsilon(T)$. Curves 1, 2 - the dependences $\varepsilon(T)$ of $TlInS_2$crystal (1 - cooling; 2 - heating); Curves 3, 4, 5 - the dependences $\varepsilon(T)$ of $TlInS_2$<Fe> crystal (3, 5 - cooling; 4 - heating). The measurement frequencies are 1 kHz (to the curves 1, 2, 3 and 4) and 1MHz (to the curve 5).

The dependence $\varepsilon(T)$ is described by Curie-Weis law with Curie constant $C^+=5.3\cdot10^3$K in the temperature region $T-T_1(216)\leq50^0$. The anomaly at 196K appears during the crystal cooling and all peaks are strongly pronounced without the signatures of the smearing. As it is obvious from figure, the dielectric hysteresis for $TlInS_2$ crystals is observed only at the temperature about 196K, while the hysteresis to the doped samples at the temperature T_m (it is a maximum temperature of $\varepsilon(T)$ curve) is about 2K (curves 3 and 4 in fig.1).

The nature of the dielectric constant in the same temperature region for $(TlInS_2)_{1-x}(Fe)_x$ crystals, where x = 0.001, is essentially distinctive namely the dependence $\varepsilon(T)$ is strongly blurred. The displacement of phase transitions to the low temperature region in 10K and the widening of region of existence of the incommensurate phase with conservation of two anomalies at 190K and 290K have been observed. In this case the natural question arises regarding the reason of such radical rearrangement of the dependence $\varepsilon(T)$ at doping 0.1-mol % of Fe.

As it is known, the composition fluctuation is a main reason of the smearing of phase transition temperatures [6, 7]. However, not any increasing in the defect concentration can be a reason to the smearing. According to [8] the defects having dipole moments are the reasons for such smearing and these defects create the electric fields in adjoining crystal regions. Besides as $TlInS_2$ is a semiconductor, the doping of impurities creates the corresponding centers of charge carrier localization, which can create the local electric fields that stimulate the initiation of the induced polarization near the phase transitions [9-11]. Important peculiarity of the ferroelectrics with smearing phase transitions is the fact that the dielectric polarization higher than T_m changes not by Curie-Weis law $(\varepsilon')^{-1}=C^{-1}(T-T_0)$ and by the law $(\varepsilon')^{-1}=A+B(T-T_0)^2$.

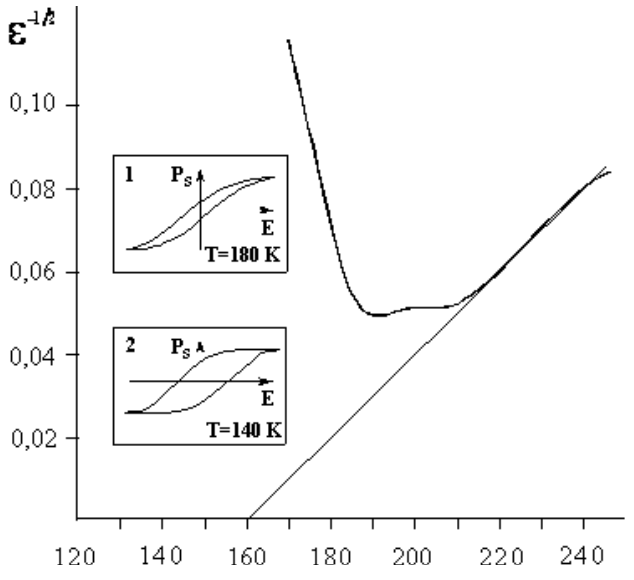

Fig. 2. The dependence $\varepsilon^{-1/2}$to $TlInS_2$<Fe> crystal. The measurements are carried out at the frequency 1MHz.The dielectric-hysteresis loops to $TlInS_2$<Fe> crystal are given in the insertions to the figure: 1 - the measurements are carried out at 180K; 2 - the measurements are carried out at 140K.

The dependence $\varepsilon^{-1/2}(T)$ for $TlInS_2$<Fe> is shown in fig. 2. This dependence line crosses the temperature axis at 164K from the side of high-temperature phase. It corresponds to the maximum value of low-temperature pyrocoefficient (fig. 3). The investigations of polarization properties of $TlInS_2$<Fe> showed that the dielectric-hysteresis loops are observed below 164K and the maximum value of spontaneous polarization (P_s) for such loops reaches up to $7.5\cdot10^{-8}$ Coulomb/sm^2. The value of P_s to the undoped $TlInS_2$ crystals is equal to $1.8\cdot10^{-7}$ Coulomb/sm^2. The value of P_s in the temperature region from 164 to 190K is $1.5\cdot10^{-8}$ Coulomb/sm^2. The dielectric-hysteresis loops for $TlInS_2$<Fe> crystals are given in the insertions to the fig.2. The first insertion to the figure reflects the observed loop in the temperature region 164 - 190K. As it is obvious from figure the loop is narrow and elongated that is a typical to the relaxor ferroelectrics. The form of dielectric-hysteresis loop below 164K has been given in the second insertion of the figure. It is obvious that the loop becomes saturated and it is a typical for the ferroelectric.

The investigations of frequency dispersion have been carried out at measurement frequencies f - 1 KHz and 1 MHz. The displacement of T_m maximums of $\varepsilon(T)$ curve with increasing frequency f in $TlInS_2$ crystals is not observed while the displacement of the smearing maximum of $\varepsilon(T)$ to $TlInS_2$<Fe> crystals is equal to 3K (figure 1, curves 3 and 5).

The temperature dependences of the pyroelectric coefficient $\gamma(T)$ for the pure $TlInS_2$ crystal (curve 1) and for the doped by Fe (curve 2) are given in the fig.3. The measurements were carried out in the quasistatic regime and the pyroelectric coefficient was calculated using the following equation: $\gamma=J/A_0\cdot dT/dt$, where J is a pyroelectric current, A_0 is an area of electrodes, dT/dt is a heating rate. The measurements were carried out using the samples, which were preliminary polarized in the external electric field. As it is obvious from figure, one peak with maximum value of the pyroelectric coefficient $1.4\cdot10^{-7}$ Coulomb/Ksm^2 in the curve $\gamma(T)$ is observed to the pure $TlInS_2$ crystal at 196K. Two anomalies at T_m=190K and T_0+164K in the curve $\gamma(T)$ are observed to $TlInS_2$<Fe> crystal. Besides, the weak current is observed in the temperature region higher than 190K, i.e. in the region of existence of the incommensurate phase.

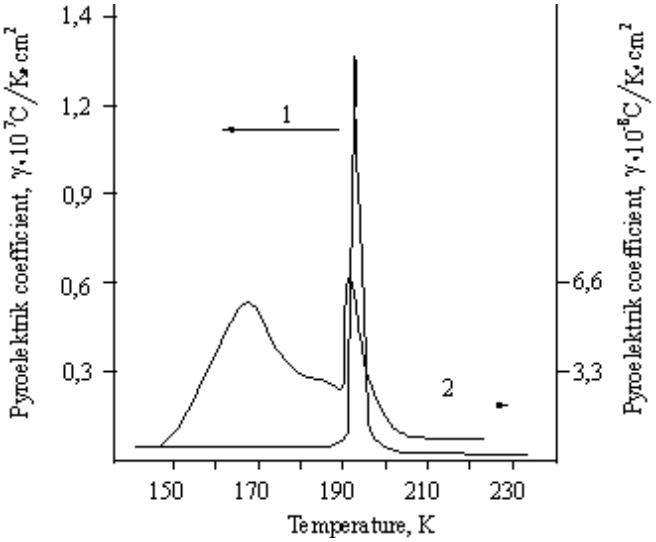

Fig.3. The temperature dependence of the pyroelectric coefficient $\gamma(T)$. Curve 1- $TlInS_2$ crystal. Curve 2- $TlInS_2$<Fe> crystal.

The analysis of the curves are given in the figures 1-3 allows to state that $TlInS_2$<Fe> crystals show all peculiarities

that are typical to the relaxation ferroelectrics namely the doping of $TlInS_2$ crystal by Fe^{3+} cations leads to the smearing of phase transitions as well as the frequency dispersion of the dielectric constant is observed. Moreover, the elongated dielectric-hysteresis loop is detected in the region of the smearing of phase transition and the temperature dependence of the dielectric constant from the side of high-temperature phase is described not by Curie-Weis law and according to the law $(\varepsilon')^{-1} = A + B(T - T_0)^2$.

The smearing of phase transitions and the peculiarities of ferroelectric properties in $TlInS_2$<Fe> crystal are unconditionally connected with the structure disorder that leads to the appearance of local distortions of both the symmetry and internal electric field in the wide temperature region. Despite the fact that the investigations of phase transitions in $TlInS_2$ crystals carried out during long period yet there are no the satisfactory understanding physical mechanisms of the processes taking place in the crystals and also the unambiguous interpretation of the observed phenomena. In our opinion it can be connected with the fact that during the investigations of phase transitions in $TlInS_2$ crystals not enough attention was given to the semiconductor properties of these crystals. Especially it concerns the crystals which are doped by the cationic impurities. These impurities can form the capture levels (traps) at the bottom of the conduction band. Here it is necessary to take into consideration both the processes of charge carrier localization on the local centers and their influence on the phase transitions. This issue has been considered in detail by Mamin in [9-11], where it was shown that the thermal filling of traps could lead to the intricate sequence of phase transitions as well as the appearance of unstable boundary state between the (incommensurate-commensurate) phases.

As it is seen in the curve $\gamma(T)$ at 164K the peak, which is not shown in the dependence $\varepsilon(T)$ (please compare fig.1and 3) is observed. According to [11] this peculiarity is a typical for the relaxors. It is connected with the fact that the oscillation frequency of the induced polarization will be determined by the characteristic relaxation time not only for the lattice subsystem as it has a place in usual ferroelectrics but also and the relaxation time of the electronic subsystem. Naturally, the characteristic time of change of parameter order $\boldsymbol{\gamma}$ and the characteristic time of electron concentration $\boldsymbol{m}$ in the traps strongly differ ($\tau_\eta/\tau_m << 1$). It allowed an author of [11] to investigate this problem by the separation method of fast and slow processes. As a result it has been established that effective temperature of the phase transition T_{cm} will be displaced below in the temperature scale due to thermal filling of the capture levels. The phase transition to the state with spontaneous polarization will occur at the temperature T_{cm}. This temperature corresponds 164K to the crystals $TlInS_2$<Fe> (fig.2). As it is seen from figure, below 164K the loop becomes saturated. As the localized charges create the local electric fields then the spontaneous polarization in the weak external fields in the separate microfields will be directed to the different directions in compliance with space distribution of the localized charges. Therefore, the hysteresis loop in the temperature region 164-190K is observed as narrow and elongated. Besides, according to the same reason, we did not observe the peculiarities in the dependence $\varepsilon(T)$ connecting with phase transition at the temperature T_{cm}.

Thus, the doping of $TlInS_2$ crystals by Fe leads to the appearance of the temperature region in which the crystals show all peculiarities that are typical for the relaxors. The phase transition from the relaxor (microdomain) to the macrodomain (ferroelectric) state occurs at the temperature 164K. The jump in the temperature dependence $\gamma(T)$ corresponds to this transition.

[1] *R.M.Sardarli, O.A.Samedov, I.Sh. Sadigov, A.I. Najafov, I.I. Aslanov, N.A. Eyubova.* «Transactions», Physics and astronomy XX11, 2002, 2, 31.

[2] *A.A.Volkov, Yu.G.Goncharov, G.V.Kozlov, K.R. Allakhverdiev and R.M. Sardarly.* (Soviet) Phys.Solid.State, 1983, 25, 2061.

[3] *R.A.Aliev, K.R.Allakhverdiev, A.I. Baranov, N.R. Ivanov, R.M. Sardarly.* (Soviet) Phys.Solid.State, 1984, 26, 775.

[4] *S.B.Vakhrushev, V.V.Zdanova, B.E.Kvyatkovski, N.M. Okuneva, K.R. Allakhverdiev, R.A. Aliev, R.M. Sardarly.* JETP letters, 1984, 39, 291.

[5] *R.A.Suleymanov, M.Yu.Seidov, F.I.Salaev, R.F.Mikailov.* Fiz. Tverd. Tela (Sankt Peterburg), 1993, 35, 2, 348.

[6] *I.P. Raevski, V.V. Eremkin, V.G. Smotrakov, E.S. Gagarina, M.A. Malitskaya.* Fiz. Tverd. Tela (Sankt Peterburg), 2000, 42, 1, 154.

[7] *M.D.Glinchuk, E.A. Eliseev, V.A. Stefanovich, B. Hilger.* Fiz. Tverd. Tela (Sankt Peterburg), 2001, 43, 7, 1247.

[8] *L. Benguigai, K. Bethe.* J.Appl.Phys., 1976, 47, 2728.

[9] *R.F. Mamin*. Fiz. Tverd. Tela (Sankt Peterburg), 1991, 33, 9, 2609.

[10] *R.F. Mamin*. JETP letters, 1993, 58, 7, 534.

[11] *R.F. Mamin*. Fiz. Tverd. Tela (Sankt Peterburg), 2001, 43, 7, 1262.

R.M. Sərdarlı, O.Ə. Səmədov, İ.Ş. Sadıqov, İ.İ. Aslanov, A.P. Abdullayev, C.H. Cabbarov

Fe AŞQARLANMIŞ $TlInS_2$ BİRLƏŞMƏNİN RELAKSOR XASSƏLƏRİ

Müəyyən edilmişdir ki, $TlInI_2$ Fe-la aşqarlandıqda, kristall relaksor seqnetoelektriklər üçün xarakterik olan xassələr göstərir. Kristalın mikrodomen (relaksor) halının varlıq temperatur intervalı və makrodomen halına keçid temperaturu tə'yin olunmuşdur.

Р.М. Сардарлы, О.А. Самедов, И.Ш. Садыхов, И.И. Асланов, А.П. Абдуллаев, Д.Г. Джаббаров

РЕЛАКСОРНЫЕ СВОЙСТВА $TlInS_2$ ЛЕГИРОВАННОГО Fe

Показано, что $TlInS_2$, легированный Fe, проявляет все особенности, характерные для релаксорных сегнетоэлектриков. Установлены температурная область существования микродоменного (релаксорного) состояния и температура перехода в макродоменное состояние.

Received: 09.12.02

PIEZOCOMPOSITES ON THE BASE OF THE TWO-COMPONENT MATRIX

M.A. KURBANOV, M.G. SHAKHTAKHTINSKIY, S.N. MUSAYEVA, G.G. ALIYEV, B.M. IZZATOV

Institute of Physics of the Azerbaijan National Academy of Sciences

H. Javid av. 33, Baku, 370143

Electrophysical and piezoelectric properties of composites on the base of two matrix: polar-polar polar-non-polar and non-polar-non-polar polymers are investigated. It is experimentally shown that by the elaboration of multiphase composites it is better to use the combination of polar and non-polar polymers than that of only non-polar or only polar polymers.

We showed before that electret, piezo- and pyroelectric properties of composites depend mainly on conditions of the injection and stabilization on various charge capture centers in the polymer phase at the electrothermopolarization [I-3]. Various structural defects, heavy-polar, low-molecular compounds in the bulk, oxide chains of the macromolecule and boundaries between amorphous and crystal phase of polymers might enter the charge capture center[1-4].It is natural to assume that the value of stabilized charges, which determines the degree of the domains orientation in composites, depends on the activation energy of stabilization centers.

It is known, that the boundaries of incompatible polymers may be effective charge capture centers (4,5). In this respect, we used the mixture of two polar and non-polar polymers, in particular, PE+PP, PE+PVDF, PP+PVDF as a matrix. Composites on the base of two-component matrixes and the piezoelectric of various structures are obtained by the method of the hot pressing.

Piezoceramics of the rhombohedral (Rh) and tetragonal (T) structure are used as a piezoelectric phase and PP, HDPE, PVDF and F_3 as a polymer phase. Electrodes of aluminum foil are applied in the process of the hot pressing. Temperature-temporary and temperature-pressure regimes of crystallization are variated with the aim of the polymer phase receipt with the various supermolecular structures (SMS). Sizes of electric phase particles are varied in the interval 50÷100 μm. Piezoelectric parameters of composites are determined by quasi-static methods.

The matrix compatibility and new phase formation in composites are determined by the research of the posistor effect. The research of the posistor effect in indicated composites allowed to determine the optimal conditions of polar composites.

Value of piezomodulus d_{33} and composites piezosensitivity g_{33} on the base of two-component matrix HDPE+PP, dispersional PCR-11 and PZT-2 versus the volume content of HDPE and PP in the matrix are shown in the Table I. It is seen, that the polymer composite with the volume relationship HDPE to PP, equal to 2:3, has the maximal value d_{33} and g_{33}.

The dependence of various composites piezomodulus, polarized at optimal values of the electric field voltage E_p and the polarization temperature T_p on the volume content F of the piezoceramics is shown on fig.1. It is seen that the piezomodulus value at all filler contents grows at the use as a matrix of the mixture HDPE and PP.

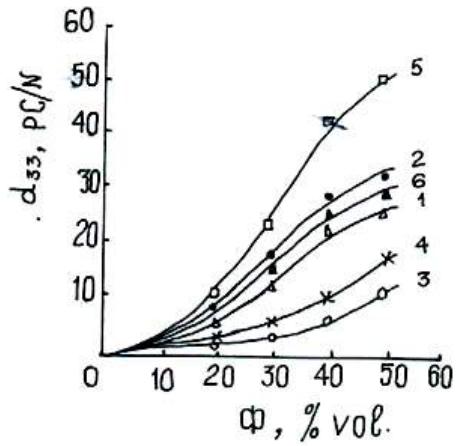

Fig.1. Piezomodulus dependence on the bulk content of the Piezoceramics: I- HDPE+PCR-11; II- PP+PCR-11; III- HDPE+PZT-2;IV- PP+PZT-2; V- HDPE+PP+PZT-2; VI- HDPE+PP+PCR-11.

The dependence of d_{33} on E_p for composites from polyolefin and PCR-11 is shown on fig.2,a. The maximal value d_{33} of HDPE+PP+PCR-11 composite is in 2 times more than the piezomodulus composite HDPE+PCR-11 and in 1,7 times more, than the piezomodulus PP+PCR-11. The d_{33} composite of HDPE+PP+PZT-2 is approximately in 2 times more, than d_{33} composite on the base of one-component matrix of HDPE+PZT-2.

Table 1.

The value of piezomodulus and composite piezosensitivity on the base of the two-component matrix.

Piezocomposites	Volume relationship HDPE:PP	Volume content of piezofillers in %	d_{33} pC/N	g_{33} Vm/N
HDPE+PP+PCR-11	1 : 4	50	34,7	0,14
	2 : 3	50	50,3	0,12
	3 : 2	50	33,8	0,15
	4 : 1	50	31,5	0,13
HDPE+PP+PZT –2	1 : 4	50	19,2	0,091
	2 : 3	50	30,4	0,145
	3 : 2	50	21,6	0,103
	4 : 1	50	17,1	0,081

The research results of the charge state of the indicated components show, that at other equal conditions of the polarization (at the stability of E_p, T_p and t_p is the polarization time) the value of stabilized volume charges (Q) in composites on the base of the two-component polymer matrix is visually more in comparison with the charge value of composites on the base of one-component polymer matrix (Table 2).

Table 2.

The charge value on the thermostimulated depolarization (TSD) and the composites piezomodulus on the base of one-component and two-component matrix.

Composites	Q,10^{-3}C/m^2	d_{33}, pC/N
HDPE+PCR – 11	0,65	21
PP+PCR – 11	0,75	33,6
PP+HDPE+PCR– 11	1,9	50,6

It is shown that more favorable conditions for the charge stabilization are realized in two-component systems. Obviously, additional centers of the charge stabilization at the electrothermopolarization occurs from non-polar polymers in the polymer-ferropiezoelectric system on the base of the matrix.

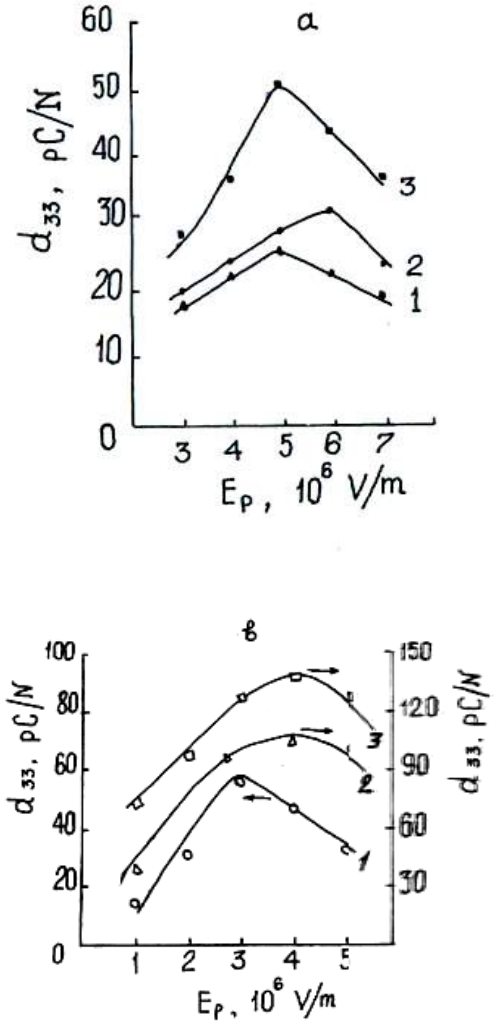

Fig.2. The dependence of piezomodulus d_{33} on the electric field voltage of the polarization E_p.
a) I- HDPE+PCR-11; II- PP+PCR-11; III- HDPE+PP+PCR-11;
b) I- PP+PCR-I; II- PVDF+PCR-I; III- PP+PVDF+PCR-I.

The dependence of d_{33} on E_p for composites as the matrix, in which polar polymer PVDF and non-polar polymer PP are used, is presented on fig. 2,b. The comparison of optimal values d_{33} versus $d_{33}=f(E_p)$ shows, that in this case the piezomodulus increment (Δd_{33}) is more, than for composites on the base of the matrix from polar or non-polar polymers. The piezomodulus increment (Δd_{33}) at the transition on the multicomponent composites was determined by optimal values of the piezomodulus dependence d_{33} on E_p and by the comparison of the piezomodulus of two matrix and more effective one-matrix composites.

Dependences of d_{33} on E_p for composites on the base of the matrix from the polar fluorine-containing polymers are shown on fig. 3 (a,b). It is seen, that d_{33} of the composite on the base of the matrix PVDF+F_3 is equal to the composite piezomodulus on the base of only PVDF (fig. 3,b) or a bit lesser (fig. 3,a).

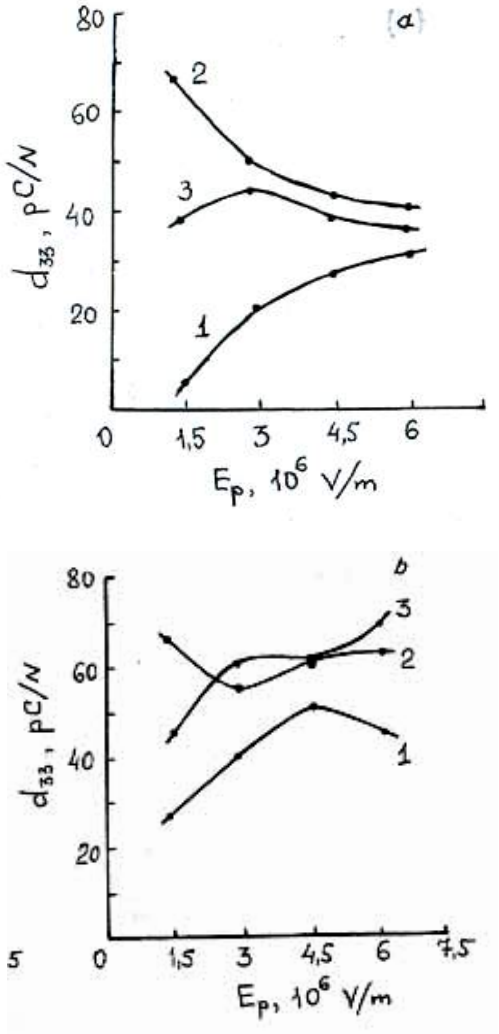

Fig. 3. The dependence of the piezomodulus d_{33} on the electric field voltage of the polarization E_p. T_p= 140° C (α)
I – F_3+PZT-I9; II – PVDF+PZT-I9; III – PVDF+F_3+PZT-I9
T_p= 180° C (δ)
I – F_3+PZT-I9; II – PVDF+PZT-I9; III – PVDF+ F_3+PZT-I9

Therefore, it may be concluded, that at the elaboration of multiphase composites, it is better to use the combination of the polar and non-polar polymer, than to use that of only non-polar or only polar polymers.

Obtained results, obviously, at first approximation may be explained with regard of changes of the supermolecular structure of matrix at their mixture and the composites receipt, and also by the compatibility of polar and non-polar polymers.

The SMS change may mainly occur in the transient layer of polymer phases. And it, in its turn, is determined by the compatibility of used polymer couples, in particular, PE+PP or PP+PVDF. As it is known, the thickness of this layer, is more exactly, the thickness of the segmental solubility layer makes dozens or hundreds Å [6]. The formation of such layer imposes limitations on the SMS formation in amorphous-crystal polymers in the direct proximity to the layer.

The thickness of the boundary layers with the changed SMS and properties on the contact surface of polymers may reach many hundreds and even thousands Å. Boundary layers may be additional phase for the change filler in the process of the composite polarization. Really, as it is seen from the table 2 at identical conditions the electrothermopolarization in the two-matrix system accumulates more changes, than in one-matrix composite. The value of the accumulated in the electrothermopolarization change, as it was proved before, determines the piezomodulus value of the composite [3]. Obviously, in two-matrix composites on the base of polar (PVDF) and non-polar (PP) polymers, a new phase, formed on the contact boundary of polymer segments has an ability to strong accumulate changes at the electrothermopolarization.

[1] *A.I. Mamedov, S.N. Musayeva, M.A. Kurbanov, A.Sh.Gasanov.* Fizika, 2001, c.VII, №3б p 50-52.
[2] *M.M. Kuliyev, S.N. Niftiyev, S.N. Musayeva, I.A. Farad-zhzade, M.G.Shakhtakhtinkiy, M.A. Kurbanov*. Fizika, 2000,c.VI, №4 p.3-5
[3] *M.A. Kurbanov*. Elektretniye, piezo, pyroelktricheskiye, varistoroniy i pozistorniy effekti v polimernikh kompozitzionnikh dielektrikakh"- Disser. d.f.-m.n.- Baku, 1985, 477.
[4] *B.I. Sajin* "Elektricheskiyi svoystva polimerov", Leningrad, 1986, 224.
[5] *V.A. Marikhin, L.P. Myasnikova.* "Nadmolekularnaya struktura polimerov", Leningrad: L:Khimiya, 1977, 230.
[6] Entziklopediya polimerov, Moskva, 1977, v.3, p.433.

M.Ə. Qurbanov, M.N. Şahtaxtinski, S.N. Musayeva, Q.Q. Əliyev, B.M. İzzətov

İKİKOMPONENTLİ MATRİSA ƏSASINDA PYEZOKOMPOZİTLƏR

Polyar-polyar, polyar-qeyri polyar və qeyri polyar-qeyri polyar polimerlər kimi iki matrisa əsasında kompozitlərin elektrofiziki və pyezoelektrik xassələri tədqiq edilmişdir. Eksperimental olaraq göstərilmişdir ki, çoxfazalı kompozitlər hazırlayarkən yalnız polyar və ya yalnız qeyri-polyar polimerlərdən deyil, matrisa kimi polyar və qeyri-polyar polimer qarışığından istifadə etmək lazımdır.

М.А. Курбанов, М.Н. Шахтахтински, С.Н. Мусаева, Г.Г. Алиев, Б.М. Иззатов

ПЬЕЗОКОМПОЗИТЫ НА ОСНОВЕ ДВУХКОМПОНЕНТНОЙ МАТРИЦЫ

Исследованы электрофизические и пьезоэлектрические свойства композитов на основе двух матриц: полярный-полярный, полярный-неполярный и неполярный-неполярный полимеры. Экспериментально показано, что при разработке многофазных композитов следует использовать сочетание полярных и неполярных полимеров, чем использовать сочетание только неполярных, или же только полярных полимеров.

Received: 18.12.02

ON THE IMPORTANCE OF THE TRANSITION *Of* - *WN* STARS FOR THE UNDERSTANDING OF STARS WOLF – RAYET TYPE EVOLUTION

J.N. RUSTAMOV, S.G. ZEINALOV
Shamakha Astrophysical Observatory of National Azerbaijan Academy of Sciences,
F.Agaev 9, Baku 370143, Azerbaijan

The similarity of the properties *WR (WN)* and *Of* stars have been considered. The possible evolutionary connections between this group stars are investigated. It is proposed that there may exist nitrogen – rich *Of* stars. Five criteria for the determination of such objects are proposed. Nitrogen – rich stars are close to *WN7-8* stars at the evolution stage . Observation of nitrogen - rich *Of* stars is important for the understanding of *Of – WN7-8* evolutionary connection.

1. Statement of the problem.

The *Of* stars are the most luminous objects among *O* stars of early subtypes. More massive *O* stars are progenitors of *Of* stars. *Of* stars are located at the Main Sequence in the region corresponding to the highest temperature and luminosity. All *Of* stars are more massive stars. The presence of emission lines with profiles *P Cyg* in the *UV* and visible region in the spectra of the *Of* stars indicate that these stars lose mass. From the similarity of spectral properties of *Of* and Wolf-Rayet (*WR*) stars Conti [1] for the first time proposed the hypothesis that the *WR* stars had evolved by stellar wind mass loss from massive *Of* stars (scenario Conti), although this statement have not been investigated completely.

In the present paper, the probable evolutionary connections between *Of* and *WR* stars are considered, and some interesting results have been obtained.

2. The comparison of the spectral properties and evolutionary connection of *Of* and *WR* stars.

The *Of* stars are those *O* stars whose optical spectra display the presence of strong emission lines *NIIIλλ* 4634, 4640,4642 and *HeIIλ*4686. Other interesting spectral lines in the visible region in the spectra of the *Of* stars are *CIII λλ*4647-4651 and *CIIIλ*5696.

It is known that the *WR* stars have been divided into three spectral types [2]: *WN* stars which exhibit emission lines of dominantly *N* (*NIII-NV*) and He ions with little evidence for *C*, have been considered as *C*-poor objects; *WC* stars showing predominantly He and *C* lines and virtually no evidence for *N*, have been considered as *N*-poor objects; *WO* stars whose optical spectra display strong *OIV*, *OV* and *OVI* lines. According to [3] the spectra of WN *WO* stars reflect an actual enhancement of the abundance of oxygen, relatively to the *WC* stars. Authors of [3, 4, 5] proposed such an evolution scheme for the *WR* types:

$$WN \rightarrow WC \rightarrow WO \qquad (1)$$

Therefore the newly formed *WR* star is a *WN* star. It is known that for the spectral classification of stars *WN*4-9 subtypes were proposed [6]. These *WN*4-9 subtypes certainly represent different ionization conditions in the stellar wind of the *WN* stars. Various observational properties : luminosity, age, spectrum, *H/He* ratio, ionization structure of the envelope set *WN*7-8 stars clearly apart from other *WR* subclasses [7]. Namely this subtype of *WR* stars may be evolved by stellar wind mass loss from *Of* stars. The difference between *WN*7-8 and *Of* spectra is that in *WN*7-8 stars the emission spectrum is more developed, and that *WN*7-8 stars have higher mass loss rate and greater envelope density than *Of* stars. The emission line *HeIIλ*4686 is present in the spectra *Of* and *WN*7-8 stars, however this line narrower in *Of* stars than in *WN*7-8 stars.

The example for the transition object is star $-67^{o}22$ in the *LMC* with both *WN* and Of properties [8]. It is difficult to classify this star because the broad emission lines and Balmer series in absorption are visible at the same time. We would like to stress that the difficulty in classification of such objects may often be not the disadvantage of the classification system but rather the fact that one deals with stars which have only slightly different properties. Because of similarity of *WN* and *Of* stars they both even fitted in same early classification schemes before.

Although *Of* and *WN*7-8 stars have similar properties there are also differences between them. We may indicate five main differences between these stars:

1. In WN7-8 stars the nitrogen overabundance is easily seen [9]. But this statement has not been revealed for the *Of* stars obviously. If some *Of* stars truly become *WN*7-8 stars we must observe much close to *WN*7-8 the *Of* stars – nitrogen rich *Of* stars (*Of – WN*7-8 transition objects). We assume that these stars are more massive *Of* stars.

2. One of the basic correlations discovered by Beals [10] was the fact that emission lines in *WR* stars arising from ions of high ionization potential had much narrower widths than those of low ionization potential. This relation is more readily seen for the *WN* stars than for the *WC* stars because of line-blending.

It is important to verify validity of this correlation for the *Of* stars. We assume that this correlation takes place namely in the transition *Of* - *WN*7-8 stars.

3. Another property of *WN*7-8 stars distinctive from other stars is the *H/He* ratio. *WN*7-8 stars are *H* – poor objects, because of loss of *H* – rich envelope by stellar wind. Therefore the transition *Of – WN*7-8 objects must be the *H* – poor objects.

4. Another difference between *Of* and *WN*7-8 stars is the mass loss rate. The mass loss rate is higher for the *WN*7-8 stars than for the *Of* stars, therefore *WN*7-8 stars have more dense envelope.

5. The *HeIIλ*4686 is present in the spectra of the *Of* and *WN*7-8 stars. Widths of this line increase with the transition from *Of* to *WN*7-8 stars.

From 1-5 we may conclude that the spectra of the *Of* -

*WN*7-8 stars transition distinguish from those *Of* and *WN*7-8 stars by the degree of emission line strength, they also have different envelope densities and mass loss rates. We think that the evolution from *Of* type to the *WN*7-8 is gradual and not dramatic. Stellar wind mass loss rate and chemical mixing can explain such behavior. Therefore we may give more exact evolution scenario for the evolution of *WR* stars subtypes:

$$O \rightarrow Of \rightarrow WN7\text{-}8 \rightarrow WN\ early \rightarrow WC \rightarrow WO \quad (2)$$

3. Conclusions

1. Some massive *Of* stars by stellar wind mass loss may gradually evolve into *WN*7-8 stars.
2. There must be the *Of* - *WN*7-8 stars transition with five properties indicated above. The spectral properties of these stars must be intermediate between those of *Of* and *WN*7-8 stars.
3. Observation and investigation of the *Of* – *WN*7-8 stars transition are important for the understanding of the evolutionary connection between *Of* and *WR* stars.

[1] *P.S.Conti*, Mem.Soc. Roy.Sci. Liege,1976. 6^{e} Ser. p. 9.
[2] *J.N.Rustamov*, Fizika. 2002. No. 2. p. 56
[3] *M.J. Barlow and D.G.Hummer, in: C.W.H. de Loore and A.J.Willis (eds).*Wolf-Rayet Stars: Observations, Physics, Evolution. IAU Symp. № 99. 1982. p.295.
[4] *B.Paczynski, in: M.K.V.Bappu and Sahade (eds.)* Wolf-Rayet and High Temperature Stars. IAU Symp. №49. 1973.p.143.
[5] *A.J.Willis and R.Wilson*, Monthly Notices Roy. Astron. Soc.1978. № 182. p. 559.
[6] *A.Karel, van der Hucht and P.S.Conti,* Space Science Reviews 1981. 28.
[7] *A.F.J.Moffat and W. Seggewiss,* Astron. Astrophys 1979. v. 77,p. 128.
[8] P.S. Conti, Wolf-Rayet Stars: Observations, Physics, Evolution. IAU Symp. №. 99. 1982. p..551.
[9] *T. Nugis,* in: Variable Stars and Stellar Evolution. 1975. p. 291.
[10] *C.S. Beals,* Monthly Notices Royal Astron. Soc. 1929. № 90. p. 202.

C.N. Rüstəmov, S.Q. Zeynalov

Of - WN KEÇİD ULDUZLARININ VOLF-RAYE TİPLİ ULDUZLARIN TƏKAMÜLÜNÜ ANLAMAQ ÜÇÜN VACİBLİYİ HAQQINDA

Of və Volf-Raye ulduzlarının spektral xüsusiyyətlərinin oxşarlığı araşdırılmışdır. Bu ulduzlar arasında mümkün təkamül əlaqələri tədqiq olunmuşdur. Azotla zəngin olan *Of* – *WN*7-8 keçid ulduzlarının mövcudluğu haqqında hipotez irəli sürülmüşdür. Bu ulduzlar təkamül nöqteyi nəzərincə *WN*7-8 ulduzlarına yaxın olmalıdır. Azotla zəngin olan *Of* ulduzlarının müşahidəsi *Of* – *WR* təkamül əlaqələrini başa düşmək üçün mühüm əhəmiyyət kəsb edir.

Д.Н. Рустамов, С.Г. Зейналов

О ВАЖНОСТИ ПЕРЕХОДНЫХ *Of- WN* ЗВЕЗД ДЛЯ ПОНИМАНИЯ ЭВОЛЮЦИИ ЗВЕЗД ТИПА ВОЛЬФА - РАЙЕ

Проанализировано подобие спектральных особенностей *WR(WN)* и *Of* звезд. Исследованы возможные эволюционные связи между этими объектами. Предложена гипотеза о возможности существования *Of* звезд с обилием азота. Предложены 5 критериев для выявления этих объектов. Эти объекты эволюционно могут быть близки к *WN*7-8 звездам. Выявление этих объектов является важным обстоятельством для понимания эволюционных связей между *Of* и *WN*7-8 звездами.

Received: 21.11.02

ON THE POSSIBILITY OF THE CREATION OF PIEZOCOMPOSITE RADIATORS FOR MEDICAL DEVICES

M.A. KURBANOV, G.M. HEYDAROV
Institute of Physics of the Azerbaijan National Academy of Sciences
H. Javid av. 33, Baku, 370143

T.A. ALIYEV, I.F. HASANOV
Azerbaijan State Oil Academy
Baku, Azadlig ave. 20

It is experimentally established that electroacoustic converters of the medical purpose may be created by the change of the polarization conditions, physico-mechanical characteristics, the configuration and geometric sizes of piezocomposite elements.

The modern medicine is inconceivable without piezoelectric diagnostic devices, operating in the ultrasound range [I]. They are necessary for the visuality of deep structures of body and internal organs for the investigation of tissues structure and the control of parameters of the moving medium and structures, for example, at the research of the blood circulation and heart work. The physiotherapical ultrasound piezoelectric technique is successfully applied at various diseases treatment, in particular, breath organs with the application of the aerosoltherapy method [2]. The main criterion, determining aerosol penetration in structural elements of lungs, is the size of aerosol particles [2]. So, for example, it is experimentally proved that particles with the radius r<5 mcm penetrate the lungs alveolus. The dispersion of the medicinal substance and its transfer in the aerodispersional system is realized by piezoelectric sprays.

It is shown in [2], that the radius (r) of aerosol particles reduces by the increase of the resonance frequency of the piezoelectric spray. It is known, that the resonance frequency of the piezoelement is determined as $f_r = \frac{\vartheta}{2d}$, where ϑ - is the sound spreading velocity, d is the piezoelement thickness. In the case of the piezocomposite the element thickness may be visibly reduced and by that f_r may be increased. High piezoelectric and physico-mechanical properties of composites allow to obtain on their base piezoelements of various configuration and resonance frequency. On principle, such task is solved even in the case of the piezoceramic elements application. However, the fragility and high internal mechanic voltage in piezoceramics do not allow to visibly reduce the piezoelement thickness. Besides, piezocomposite element may have because of the high possibility of the thickness reduction resonance at relatively high frequencies in comparison with the piezoceramic material. In the given paper possibilities of piezocomposite materials application as a piezoelectric resonator for aerosoltherapy devices are investigated. Composites are obtained on the base of the hot pressing. The piezoelement thickness is variated from 250 to 1500μm.

Piezoelements are obtained on the base of polyvinylidene-fluoride and polypropylene (table 1) of lead-zirconate-titonate family of various structures. Piezoelements are polarized at voltages of the polarization electric field from 1,0 to 16 mV/m and temperature from 373 to 450 K. The cubic content of the piezophase in composites is changed in limits from 10 to 70%.

The dependence of piezoelectric characteristics of composites on conditions are presented on fig.1 and 2. It is seen, that composites have high piezosensitivity g_i and piezomodulus d_i. The piezomodulus dependence on the temperature (T_p) and the voltage of the polarization electric field (E_p) has extreme nature, at first by the growth of E_p and T_p the value d_{33} increases and achieve maximum, and then reduces. The value d_{33} from the cubic content of piezophase (F) grows quicker, than by the linear law. And g_{33} from F grows at first and 40% achieve the maximal value. Main parameters of piezoceramics –PCR-3M and PCR-7M, and also composites on their base and polymers PVDF, PP are presented in tables 1 and 2.

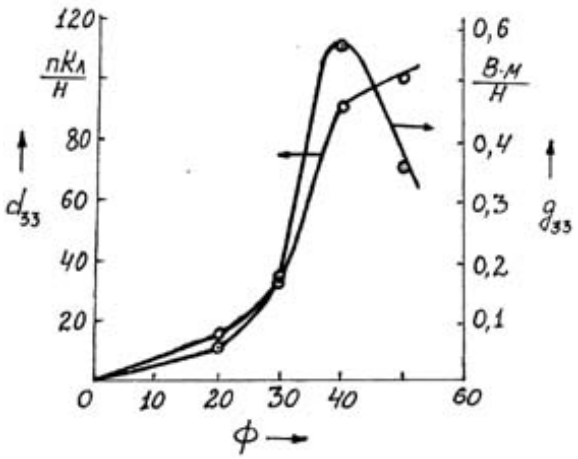

Fig.1 The dependence of d_{33} and g_{33} on F of the composition PP+PCR-3M T_p=393K, E_p =3mV/m.

Table 1.

The polymer Name	Polypropylene	Polyvinylidenefluoride
Thechemical composition Of links	$-CH_2 - CH_2 - CH_3$	$-CH_2 - CF_2$ |
The polymer code	PP	PVDF (F_2)
$\rho_{v\ (ohm.\ cm)}$	10^{14}-10^{15}	2.10^{14}
ε	2.3	13
D_{33}, (pC/N)	-	6.3
tanδ	4.10^{-4}	0,017
T_g , к	203	233
T_{pr} , к	463	473
ρ, (g/sm)	0,92-0,93	1,76
D_{31} , pC/N	-	15
E_{31} ,V.m/N	-	0,11

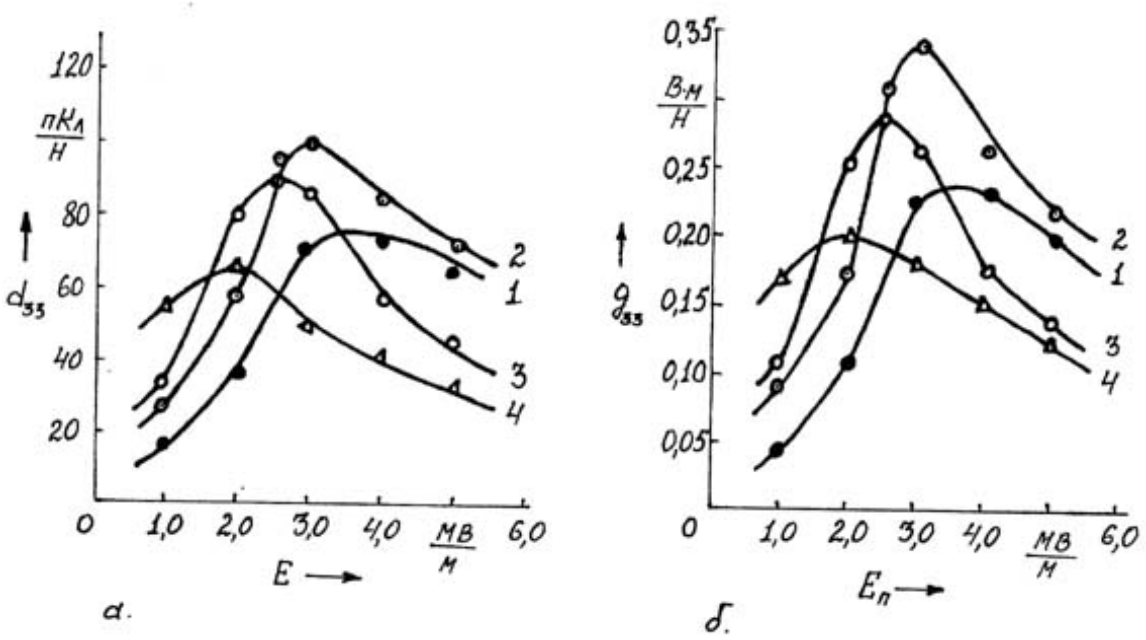

Fig.2 a. The dependence of d_{33} on E_p of the composition PP+PCR-3M: T_P=373 K, 2- T_P =393 K, 3- T_P=413 K, 4 – T_P=433 K.
b. The dependence of g_{33} on E_p of the composition PP+PCR=3M: T_P=373 K, 2- T_P =393 K, 3- T_P=413 K, 4 – T_P=433 K

Piezocomposites, in their turn, have in comparison with piezoceramics defects (faults), connected with the low radiation power and capacity. Therefore, it is necessary to work out piezocomposites with radiation power no lesser (0,15÷5) Pa/V. If in the regime of the acoustic wave receipt the piezocomposites in comparison with the piezoceramics are more sensitive, at least to an order (table 2 and 3), then in the radiation regime they yield to the piezoceramics (table 3). Therefore it is better to variate physico-mechanical properties of piezocomposites. So, that in the radiation regime their efficiency is to be equal and close to the piezoceramics efficiency. One of the factor of the piezoelectric materials efficiency is the coefficient of the electromechanical coupling. If the sample has the shape of the plate with cross sizes, which is far more than the thickness, and vectors of the polarization and the voltage of the electric field are directed perpendicularly to electrodes, then all values, included in the equation of the direct and inverse piezoeffects, have only one component and the coefficient of the electromechanical coupling is determined by the expression:

$$\beta^2 = \frac{d^2}{\varepsilon^\sigma S^E} = \frac{h^2 \varepsilon^u}{C^D} = \frac{g^2 \varepsilon^u}{S^D}$$

where d-is the piezomodulus, ε^σ, ε^u are dielectric constant at $\sigma = 0$ and $u = 0$, respectively, S^E - is the pliability, h-is the piezocoefficient, g-is the piezosensitivity, C^D -is the elasticity coefficient at D=0.

Table 2.

Characteristics of compositions and pizoceramics	Composites and conditions of their polarization	d_{33}^k pC/N	g_{33} V.m/N	ε_{ik}	d_{33}^k pC/N	d_{33}^k/ε_k V.m/N
PP+50% com PCR-7M T_p=393 K	E_p=3 MV/м E_p=6 MV/м E_p=12 MV/м E_p=9 MV/м	16,5 23 40 45	0,072 0,135 0,157 0,212	5000 - - -	760 - - -	0,0108 - - -
PP+50% com. PCR-3M T_p=393 K	E_p=1 MV/м E_p=2 MV/м E_p=3 MV/м E_p=5 MV/м	28 59 120 74	0,086 0,17 0,339 0,213	400 - - -	99 - - -	0,028 - - -
PVDF+50% com. PCR-3M T_p=413 K	E_p=4,5 MV/м	160	0,290	400	99	0,028

The square of the electromechanical coupling coefficient β^2 is determined by the piezoconverters sensitivity at the emission (radiation) and the receipt of sound waves. We compare the value β^2 of the piezoceramics and piezocomposites with the aim to determine the application possibilities of polymer-piezoceramics composites for the creation of medical devices radiators. Parameters, included in the formula β^2

and values β^2 for various piezoceramics and PVDF+PCR-3M composite, are presented in the table 3.

Table 3.

Piezoelectric materials	Piezomodulus $d_{ij\text{ж}} \cdot 10^{12}$, C/N	Elastic pliability $S_{ik} \cdot 10^{12}$, m^2/N	Relative dielectric constant ε_{33}	Piezosensitivity g_{ij}, Vm/N	β^2
PZT-19 ZTPNB –1 \ZTBP-3	250 400 300	14.9÷10.4 16.8÷14.7 12.2÷10.7	1725±326 2250±560 2350±500	0,013 0,02 0,016	2,6 3,6 3,0
Piezocomposite PVDF+PCR-3M	160÷200	160	100±10	0,25	1,6÷2,5

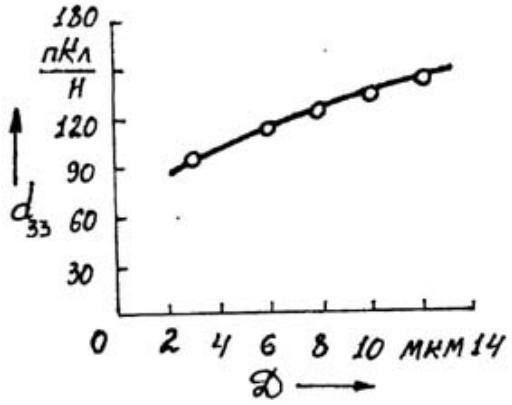

Fig. 3. The dependence of d_{33} of the composite PP+50 % PCR-5 on the grain diameter of the piezoparticle PCR-5

It is seen from the table 3, that values β^2 for high effective piezoceramics PZT-19, ZTBP and ZTPNB-I and the composite PVDF+PCR-3M, distinguish a little. So, for example, values ratio β^2 for ZTPNB-I and PVDF+PCR-3M is equal to ~1,5. Piezoceramics factors (indices) may be obtained in the radiation regime in composites by the small growth of the value d_{ij} and the reduction of s_{ic} by means of the variation of the cubic content and the grains size (D) (fig.3) of the piezofiller in the composite and the improvement of technical regimes of the composites receipt and also small increase of the excitation voltage. S_o, for example, the piezomodulus value (d_{33}) of the composite PP+50 % PCR-5 may be regulated by the variation of the size of the piezoparticles (piezophase) grain PCR-5. The grain diameter (D) is variated by the change of the pressure and sintering temperature of the piezoceramics PCR-5. It is seen, that d_{33} of the composite grows visibly by the increase of D. The simplicity of the receipt technology, high physico-mechanical and piezoelectric characteristics, and the possibility of the piezoelement receipt of the various configuration make the piezocomposite more effective piezomaterial for the creation of electroacoustic converters of the new generation, distinguished by high exploitational characteristics. We should note, that the research on the creation of medical devices, in particular, aerosoltherapy devices on the base of piezocomposites is in present time on the initial stage. It is necessary to work out the physical principles of the composite material creation for radiators and receivers, to calculate optimal constructions of separate converters, to determine configurations and geometric sizes of the piezocomposite element, and also optimal regimes of the polarization. It is necessary to especially note, that the amplitude-frequency characteristic (AFC) and the radiation power of piezocomposite converters essentially depend on the configuration of the piezocomposite element (table 4). Results are obtained at the application to the piezoelement of 10V voltage.

The possibility of the wide variation of the configuration, what is impossible to obtain in the case of the piezoceramics capacity and piezomodulus d_{ij}, and, respectively, g_{ij}. It gives the chance of the creation of high effective piezocomposite radiators of the medical purpose.

Table 4

f, Hz	P, Pa, the flat (plane) element	P, Pa, the domed (dome-shape) element $\tau_{cr} = 1mm$
1000	26,0	9,0
1200	6,25	16,0
1300	4,0	24,5
1400	3,0	45
1500	2,82	68
1800	4,0	11,0
2000	1,8	7,5
2500	1,9	2,25
3000	0,1	2,25
4000	0,17	2,4

Amplitude-frequency characteristics of piezoresonators from the composite PP+50 % PCR-3M (the curve 3) and the piezoceramics PZT-19 (curve 2) are compared on fig. 4.

It is seen that the value of the resonance frequency f_r of the inhaler piezoresonator of the TUMAN-1.1 type may be increased at the piezocomposite application as a piezoresonator. The growth of f_r, as it has been already noted, leads to the reduction of the diameter of the medicinal aerosol particles of the inhaler, and consequently, increases the efficiency of this device.

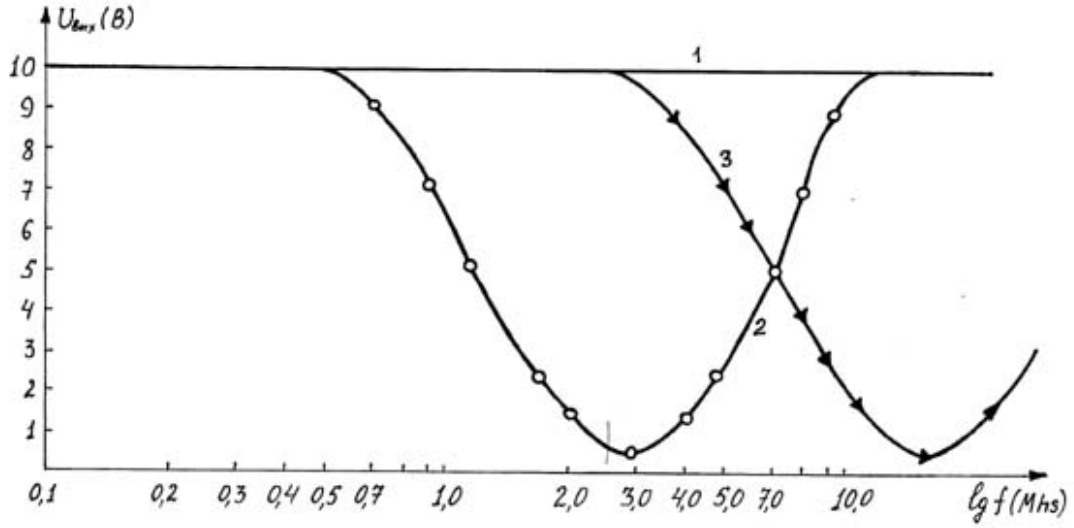

Fig. 4 The amplitude-frequency characteristics of the signal generator in the regime of the inverse piezoelectric effect
1. The regime of the idle run
2. The regime with the use of piezoceramics PZT-19
3. The regime with the use of piezocomposites PP+PCR-3M

The thickness of the piezoceramic element PZT-19 is 1,5 mm
The thickness of the piezocomposite element PP+PCR-3M is 0,5 mm.

Therefore, piezoelectric acoustic converters of the medical purpose may be created by the change of physico-technological regimes of the polarization condition, physico-mechanical characteristics, the configuration and geometric sizes of the piezocomposite elements receipt.

[1] Primineniye ultrazvuka v medizine, edited by Hill,Izd. "Mir", Moscow, 1989
[2] *S.A. Glukhov, S.I. Eidelshtein*. Technicheskoye osnosheniye aerosolterapiyi. Medizina, 1974
[3] Pribori dlya nerazrushayushego kontrolya matarialov i izdeliy. Reference book, II volume, edited by *V.V. Kluyeva.*
[4] *M.V. Korolev, A.E. Kaprelson*. Shirokopolosniye ultrazvukoviye piezopreobrazovateli. M: Mashinostroyeniye (Engineering), 1977, p.48
[5] *L. Bergmann*. Ultrazvuk i ego primeneniye v nauke i technike. M: Inostran. Liter., 1957, p.726.

M.A. Qurbanov, Q.M. Heydərov, T.A. Əliyev, İ.F. Həsənov

TİBB MƏQSƏDLİ APARATLAR ÜÇÜN PYEZOKOMPOZİT ŞÜALANDIRICILARIN HAZIRLANMA İMKANLARI HAQQINDA

Təcrübi olaraq müəyyən edilmişdir ki, kizokompozit elementlərin polyarizasiya şərtlərini, fiziki-mexaniki xarakteristikalarını, konfiqurasiyasını və həndəsi ölçülərini dəyişməklə tibbi məqsədlər üçün elektroakustik çeviricilər hazırlamaq mümkündür.

М.А. Курбанов, Г.М. Гейдаров, Т.А. Алиев, И.Ф. Гасанов

О ВОЗМОЖНОСТИ СОЗДАНИЯ ПЬЕЗОКОМПОЗИТНЫХ ИЗЛУЧАТЕЛЕЙ ДЛЯ АППАРАТОВ МЕДИЦИНСКОГО НАЗНАЧЕНИЯ

Экспериментально установлено, что изменяя условия поляризации, физико-механические характеристики, конфигурации и геометрические размеры пьезокомпозитных элементов, можно создать электроакустические преобразователи медицинского назначения.

Received: 27.09.02

ELECTRON TRANSPORT PHENOMENA IN SIZE-QUANTIZED n-Ge AND n-Si FILMS

G.B. IBRAHIMOV
Institute of Physics, Azerbaijan National Academy of Sciences,
Javid Avenue 33, 370143, Baku, Azerbaijan Republic

V.M. HAJIYEV
Schlumberger Logelco Inc.,
Salyan Highway, Shikh District, 370023, Baku, Azerbaijan Republic

The behavior of some kinetic coefficients depending on *n*-Ge and *n*-Si films surface orientation is investigated in the nonquantized magnetic field. The general solution of transport equation and expressions for the relaxation time at various electron scattering cases are obtained. Also the expressions for halvanomagnetic and thermomagnetic tensors are obtained at the arbitrary degeneration of electron gas. The Hall constant and thermopower of *n*-Ge and *n*-Si films in a strong and weak transverse magnetic field are calculated.

1. Introduction

At present thin semiconducting films are intensively investigated in the size-quantized conditions connected with microelectronics development. When the specimen sizes are of de Broglie wavelength of the current carriers' the quantum-sized effects occur and the wave functions form changes. Some thermodynamic and kinetic properties of conducting films with standard zone (simple isotropic model) have been considered in the works [1-4]. In the work [5] the electron states in anisotropic size-quantized *n*-Ge and *n*-Si films have been considered and the so-called size-quantized anisotropy (dependence of physical values on film surface orientation) was predicted. Evidently, such dependence can be observed in kinetic properties of *n*-Ge and *n*-Si films.

2. Transport equation

The energy spectrum of electrons in the size-quantized *n*-Ge and *n*-Si films takes a form:

$$\varepsilon_s\left(n_s,k_x,k_y\right)=\frac{\hbar^2}{2m_{II}}\left(\frac{\pi}{d}\right)^2\varphi_s^{\,2}(\alpha)n_s^2+\frac{\hbar^2}{2m_{\perp}}\left[\varphi_s^{-2}(\alpha)k_x^2+k_y^2\right], \tag{1}$$

where $m_{||}$ and $m_{\perp}$ are the longitudinal and transverse effective electron masses, respectively; d is the film thickness, s is the ellipsoid number, n_s=1, 2, 3,… is the sized quantum number, α is the angle of rotation of a normal to the [001] film surface around one of the crystallographic axes, $\varphi_s(\alpha)$ are anisotropy functions characterizing ellipsoids orientation as regard to the system of reference (see [5]).

To consider some kinetic properties of the system it is necessary to solve the Boltzmann transport equation in the external nonquantized magnetic field. The solution of the same equation for *n*-Ge and *n*-Si bulk specimens was obtained in the works [6,7]. In our case of size-quantized *n*-Ge and *n*-Si films we have to solve the two-dimensional transport equation in film's plane.

If one represents the nonequilibrium distribution function of electrons in the form:

$$f_1=\left(-\frac{\partial f_0}{\partial\varepsilon_s}\right)\left(\vec{v}\vec{P}\right), \tag{2}$$

and assumes that the external nonquantized magnetic field is directed along a normal to the film surface (transverse field) then the following solution of equation is obtained:

$$\vec{P}=\frac{1}{1+\nu^2}\left\{\hat{\tau}\vec{\Phi}_0+\frac{e}{c}\hat{\tau}\left[\vec{H}\hat{M}^{-1}\left(\hat{\tau}\vec{\Phi}_0\right)\right]\right\}, \tag{3}$$

where f_0 is the Fermi-Dirac function, $\nu=\dfrac{e\left|\hat{\tau}\right|^{1/2}}{c\left|\hat{M}\right|^{1/2}}H$,

$\vec{\Phi}_0=-e\vec{E}-\dfrac{\varepsilon_s-\xi}{k_0T}k_0\vec{\nabla}T$, $\hat{\tau}$ is the tensor of relaxation time, $\hat{M}^{-1}$ is the inverse tensor of electron effective masses, $\left|\hat{\tau}\right|$ and $\left|\hat{M}\right|$ are determinants of the relaxation time and effective masses tensors, respectively.

As we see from (2) and (3) $\vec{P}$ like nonequilibrium function depends on components of the relaxation time tensor. Therefore, to calculate the kinetic coefficients it is necessary to obtain the relaxation time expression for different electron scattering cases. In *n*-Ge and *n*-Si films plane $\vec{P}$ has two components depending on only one relaxation time parameter τ_s.

The τ_s expression for electrons scattering on acoustical and non-polar optical phonons, point defects and ionized impurities in films plane takes a form:

$$\tau_s^{-1}(\varepsilon_s)=\sum_{\beta_s'} W_{\beta_s'\beta_s}\left(1-\frac{k_x'k_x+\varphi_s^4(\alpha)k_y'k_y}{k_x^2+\varphi_s^4(\alpha)k_y^2}\right), \quad (4)$$

where $W_{\beta_s'\beta_s}$ is the probability of electron transition from a $\beta_s=(n_s,k_x,k_y)$ state to a $\beta_s'=(n_s',k_x',k_y')$ state and back.

The exact calculations in the cases of electron scattering on phonons and point defects give us:

$$\tau_s(\varepsilon_s)=\tau_0\varphi_s^{-1}(\alpha)\left(\overline{n_s}+\frac{1}{2}\right)^{-1}, \quad (5)$$

where $\overline{n_s}=\left[\sqrt{\frac{\varepsilon_s}{\varepsilon_{1s}}}\right]$ is an integer part of $\sqrt{\frac{\varepsilon_s}{\varepsilon_{1s}}}$ (the average number of film subbands below energy ε_s), $\varepsilon_{ls}=\varepsilon_s$ ($n_s=1$, $k_x=k_y=0$), τ_0 is the multiplier that doesn't depend on energy but proportional to the film thickness.

As it is seen from (5) τ_0 depends on energy only through $\overline{n_s}$. Moreover, τ_s essentially depends on *n*-Ge and *n*-Si films surface orientation and this dependence vanishes only at the $\overline{n_s}>>1$ limit when the result for bulk specimen is obtained.

In the case of electrons scattering on ionized impurities the τ_s analytical expression for arbitrary $\overline{n_s}$ values is n't obtained. However, if we assume that the scattering on ionized impurities occurs without the transition between film subbands then the following result for relaxation time is obtained:

$$\tau_s(\varepsilon_s)=\tau_0\varphi_s^{-1}(\alpha)\left(\overline{n_s}+\frac{1}{2}\right)^{-1}\left(\frac{\varepsilon_s-\varepsilon_{ns}}{k_0T}\right)^2, \quad (6)$$

where ε_{ns} is the discrete part of the energy spectrum (1).

3. Hall constant and thermopower

Having knowledge of the transport equation solution and expression for the relaxation time one can calculate the current and the energy stream densities and then we can determine components of kinetic tensors. For the σ_{ik} and β_{ik} ($i,k=1, 2,; i\le k$) tensors connecting the current and the energy stream densities with the electric field and the temperature gradient the following expressions are obtained:

$$\sigma_{ik}=\frac{e^2m_\perp}{\pi d\hbar^2}\left(-\frac{eH}{c}\right)^{k-i}\sum_{s=1}^{N}\left\{\varphi_s(\alpha)\sum_{ns}\int_{\varepsilon_{ns}}^{\infty}\frac{(\varepsilon_s-\varepsilon_{ns})\left(-\frac{\partial f_0}{\partial\varepsilon_s}\right)K_k(\varepsilon_s)K_{k-i}(\varepsilon_s)d\varepsilon_s}{1+\nu^2(\varepsilon_s)}\right\}, \quad (7)$$

$$\beta_{ik}=\frac{em_\perp}{\pi d\hbar^2T}\left(-\frac{eH}{c}\right)^{k-i}\sum_{s=1}^{N}\left\{\varphi_s(\alpha)\sum_{ns}\int_{\varepsilon_{ns}}^{\infty}\frac{(\varepsilon_s-\varepsilon_{ns})(\varepsilon_s-\xi)\left(-\frac{\partial f_0}{\partial\varepsilon_s}\right)K_k(\varepsilon_s)K_{k-i}(\varepsilon_s)d\varepsilon_s}{1+\nu^2(\varepsilon_s)}\right\}, \quad (8)$$

where

$$K_0=1, K_1(\varepsilon_s)=\frac{\tau_s(\varepsilon_s)\varphi_s^{-2}(\alpha)}{m_\perp}, K_2(\varepsilon_s)=\frac{\tau_s(\varepsilon_s)}{m_\perp},$$

N=4(*n*-Ge) and N=6(*n*-Si).

On a base of the general expressions (7) and (8) for kinetic tensors we can calculate all kinetic effects in various conditions. Let us show some of them in a strong ($\nu>>1$) and weak ($\nu<<1$) transverse magnetic fields.

So, for the Hall constant in the strong magnetic field we obtain:

$$R_f=-\frac{1}{n_{ef}ec}, \quad (9)$$

where n_{ef} is the concentration of electrons in film. Therefore, in this case R_f doesn't depend on the film surface orientation, degree of electron gas degeneration and electron scattering mechanisms. But unlike the bulk specimen n_{ef} depends on film thickness and this dependence characterizes the quantum-sized effect.

For the thermopower in this case we have:

$$\alpha_f=-\frac{k_0}{e}\frac{B(\alpha)}{A(\alpha)}, \quad (10)$$

where

$$A(\alpha)=\sum_{s=1}^{N}\left\{\varphi_s(\alpha)\sum_{ns}F_1(\eta_{ns})\right\},$$

$$B(\alpha)=\sum_{s=1}^{N}\left\{\varphi_s(\alpha)\sum_{ns}\left[F_2(\eta_{ns})-\eta_{ns}F_1(\eta_{ns})\right]\right\}.$$

Here $F_t(\eta_{ns})=\int_0^{\infty}x_s^t\left(-\frac{\partial f_0}{\partial x_s}\right)dx_s$ are the uniparametric Fermi integrals of t index,

$$x_s=\frac{\varepsilon_s-\varepsilon_{ns}}{k_0T},\eta_{ns}=\frac{\xi-\varepsilon_{ns}}{k_0T}.$$

The analysis of expression (10) for α_f shows us that in this case thermopower doesn't depend on scattering mechanisms and for degenerated electron gas we obtain:

$$\alpha_f=-\frac{(\pi k_0)^2T}{3en_{ef}}g_f(\alpha), \qquad (11)$$

where $g_f(\alpha)=\frac{m_\perp}{\pi d\hbar^2}\sum_{s=1}^{N}\left\{\varphi_s(\alpha)\overline{n_s}\right\}$ is the density of electron states in *n*-Ge and *n*-Si films [5].

Therefore, the α_f behavior in this case is the same like for the density of electron states near the Fermi energy at the fixed n_{ef}. Otherwise, the thermopower depends on the film thickness as *1/d* until the film subband coincides with the Fermi energy. In this case α_f has a leap and is equal to the thermopower value in bulk specimen. Therefore, the thermopower dependence on film thickness has a saw-toothed character.

In another case of nondegenerated electron gas for α_f we have:

$$\alpha_f=-\frac{k_0}{e}\left\{2-ln\frac{\pi d\hbar^2n_{ef}}{m_\perp k_0TC(\alpha)}+\frac{D(\alpha)}{C(\alpha)}\right\}, \qquad (12)$$

where

$$C(\alpha)=\sum_{s=1}^{N}\left\{\varphi_s(\alpha)\sum_{ns}exp(-x_{ns})\right\},$$

$$D(\alpha)=\sum_{s=1}^{N}\left\{\varphi_s(\alpha)\sum_{ns}x_{ns}\,exp(-x_{ns})\right\},\ x_{ns}=\frac{\varepsilon_{ns}}{k_0T}.$$

The α_f behavior on film thickness in this case differs from the one for degenerated electrons. The analysis of expression (12) shows us that for fixed n_{ef}. Otherwise, thermopower in this case also is a nonmonotonous function of film thickness. When $\overline{n_s}>>1$ limit the result for bulk specimen is obtained that doesn't depend on a film thickness.

The same kinetic coefficients in the weak magnetic field take forms:

$$R_f=-\frac{1}{n_{ef}ec}\frac{A(\alpha)C'(\alpha)}{A'^2(\alpha)}, \qquad (13)$$

$$\alpha_f=-\frac{k_0}{e}\left\{\frac{D'(\alpha)}{A'(\alpha)}+\nu_0^2\left[\frac{F'(\alpha)C'(\alpha)+B'(\alpha)D'(\alpha)}{A'^2(\alpha)}-\frac{D'(\alpha)C'^2(\alpha)}{A'^3(\alpha)}-\frac{E'(\alpha)}{A'(\alpha)}\right]\right\}, \qquad (14)$$

where

$$\nu_0=\frac{e\tau_0}{m_\perp c}H,\ A'(\alpha)=\sum_{s=1}^{N}\left\{\frac{\left[\varphi_s^{-2}(\alpha)+1\right]}{2}\left(\overline{n_s}+\frac{1}{2}\right)^{-1}\sum_{ns}F_{r+1}(\eta_{ns})\right\},$$

$$B'(\alpha)=\sum_{s=1}^{N}\left\{\frac{\left[\varphi_s^{-4}(\alpha)+\varphi_s^{-6}(\alpha)\right]}{2}\left(\overline{n_s}+\frac{1}{2}\right)^{-3}\sum_{ns}F_{3r+1}(\eta_{ns})\right\},$$

,

$$D'(\alpha)=\sum_{s=1}^{N}\left\{\frac{\left[\varphi_s^{-2}(\alpha)+1\right]}{2}\left(\overline{n_s}+\frac{1}{2}\right)^{-1}\sum_{ns}\left[F_{r+2}(\eta_{ns})-\eta_{ns}F_{r+1}(\eta_{ns})\right]\right\},$$

$$E'(\alpha)=\sum_{s=1}^{N}\left\{\frac{\left[\varphi_s^{-4}(\alpha)+\varphi_s^{-6}(\alpha)\right]}{2}\left(\overline{n_s}+\frac{1}{2}\right)^{-3}\sum_{ns}\left[F_{3r+2}(\eta_{ns})-\eta_{ns}F_{3r+1}(\eta_{ns})\right]\right\},$$

$$F'(\alpha)=\sum_{s=1}^{N}\left\{\varphi_s^{-3}(\alpha)\left(\overline{n_s}+\frac{1}{2}\right)^{-2}\sum_{ns}\left[F_{2r+2}(\eta_{ns})-\eta_{ns}F_{2r+1}(\eta_{ns})\right]\right\},$$

r=0 for phonons and point defects and r=2 for ionized impurities.

Therefore, in this case unlike the strong field R_f depends on film surface orientation. Thermopower α_f depends on magnetic field like small correction proportional ν_0^2.

In conclusion, we note that kinetic coefficients in size-quantized n-Ge and n-Si films essentially depend on film surface orientation. Therefore, they possess the so-called size-quantized anisotropy. It is the most particular feature of kinetic quantum-sized effects in the anisotropic n-Ge and n-Si films.

[1] *V.B. Sandomirsky*, J. Eksp. I Teor. Fiziki, 52 (1967) 158 (in Russian).
[2] *B.A. Tavger*, Physica Status Solidi, 22 (1967) 31.
[3] *B.A. Tavger*, V.N. Demikhovsky, Uspehi Fiz. Nauk, 96 (1968) 61 (in Russian).
[4] *B.M. Askerov, B.I. Kuliev, R.F. Eminov*, Fizika Nizkih Temp., 33 (1977) 344 (in Russian).
[5] *B. Kuliev, V. Hajiyev*, Turkish J. of Physics, 22 (1998) 1047.
[6] *B.M. Askerov*, Electron Transport Phenomena in Semiconductors, World Scientific, Singapore (1994) 210.
[7] *L.I. Baransky,* Elektricheskiye I Galvanomagnitniye Yavleniya v Anizotropikh poluprovodnikaxrs, Naukova Dumka, Kiev (1977) 17 (in Russian).

H.B. İbrahimov, V.M. Hacıyev

n-Ge VƏ *n*-Si ÜÇÜN KVANTLANMIŞ NAZİK TƏBƏQƏLƏRDƏ ELEKTRON KEÇİRMƏ HADİSƏLƏRİ

n-Ge və *n*-Si nazik təbəqələrin səthindən asılı olaraq kvantlanmamış maqnit sahəsində kinetik əmsalların xassələri təhlil olunur. Kinetik tənliyin ümumi həlli alınmışdır və müxtəlif elektron səpilmələri üçün relaksasiya zamanı hesablanmışdır. Həmçinin ixtiyari cırlaşmış elektron qazının qalvanomaqnit və termomaqnit tenzorlar üçün ifadələr alınmışdır. Və nazik təbəqələrdə güclü və zəif eninə maqnit sahəsində Holl əmsalı və termol-EHQ hesablanmışdır.

Г. Б. Ибрагимов, В.М. Гаджиев

ЭЛЕКТРОННЫЕ ЯВЛЕНИЯ ПЕРЕНОСА В РАЗМЕРНО-КВАНТОВАННЫХ ПЛЕНКАХ *n*-Ge И *n*-Si

Исследовано поведение некоторых кинетических коэффициентов для размерно-квантованных пленок n-Ge и n-Si в неквантованном магнитном поле в зависимости от ориентации их поверхности относительно кристаллографических осей. Получено общее решение для кинетического уравнения и выражения для времени релаксации при различных механизмах рассеяния. Также получены выражения для компонент гальваномагнитных и термомагнитных тензоров при произвольном вырождении электронного газа. Вычислены коэффициент Холла и термо-ЭДС для пленок n-Ge и n-Si в сильных и слабых поперечных магнитных полях.

Received: 28,11.02

CONDITIONS FOR THE TEMPERATURE STABILIZATION OF THE THERMOELECTROMOTIVE FORCE IN SEMICONDUCTIVE MATERIALS

T.G. OSMANOV, R.S. MADATOV
The Institute of Radiation Problems of NASA

F.K. ALESKEROV, N.M. ABDULLAYEV, S.A. NABIYEVA
NPO "Selen" at the Institute of Physics NASA

The possibility of the stabilization of the common thermoelectromotive force versus the temperature is observed for materials with the standard band structure of one-type charge carriers and for those, having the complex construction of the valent band or)and) the conduction band (two-band model). It is shown, that the stabilization of the common thermoelectromotive force α is possible for the energy spectrum of the charge carriers corresponding to the two-band model if the width of the forbidden band ΔE is more than the value of the energy gap $\Delta\varepsilon$ between subbands.

The practical value of the semiconductive substance, which is applied in various thermal converters is determined firstly by the average value of the dimensionless parameter *ZT*, in which at the given temperature *T* the value of the thermal efficiency *Z*, according to the A.F. Ioffe criterion, is equal to:

$$Z = \frac{\alpha^2\sigma}{\chi_{com}} \sim \frac{u}{\chi_{cat}} \qquad (1)$$

where α, σ, χ_{com} are the common thermoelectromotive force, electroconductivity and heat conductivity, respectively, *u* is the mobility of the charge carries, χ_{lat} is the lattice heat conductivity.

The maximum of *Z* (Z_{max}) at the given temperature *T* [1] depends on: 1) the reduced Fermi level μ^*; 2) the dimensionless coefficient:

$$\beta = \frac{2(2\pi)^{3/2}}{h^3 e}(\kappa o)^{7/2}\frac{u}{\chi_p}\left(\frac{m^*}{m_o}\right)^{3/2} T^{5/2} \qquad (2)$$

and 3) the parameter of the charge carriers scattering *r*, where h is the Planck's constant, *e* is the electron charge, k_0 is the Boltzmann's constant, $\left(\frac{m^*}{m_o}\right)$ is the effective mass, *T* is the temperature.

The dependence of *Z T* on the reduced Fermi level μ^* has maximum, the sharpness and value of which depend on β [1] and respective thermoelectromotive force α and electroconductivity are optimal - α_{opt} and σ_{opt}.

The stabilization of the reduced Fermi level μ^* in the determined temperature interval corresponding to the value α_{opt} leads to the considerable growth of the parameter $Z_{ave}\ \Delta\ T$ and, consequently, to the maximal temperature gradient ΔT_{max}, the maximal cooling coefficient K_{max} and maximal efficiency ζ_{max}, in this interval, what has a great value for the development and practical use of the applied material in various cooling and generator devices.

The term "stabilization" means not the expression $\alpha(T)$ and $\alpha(n)$; $\alpha(p)=const$, but the change of the value α in determined limits, usually ±5-7% from the value of α_{opt}. At present time in the applied thermal material of *n* and *p*-type the value of the thermoelectromotive force α corresponds to the case of weak electrons and holes degeneration and its value versus the Fermi level μ^* is determined as:

$$\alpha = \frac{\kappa_o}{e}\left[\frac{(2r+5)F_{r+3/2}(\mu^*)}{(2r+3)F_{r+1/2}(\mu^*)} - \mu^*\right] \qquad (3)$$

where $F_r = \int_0^\infty \chi^r\left[exp(x-\mu^*)+1\right]dx$ is the Fermi integral, the value of which is tabulated in [2], *r*-is the scattering parameter.

The reduced Fermi level μ^* is connected with the charge carriers concentration *p(n)*, the effective mass of the state density m^*/m_0 (electrons and holes) and the temperature *T* through the Fermi integral as:

$$F_{1/2}(\mu^*) = \frac{p(n)\sqrt{\pi}h^3}{4(2\pi k_0 T m^*/m_o)^{3/2}} \qquad (4)$$

It is seen from the formula (2) that at conditions $m^*/m_0(T)=const$, $r=const$, $p(n)\sim T^{3/2}$ the Fermi integral $F_{1/2}(\mu^*)$, and consequently μ^* and α, for substances with the standard parabolic band and one-type charge carriers, do not depend on the temperature, i.e. they are stabilized.

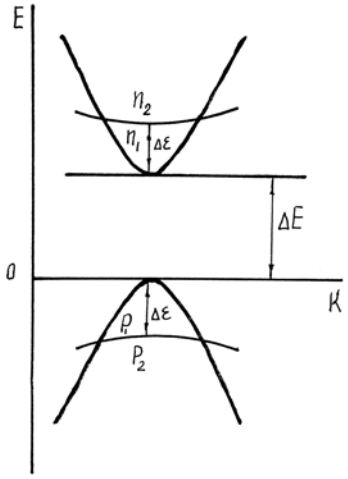

Fig. 1. Schematic picture of the energy bands of the complex structure.

For known semiconductive materials the theory of the transfer phenomena gives much stronger dependence *n(T)* and *p(T)*, and therefore the stabilization of the thermoelectromotive force *α(T)* is impossible in them. For substance with the complex band structure, to which Bi_2Te_3 of *p* and *n*-type, Sb_2Te_3 of *p*-type and etc. refer, it is possible to suppose the possibility of the condition fulfillment $F_{1/2}(\mu^*)\approx const$ at the stability of the common charge carriers concentration in the subzone $(p_{com}(T)=const)$ (fig.1).

At such condition the common thermoelectromotive force is:

$$\alpha_{com} = \frac{\alpha_1\sigma_1 + \alpha_2\sigma_2}{\sigma} \qquad (5)$$

the common electroconductivity is:

$$\sigma = \sigma_1 + \sigma_2$$

the common charge carriers concentration is:

$$p = p_1 + p_2 \qquad (6)$$

$$n = n_1 + n_2 \qquad (7)$$

where indices 1,2 refer to the first and second subzone of the valent band or the conduction band.

At the primary carriers scattering at the acoustic oscillation of the lattice (*r=-1/2*), the partial thermoelectromotive force, electroconductivity and the carriers concentration in the subbands have the form:

$$\alpha_1 = \frac{\kappa_0}{e}\left|\frac{2F_1(\mu^*)}{F_0(\mu^*)} - \mu^*\right| \qquad (8)$$

$$\alpha_2 = \frac{\kappa_0}{e}\left|\frac{2F_1(\mu^* - \Delta\varepsilon)}{F_0(\mu^* - \Delta\varepsilon)} - (\mu^* - \Delta)\right| \qquad (9)$$

$$\sigma_1 = 2e\frac{(2\pi m_0 k_0 T)^{3/2}}{h^2} F_0(\mu^*) u_{01}\left(\frac{m_1^*}{m_0}\right)^{3/2} \qquad (10)$$

$$\sigma_{21} = 2e\frac{(2\pi m_0 k_0 T)^{3/2}}{h^2} F_0(\mu^* - \Delta) u_{021}\left(\frac{m_2^*}{m_0}\right)^{3/2} \qquad (11)$$

$$p_1(n_1) = 4(2\pi\, m^*/m_0 k_0 T)^{3/2} F_{1/2}(\mu^*) \qquad (12)$$

$$p_2(n_2) = 4(2\pi\, m_2^*/m_0 k_0 T)^{3/2} F_{1/2}(\mu^* - \Delta) \qquad (13)$$

where u_{01}, u_{02} are the mobility of non-degenerated carriers in the first and second subbands, respectively.

For the analysis of the thermal and concentration dependence of the common thermoelectromotive force α_{com}, the ratio of the effective mass of the state density in the subbands $\left(\frac{m_2^*}{m_1^*}\right)$, the charge carriers mobility $\left(\frac{u_1}{u_2}\right)$, and also the value of the energy gap $\Delta\varepsilon$, and the width of the forbidden band ΔE are usually accepted as constant values, subbands are parabolic, and the mechanism of the charge carriers scattering is equal. At low temperatures ($kT \ll \Delta\varepsilon$) the charge carriers of the first subband mainly take part in the conduction process, the second subzone is almost empty and therefore (formulae 5-7)

$$\sigma \approx \sigma_1;\ p \approx p_1;\ \alpha \approx \alpha_1$$

by this

$$\frac{p_1}{p_2} \gg 1,\ \sigma_1 \gg \sigma_2,\ \alpha_1 \ll \alpha_2$$

and the common thermoelectromotive force α_{com} grows in a linear fashion with the temperature increase (part 1; fig. 2).

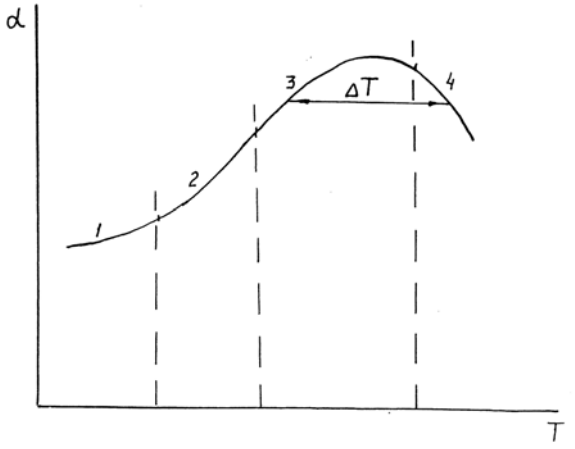

Fig.2. The temperature dependence of the thermoelectromotive force for n/n materials of *p*-type and with $\Delta E > \Delta\varepsilon$.

The redistribution of the charge carriers between subbands occurs with the further temperature growth, the behavior of the thermoelectomotive force α_{com} and electroconductivity σ_{com} will depend on the relation between the thermal activation energy of the charge carriers ΔE_T and the width of the energy gap $\Delta\varepsilon$ between subbands. Two cases are possible by this: 1) $\Delta\varepsilon < \Delta E$ and 2) $\Delta\varepsilon = \Delta E$.

1. In the first case the reduction of the carriers concentration in the low subzone $p_1(n_1)$ and its growth in the second $p_2(n_2)$ lead to the increase of the thermoelectromotive force α_1 and electroconductivity σ_2, the reduction of the elctroconductivity σ and thermoelectromotive force α_2.

By the temperature growth the reduced Fermi level μ^* approaches the top of the "heavy" holes subbands; the contribution of its carriers in the transfer process increases and at the determined *T* (depending on subbands parameters $\Delta\varepsilon$, ΔE, $\left(\frac{m_T^*}{m_{JI}^*}\right)$ and etc.) the product $\alpha_2\,\sigma_2$ becomes more than $\alpha_1\,\sigma_2$ and the common thermoelectromotive force α_{com} grows according to much stronger law, it follows from the theory for substances with one-type carriers in the degenerated state

$T \approx \left(\frac{\Delta\varepsilon}{K_0}\right)$, the primary contribution of the second subband carriers is shown in the conduction process

$$\alpha_{com} \approx \alpha_2, \sigma_{com} \approx \sigma_2, p_{com} \approx p_2$$

The further increase of the charge carriers concentration in the second subzone leads to the reduction of the thermoelecromotive force α_2 (the formula Pissarencko) and in spite of the growth of σ_2(T) the product $\alpha_2\ \sigma_2$ reduces and the common thermoelectromotive force α_{com}, passing through the maximum, reduces (the formula 5) part 4.

The common electroconductivity σ_{com} falls by this, both in the consuquence of the carriers number growth with the high effective mass of the state density $\left(\frac{m_2^*}{m_0}\right)$ and the low mobility u_2, and the dependence of u_2 on the temperature, the exponent «K» in the expression $\sigma_{com} \approx T^k$ as it is more than 3/2 by this (at the charge carriers scattering in the second subzone on the acoustic oscillation of the lattice r = - ½).

Therefore, in the observed case the temperature dependence $\alpha_{com}(T)$ differs a bit from the value α_{max} and they might be concerned stabilized to a required precision. The interval value ΔT (its length) depends on the relation $\Delta\varepsilon$ and ΔE.

2. $\Delta\varepsilon = \Delta E$. In this case the contribution in the common thermoelectromotive force α_{com} and electrons electroconductivity σ_{com} of the conduction band α_n and σ_m occurs at determined temperatures, respectively, formulae (5)-(6) have the form:

$$\alpha_{экс} = \frac{\alpha_1\sigma_1 + \alpha_2\sigma_2 - \alpha_n\sigma_n}{\sigma_1 + \sigma_2 + \sigma_n} \qquad (14)$$

Creating solid solutions on the base of the matrix (basic) materials, it is possible to obtain optimal values ($\Delta\varepsilon < \Delta E$) at ($\Delta\varepsilon = \Delta E$) the common electroconductivity σ_{com} will increase - it is seen from the formula (13) at the whole temperature interval.

From applied in the present time in the thermal converters materials of the complex energy spectrum of the charge carriers, allowing to explain the behavior of kinetic parameters α_{com}, σ_{com}, R_x versus the temperature and concentration, have mainly tellurides GeTe, SnTe, PbTe [3,4'; $SbTe_3$, Bi_2Te [5,6]. In all indicated tellurides the value of the energy gap $\Delta\varepsilon$ is lesser than the width of the forbidden band ΔE, i.e they meet the first case and it is possible by means of the solid solution creation on their base to achieve the stabilization of the common thermoelectromotive force α_{com} in the respective temperature interval.

[1] *B.M. Holtzmann, V.A. Kudinov, I.A. Smirnov*. Poluprovodnikoviye termoelektricheskiye materiali na osnove Bi_2Te-M. Nauka, 1972, p. 320

[2] *B.M. Askerov*. "Kineticheskiye effekti v poluprovodnikakh". Nauka, L:1970, p. 302.

[3] *Y.I. Ravich, B.A. Yefimov, I.A. Smirnov*. "Metodi issledovaniya poluprovodnikov v primeneniyi k khalkogenidam svintza PbTe, PbSe, PbS", Nauka, M, 1968, p.383.

[4] *N. Kh. Abrikosov, V.M. Bankina, L.V. Poretzkaya, E.V. Skudnikova, V.F. Chijevskaya.* Poluprovodnikoviye khalkogenidi i splavi na ikh osnove, Nauka M., p. 220.

[5] *A.A. Andreyeva, I.A. Smirnov, V.A. Kutasov*. FTP 10, 3000, 1968.

[6] *B.Ronland, O. Beckmann, H. Leby*. Z. Phys. Chem. Sol., 26, 1281, 1965.

T.Q. Osmanov, R.S. Mədətov, F.K. Ələsgərov, N.M. Abdullayev, S.A. Nəbiyeva

YARIMKEÇİRİCİ MADDƏLƏRDƏ TERMO-ELEKTRİK HƏRƏKƏT QÜVVƏSİNİN TEMPERATURDAN ASILI OLARAQ STABİLLƏŞDİRMƏ ŞƏRTLƏRİ

Məqalədə mürəkkəb quruluşlu keçirici və valent zonaya malik olan və bir növ yükdaşıyıcı, standart zolaqlı maddələr üçün temperaturdan asılı olaraq ümumi T.E.h.q-nin stabilləşməsi halı araşdırılmışdır. Göstərilmişdir ki, ΔE qadağan olunmuş zolağın eni $\Delta\varepsilon$ - energetik məsafənin qiymətindən böyük olduqda yükdaşıyıcılarının energetik spektri iki zolaqlı modula uyğun gələn maddələr üçün T.E.h.q-nin stabilləşdirilməsi mümkündür.

Т.Г. Османов, Р.С. Мадатов, Ф.К. Алескеров, Н.М. Абдуллаев, С.А. Набиева

УСЛОВИЯ ТЕМПЕРАТУРНОЙ СТАБИЛИЗАЦИИ ТЕРМОЭДС В ПОЛУПРОВОДНИКОВЫХ МАТЕРИАЛАХ

Рассмотрена возможность стабилизации общей термоэдс в зависимости от температуры для материалов со стандартной зонной структурой с одним сортом носителей заряда или обладающими сложным строением валентной зоны и, или зоны проводимости (двухзонная модель). Показано, что для веществ с энергетическим спектром носителей заряда, соответствующих двух-зонной модели, возможна стабилизация общей термоэдс α, если ширина запрещенной зоны ΔE больше величины энергетического зазора $\Delta\varepsilon$ между подзонами.

Received: 04.12.02

THE SHAPER OF MODULATING SQUARE WAVES

CH.O.QAJAR, S.A.MUSAYEV, I.Z.MOVSUMOV, M.R.MENZELEYEV
Institute of Physics of National Science Academy of Azerbaijan

The displacement of measured value of the resonant frequency of centers of microwave spectral lines of some rotational and rotationally vibrational transitions of asymmetric top molecules was observed. The shaper of zero-based square-waves eliminating of such displacements was designed and tested in a hybrid microwave spectrometer.

The Stark modulation in microwave spectroscopy has many advantages, but sometimes the values of frequency of spectral lines centers measured by this method were displaced. The careful analysis of such spectral lines has shown, that the displacement of their resonant frequencies is caused by a displacement of zero level of modulating square-waves. It was confirmed by dependence of the resonant frequency of transition $s4_{32}$-$s4_{22}$ 28543,079 MHz (ethanol, gauche form) on magnitude of displacement of zero level of square-wave (fig. 1). As it follows from this figure, even a little change of voltage of zero level of zero-based square-wave displaces measured value of frequency of a spectral line center on a few megahertz.

Fig.1 A curve of dependence of displacement of resonant frequency of transition $s4_{32}$-$s4_{22}$ 28543,079 MHz of spectral line of gauche-ethanol molecule on magnitude of voltage of displacement of zero level of modulating square wave

The purpose of the present paper was working out the square-wave shaper with minimum displacement of a zero level. In well-known analogs of such shaper [1-3] a displacement of zero level sometimes reaches too high values, because of use of high-voltage bipolar transistors in output stages of shaper. Switchover of such transistors into state of saturation requires the particular shape and power of controlling impulses with necessity of high-voltage uncoupling. However even residual voltage of collector - emitter transition of the bipolar transistors in the opened state creates a displacement of zero level of square wave. Therefore special monitoring and compensation of such displacement is required. The presented shaper of modulating square waves (SMSW) is constructed on the basis of modern MOSFET-transistors having low values of resistance of a conducting drain - source channel in an opened state [4]. The control of the transistors is carried out by a special chip of high voltage, high-speed power MOSFET and IGBT drivers with dependent high and low side referenced output channels [5].

The shaper consists of the following functional blocks (fig. 2):

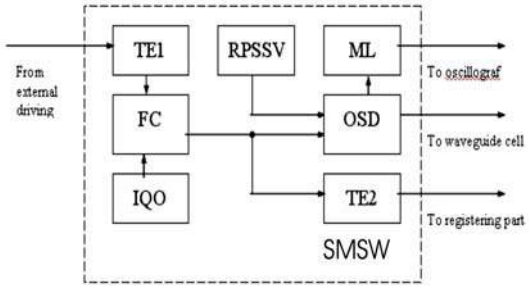

Fig.2. Functional diagram of shaper of modulating square waves.

- Regulated power source of stabilized voltage RPSSV;
- Internal quartz oscillator IQO;
- Frequency converter FC;
- Input and output threshold elements TE1, TE2;
- Output shaping device OSD;
- Measuring limiter ML.

The schematic diagram of SMSW is presented on a fig. 3.

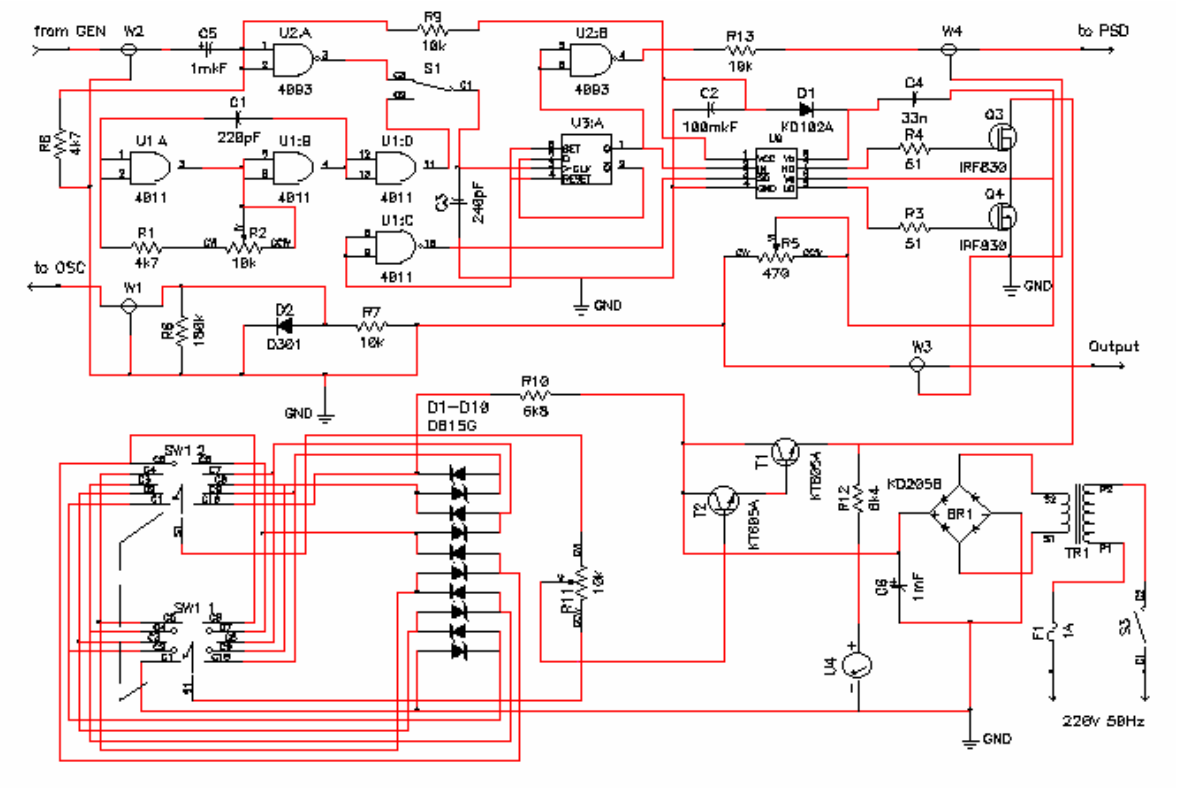

Fig.3. Schematic diagram of shaper of modulating square waves

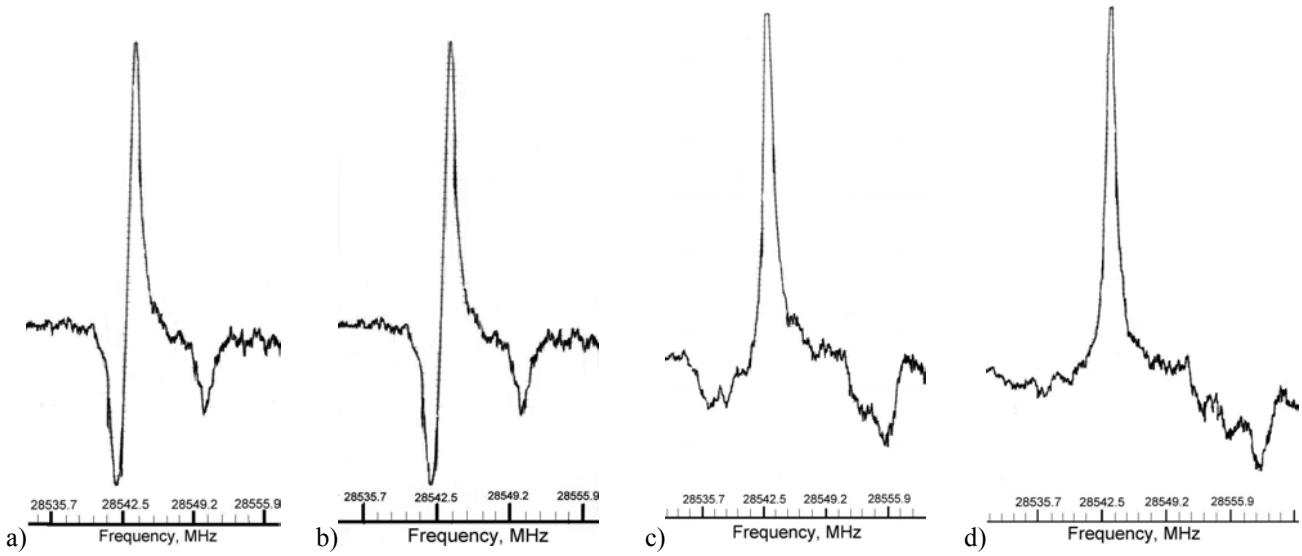

Fig. 4. Records of transition $s4_{32}$-$a4_{22}$ 28543,079 MHz of spectral line of gauche-ethanol molecule at different values of amplitude of modulating square wave a) U=2,5V; b) U=5V; c) U=7,5V; d) U=10V

The harmonic signal of external driving generator incoming to input of the threshold element TE1 is converts to impulse. The frequency of these impulses sequence is divided on 2 in the FC constructed on basis of flip-flop circuit (chip 4013). The pulse signal from an exit of a frequency converter transits into an input of the shaping device consisting of the half bridge driver U9 (chip IRF2104) [5] and shaping output switches Q3, Q4, as which the MOSFET transistors with an isolated gate and 1.4 Ohm resistance of an open channel IRF 830 is used [4]. The amplitude of output zero-based square wave is determined by a value of voltage of RPSSV. The exit of the shaper is in accord with a load (wavequide cell) by adjusting of a potentiometer R5. The reference signal of phase-sensitive detector of the registering part of spectrometer is formed in a frequency converter and through a threshold element TE2 (Schmidt flip-flop U2в of a chip 4093) comes to the corresponding SMSW exit.

During the process of testing of the shaper the value of voltage of zero level displacement was measured by oscilloscope by instrumentality of amplitude limiter ML (R7, R6, D2).

The use in the shaper of modern element base has allowed to reduce a voltage of zero level displacement up to values, at which its influence to an accuracy of measurement of spectral lines centers frequencies becomes negligible. It is confirmed by record of spectral line mentioned above (fig. 4).

Thus, necessity for monitoring and compensation of a zero level displacement of modulating impulses for separate transitions has disappeared and it enables to realize continuous record of a spectrum in an automatic mode. Moreover, range of operating frequencies has essentially extended, that enables to select an optimum relation of sensitivity and resolution of the measuring equipment at the record of spectral lines.

SMSW stably works in a frequency range from 20 Hz up to 600 kHz and in all range of operating frequencies has the following characteristics:

- Amplitude of output impulses 0÷100 V;
- Off-duty factor 2;
- Duration of front of impulses, no more than 300 ns;
- Duration of cutoff of impulses, no more than 250 ns;
- Loading capacitance, not less than 1000 pF;
- Displacement of a zero level, no more than 10 mV.

[1] Radiospectrometer with electrical molecular modulation. Int. of AS of Azerb. SSR, part of PTMS, 1979, № 1 pp.100-107.
[2] *Ch.Townes, A.Shavlov* Radiospectroscopy., 1959. p.756.
[3] C.O. Britt. Solit state microwave spectrometer. Rev. Sci. Instrum , 1967, v. 38, № 10, p.1496-1501.
[4] SMPS MOSFET IRF830A, Data Sheet № PD-91878C, International Rectifier, 05/2000.
[5] High and low side driver IRF2104(s), Data Sheet № PD-60046-O, International Rectifier, 02/15/2001.

Ç.O. Qacar, S.A. Musayev, İ.Z. Mövsümov, M.R. Menzeleyev

MODULYASİYAEDİCİ İMPULSLARIN FORMALAŞDIRICISI

Asimmetrik fırfıra tipli molekulların bəzi fırlanma və rəqsi fırlanma keçidlərinin rezonans tezlikli mikrodalğalı spektral xətlərinin mərkəzlərinin ölçülən qiymətlərinin sürüşməsi müşahidə olunmuşdur. Bu sürüşmənin yaranma səbəblərini aradan qaldırmağa imkan verən modulyasiyaedici unipolyar impulsları formalanşdıran qurğu hazırlanmış və hibrid spektrometrin tərkibində sınaqdan çıxarılmışdır.

Ч.О. Каджар, С.А. Мусаев, И.З. Мовсумов, М.Р. Мензелеев

ФОРМИРОВАТЕЛЬ МОДУЛИРУЮЩИХ ИМПУЛЬСОВ

Обнаружено смещение измеряемого значения резонансной частоты центров микроволновых спектральных линий некоторых вращательных и вращательно-колебательных переходов молекул типа ассиметричного волчка. Разработан, изготовлен и испытан в гибридном спектрометре формирователь модулирующих электрических импульсов, устраняющий причины возникновения таких смещений.

Received: 09.12.02

THE PHASE TRANSITION SPREADING IN BISMUTH HTSC

S.A. ALIYEV
The Institute of Physics, Azerbaijan NAS,
370143, Baku, H. Javid ave. 33

Results of electric properties of bismuth crystals (2212) and (2223) are interpreted in a framework of the theory of spreaded phase transitions. Parameters, characterizing the spreading degree of *PT*, are determined. It is shown, that in bismuth *HTSC* phase transitions have strongly spreaded nature and the spreading degree grows to an order under the influence of the magnetic field.

INTRODUCTION

The research of phase transitions is one of the most studied directions in solid-state physics. This is caused by the close relation of *PT* theory with many branches of physics and has always both the scientific and practical interest.

Irrespective of the *PT* nature, they are followed by the jump-shaped changes of electric, segnetoelectric, heat, magnetic and other properties, which are successfully applied for the creation of converters of various types. The information on the rules of investigated effects changes in the *PT* region, on the influence of the external factors on these effects is necessary for the stable work of such converters. The interest to the *PT* research in solid states has grown after the discovery of high-temperature superconductors (*HTSC*).

One of the actual issues of the given directions is to find out the rules of the phase coexistence in the *PT* region. Theoretical aspects of this issue are observed in papers [1,2]. Experimental data can be found in papers [3,6]. In the paper [6] results of electric and heat properties of Ag_2Te in the *PT* region are interpreted in a framework of the theory of spreaded PT [1,2]. The parameters, determining the spreading degree of *PT*, are calculated. It is established, that structural phase transitions in Ag_2Te have the spreaded nature, electric and magnetic fields, impurities, and also the excess of Te or Ag do not essentially influence on the spreading degree. It is shown, that parameters, calculated from heat and electric properties, are in agreement with data, obtained from temperature dependences of roentgen reflections intensities and may be applied to determine the *PT* parameters.

The analysis of temperature dependences of *HTSC* electric properties in the *PT* region indicates on their analogous to the second type of superconductors, have peculiarities, which should be followed by the strong spreading of *PT*. Among such peculiarities the unusual mechanism of the interaction with magnetic, electric fields can be counted too in consequence of which the strong spreading of the transition region *BT (B,E)*, the asymmetry growth relatively to T_0, the fracture appearance on B_{c2} *(T)*. Therefore in the present paper the task is to observe the data of electric properties of bismuth superconductors (Bi (2212) and Bi (2223)) in the transition region in a framework of the *DPT* theory by methods, suggested in [1,2,6], to calculate *PT* parameters, determining the spreading degree and the influence of the magnetic field on it as well as to find superconductive one.

THE THEORY AND METHODS OF THE DETERMINATION OF PHASE TRANSITION PARAMETERS

Theoretical aspects of phases coexistence issues and the DPT parameters determination in solid states are considered in papers [1,2]. With this aim the theory of the spreaded phase transitions in condensed systems, based on the introduction of the switching function *L(T)* was used. It is assumed that if thermodynamic potentials of α and β-phase denote as Φ_α и Φ_β , then the thermodynamic potential *Φ(T)* in the phases coexistence region may be represented in the form:

$$\Phi(T) = \Phi_\alpha(T) - \Delta\Phi(T)\cdot L(T), \qquad (1)$$

where $\Delta\Phi(T) = \Phi_\alpha(T) - \Phi(T)$. In the case when the phase transition occurs in the temperature interval $\Delta T = T_2 - T_1 (T_2 \rangle T_1)$ the switching function should fulfill the conditions:

$$L(T) = \begin{cases} 0 , & T \langle T_1, \\ 0 \langle L \langle 1 , & T_1 \langle T \langle T_2, \\ 1 , & T_1 \rangle T_2. \end{cases} \qquad (2)$$

According to the *DPT* theory, the expression obtained for the function *L(T)* looks as:

$$L(T) = \{1+exp[-a(T-T_0)]\}^{-1}, \qquad (3)$$

where T_0 is the temperature, at which masses of both phases are quantitatively equal, α is the constant, characterizing the spreading degree of phase transitions and depends on the bulk of possible fluctuations and also the energy and *PT* temperatures. Taking into consideration the fact that the function *L(T)* characterizes the relative part of phase in the region of their coexistence, it may be represented in simple form:

$$L(T) = \frac{m_\beta(T)}{m_\alpha(T) + m_\beta(T)} = \left[1 + \frac{m_\alpha}{m_\beta}(T)\right]^{-1}, \qquad (4)$$

where m_o and m_β are masses of α and β-phases. Temperatures T_0 may be determined from the temperature dependences $ln\left(\frac{m_\alpha}{m_\beta}\right)$. We obtain from the joint solution of (3) and (4):

$$\alpha = \frac{1}{T_0 - T} ln \frac{m_\alpha}{m_\beta} \qquad (5)$$

If α is some constant, then the factor $ln\frac{m_\alpha}{m_\beta}$ should be the line function of the temperature.

No less informative is the derivative of $L(T)$ with respect to the temperature:

$$dL\Big/dT = \frac{a}{2}\cdot\frac{1}{1+ch(a\cdot(T-T_0))} \quad , \qquad (6)$$

expressing the temperature velocity of phase transformations of each phase.

The possibility of $L(T)$ determination on the base of the structural research of phase transitions of solid states was shown in the paper [5,6]. It was supposed by this, that in the indicated regions of the phases coexistence the temperature changes of roentgen reflections intensities were caused by the quantitative changes of phases. In paper 6 assuming, that in the PT region temperature changes of the differential thermal analysis (DTA) and electric properties are also caused by mainly quantitative changes of α-β phases of Ag_2Te and α, T_0, $L(T)$, dL/dT and other thermodynamic parameters are determined. It was necessary to achieve the line change of the temperature near and in the PT region. Then from the beginning of the transition to the end the interval $\Delta\boldsymbol{T}$ may be divided on equal periods and corresponding values of the investigated effect relate to the supposed phases, for example:

$$\Delta T_y = T_{y,\alpha}(1-m_\beta/m_\alpha)+\Delta T_{y,\beta}\left(\frac{m_\beta}{m_\alpha}\right) \quad , (7)$$

The results comparison of a, T_0, $L(T)$, dL/dT and other thermodynamic parameters, obtained for Ag_2Te on data of roentgen reflections intensities [3,4] with DTA results and electric properties gave almost coinciding values.

EXPERIMENTAL RESULTS AND THEIR DISCUSSION

If by the analogy to Ag_2Te, we take one phase as normal and another one as a superconductive (SC), then the suggested method may be applied for $HTSC$ too. Then corresponding messes will have values m_n and m_{cn}. Dependences $\rho(T,B)$ (a) and $\alpha(T,B)$ ($в$) for the crystal sample $Bi_2Sr_2CaCu_2O_x$ are represented on fig.1.

The characteristic dependences $\ln(y=\frac{m_{cn}}{m_n})$ on T at B=0(1) and B=2,2T(2) are represented on fig.2. The corresponding masses m_n and m_{cn} are determined from data $\rho(T,B)$ and $\alpha(T,B)$. Nominal temperatures T_0 are determined by the cross point of straight lines with the abcissa axis. The represented straight lines are described by the formula:

$$y=exp[-a\ (T-T_0)], \qquad (8)$$

where the values of α, determined from the straight lines slope $\left(\frac{ln\,y}{\Delta T}\right)$, are temperature constant of the transition. As it is seen, points of the «untime» reduction of $\rho(T)$ and $\alpha(T)$ part are declined from straight lines in the indicated coordinates. It indicates on the correctness of the applied method of m_{cn}/m_n determination for the main PT part. It is seen, T_0 and α reduce under the influence of the magnetic field. In spite of the strong stretching of the low-temperature part of curves $\rho(B,T)$ and $\alpha(B,T)$ in the magnetic field, they fully placed on the straight lines. Curves of the switching function $L(T)$ (at B=0 and B=2,2T), calculated by formulae 4(a) and 3(b) with the data application α and T_0, are represented on fig.3.

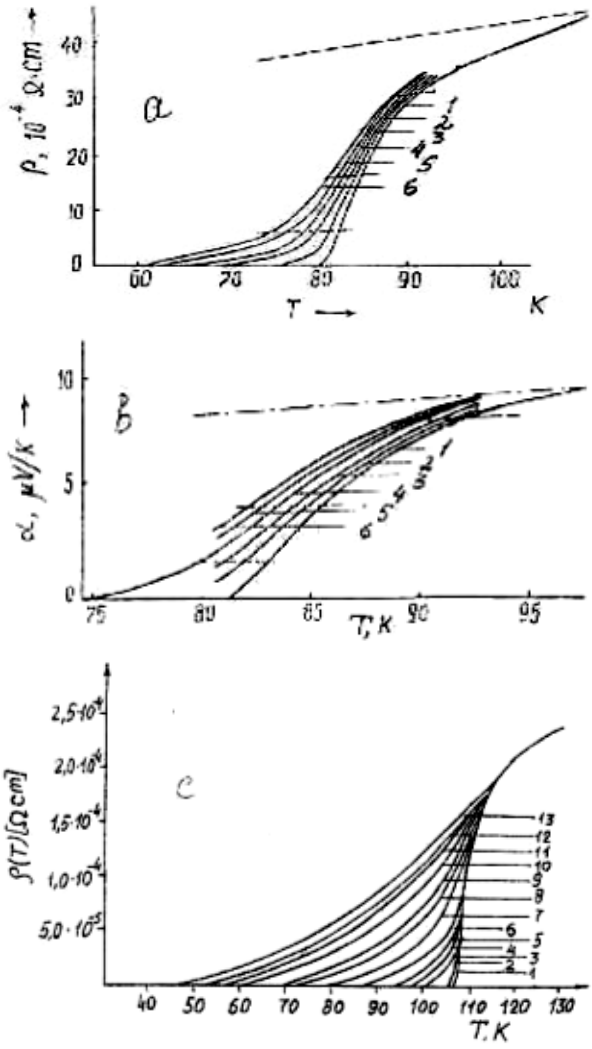

Fig.1 Temperature dependences of resistance (a) and thermo e.m.f. (b) in Bi (2212) B:1-0;2-0,1;3-0,2;4-0,5;5-0,9:6-2,2T и Bi (2223)(c) данные [7] B:1-0;2-0,01;3-0,05;4-0,1;5-0,2;6-0,5;7-1;8-2;9-3;10-5;11-7;12-9;13-12T

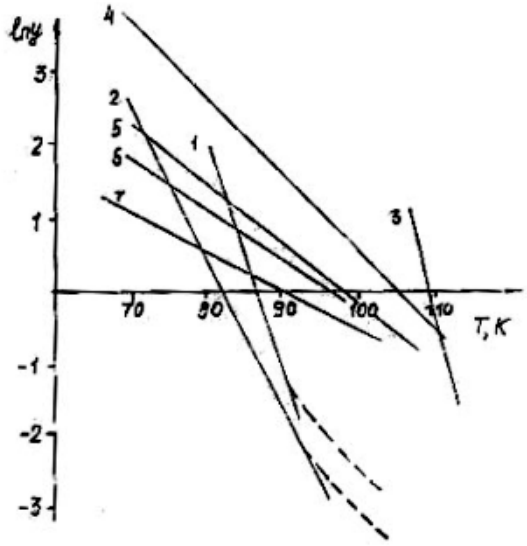

Fig.2 Temperature dependences of the masses distribution lny at various values of the magnetic field for Bi (2212) (1-at B=0;2-at B=2,2T) and Bi (2223) (3-B=0;4-2T;5-5T;6-7T;7-12T).

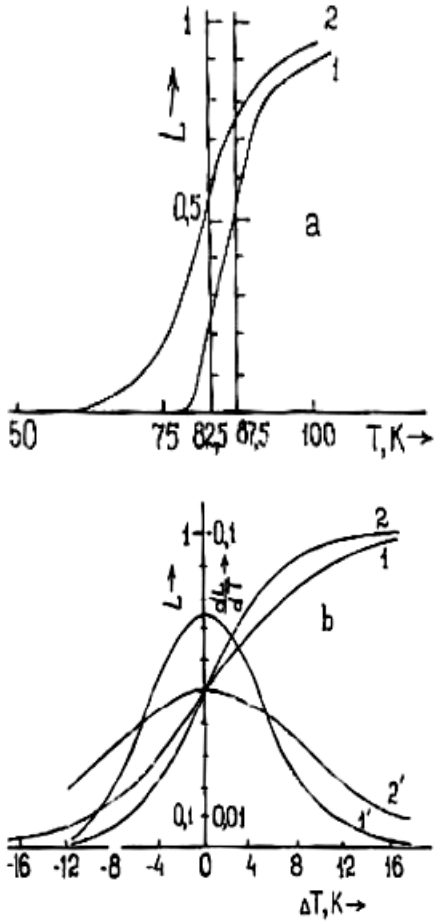

Fig.3 Temperature dependences of the switching function, calculated by formulae (4) (a) and (3) (b) and its derivative *dL/dT* for Bi (2212)

As it is seen, temperature dependences *L(T)* in separate parts differ quantitatively. It is connected with values change T_0 and α in the magnetic field, it leads to the *L(T)* bias on the temperature. Therefore the *L(T)* analysis is convenient to carry out on the formula (3) data. It is seen, that curves *l(T)* approach the zero value at $T \approx T_k$, they cross the axis at L=0,5 curves are spreaded by the growth of the magnetic field.

The derivatives L on the temperature *dL/dT* (1′,2′) are represented on fig. 3(b). As it is seen, curves *dL/dT (ΔT)* pass through the maximum at ΔT, and moreover the maximal value corresponds to $dL/dT=\frac{a}{4}$. As far as *B* grows, the curve *dL/dT* becomes more sloping and the values when $\Delta T= 0$ reduce proportionally to *a*.

Let us note, that weak magnetic fields, at which research for Bi (2212) was carried out, make it difficult to conclude about PT parameters dependence on the magnetic field with this aim, the data of authors of paper [7], in which the detailed research of *ρ(T,B)* in crystals $Bi_{1.72}Pb_{0.34}Sr_{1.83}Ca_{1.97}Cu_{3.13}O_{10+\delta}$ in magnetic fields to 12 T (fig (1c)) is carried out, are used, These data are useful not only because of high values of B, but as the another phase Bi (2223) of bismuth HTSC, having high values T_k. Straight lines *lny(T)* are represented on fig (2-7). In the case of Bi (2223) high-temperature parts points of curves fell out the straight lines. It is seen, that values α and T_0 reduce strongly by the *B* growth. Data of *α(B)* are represented on fig.4, from which it is seen, that the strong reduction of α occurs at relatively weak fields (0-1 T). Data of *L(ΔT)* (1-5) at various values B are presented on fig.5. It is seen clearly from data, that L approaches the zero value at $\approx T_k$ and curves *L(T)* are spreaded by the B growth analogous results are obtained from temperature dependences of derivatives on the temperature *dL/dT* (fig.5) (1′-5′). As it is seen, the curve *dL/dT* at *B=0* has more sharp peak and it losses the velocity as far as it removes from $\Delta T=0$, the asymmetry is observed at high sloping form, cross the curve $(dL/dT)_{B=0}$ and decrease slower. By this the low-temperature part of curves falls behind from it more, than high temperature.

It follows from data a *(B)* and *L(T/B)*, the spreading degree is inversely proportional to the temperature constant *ρT-a*. The obtained value a for Bi (2212) and Bi (2223) tells about the strong spreading of PT in them, moreover the spreading degree in Bi (2212) is higher, than in Bi (2223). Estimations show, that the spreading degree is higher in phase Bi (2001), than in these two phases. The spreading degree of PT strongly increases in the magnetic field, especially at relatively weak values *B*. The temperature velocity of PT grows as far as the spreading degree reduces, what leads to more sharp realization of PT.

The points derivation of the premature reduction part *ρ(T)* and *α(T)* from the straight line *(T,B)* tells in favor of the fact, that, actually, the mechanism of SC couples formation and their uncoupling under the influence of the magnetic field in the main transition part and high-temperature part distinguish essentially.

The physical nature of defects, leading to the PT spreading in the absence of magnetic field, may serve heterogeneity, connected with the presence of other bismuth *SC* phase (2201, 2212 and 2223) in each *SC* phase, the derivation from the stechiometry of multicomponent ingredients, the slightest oxygen lack and other imperfections [8,9]

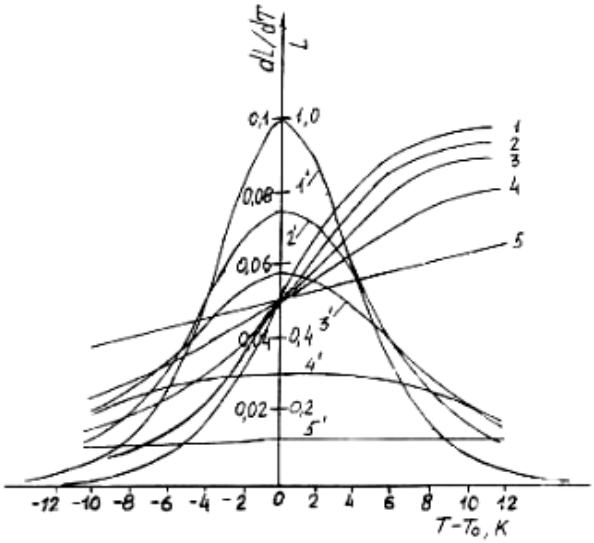

Fig.4. Temperature dependences L(1-5) and dL/dT (1′-5′) for Bi (2223) B: 1,1′-0; 2,2′-0,1; 3,3′-0,2; 4,4′-2; 5,5′-12T.

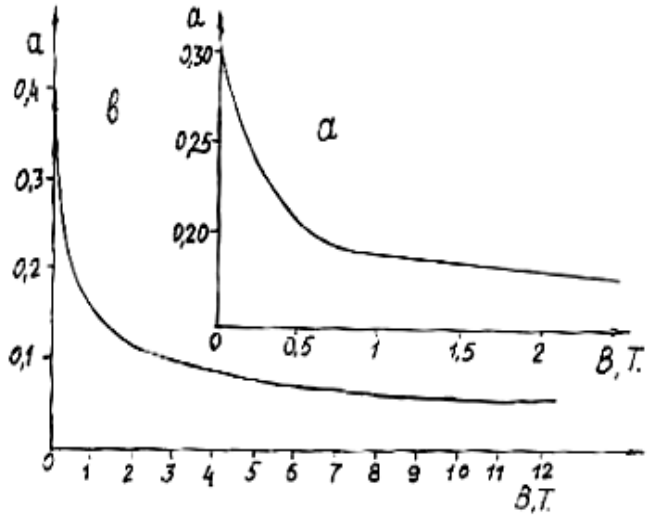

Fig.5 The dependence of the temperature constant of PT *a* on the magnetic field: *a* -Bi (2212), b-Bi (2232)

Defects, leading to the spreading in the magnetic field are caused by the vortical state of super conductors of the second type, in which the vortical currents occurs spontaneously beginning from very weak fields B_{C_1} ($B_{C_1} \langle\langle B_{C_2}$).

At the further *B* growth the vortex size and the value of the magnetic field flow, which they conduct, remain stable, the vortex number grows, forming alike crystals atoms the right lattice *L* in the cross-section of the trigonal shape, which causes the growth of the spreading degree in them.

[1] *N. Rolov*. Razmitiye fazoviye perekhodi, Riga-1972, p.311

[2] *B.N. Rolov*. Izv. AN Latviya SSR, ser. phys.techn. nauk,4,33, 1983

[3] *K.P. Mamedov, M.F. Cajiyev, Z.D.Nuriyev*. DAN SSR, 321, 1, 94, 1976

[4] *K.P. Mamedov, M.F. Cajiyev, Z.D.Nuriyev*. FTT, 19,7, 1977

[5] *S.A. Aliyev, F.F. Aliyev, G.P. Pashayev*. Neorganicheskiye materiali, 29, № 8, 1073, 1993

[6] *S.A. Aliyev, F.F. Aliyev, Z.O. Gasanov*. FTT, 40, №9, 199

[7] *G.Grassj, F.Marti, Y.Huang, A.Perin, R.Flukiger*. Physica,281,271,1997.

[8] *S.A.Aliev, D.A.Bagirov,S.S.Ragimov.at.al.* J.RareEarths,№3,1060, 1991

[9] *S.A.Aliev, S.S.Ragimov and V.M.Aliev*. Fiz.Nizkich Temperatur, 22, 679, 1996.

S. A. Əliyev

YTİK BİSMUTDA FAZA KEÇİDİNİN YAYILMASI

Bismut (2212) və (2223) kristallarının elektrik xassələri yayılmış faza keçidləri nəzəriyyəsi çərçivəsində izah edilmişdir. Faza keçidlərinin yayılma dərəcəsini xarakterizə edən parametrlər müəyyən edilmişdir. Göstərilmişdir ki, yüksək temperaturlu ifratkeçirici (YTİK) vismutda faza keçidləri güclü yayılma xarakterinə malikdir və maqnit sahəsinin tə'siri ilə yayılma dərəcəsi bir tərtib artır.

С.А. Алиев

РАЗМЫТИЕ ФАЗОВОГО ПЕРЕХОДА В ВИСМУТОВЫХ ВТСП

Результаты исследования электрических свойств висмутовых кристаллов (2212) и (2223) интерпретированы в рамках теории размытых ФП. Определены параметры, характеризующие степень размытия ФП. Показано, что в висмутовых ВТСП фазовые переходы носят сильно размытый характер и под действием магнитного поля степень размытости возрастает до одного порядка.

Received: 25.07.02

SHOTTKY FIELD EFFECT TRANSISTOR WITH SUPERHIGH SPEED

F.D. KASIMOV
Azerbaijan National Aerospace Agency, 370106, Baku, ave. Azadlig 159

A.A. MAMEDOV
Azerbaijan Technical University,370073, Baku, H. Javid ave. 25

Field transistors with controlling Shottky type junctions of vertical structures on the basis of SiC/Si material with various length of channels have been investigated.

It is shown, that increase of fast action in the wide band of temperature (up to 700 °C) is reached under extremely low lengths of the channel (<100 nm) and thermocorrelated supply voltage.

Field effect transistors (FET) with controlling Shottky type junctions have some advantages in comparison with bipolar and MOS-transistors, related with possibility to use more short channels and providing for higher speed [1].

One of major limitations for minimal length of ShFET is connected with effect of modulation of channel's length, which leads to triode character of V-A characteristics [2].

In order to eliminate the modulation of the channel, special constructions of normally closed ShFET with vertical channels of *n*- and *p*-type, named as transistors with static induction (SIT) were developed [3], where the channel was the area of space charge (ASC) for whole band of working voltage at the transistor exit leads. Control of the drain current I_d is carried out through changing of the height of potential barrier of source-channel, occurred as a result of diverse level of alloying of source and drains areas (fig. 1).

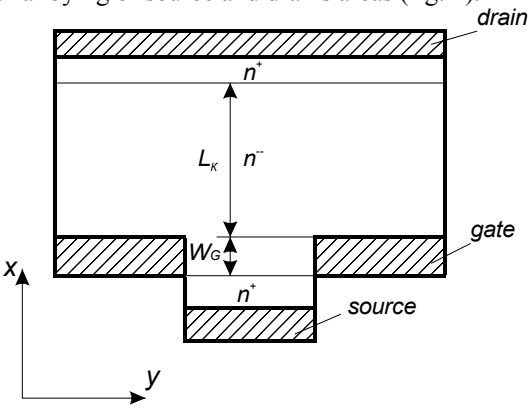

Fig. 1. Structure of n-channel SIT with Shottky barrier.

Height of the potential barrier is determined by a voltage gate-source U_s and lightly depends on voltage of drain-source U_d due to low thickness of channel by source.

Major factors restricting a wide use of SIT as submicron elements of superhigh speed integral circuits, are:

- triode character of V-A characteristics of SIT, conditioned by dependence of height of potential barrier in the channel from voltage gate-source and drain-source, also by modulation of ASCs width in the channel by voltage U_d;
- presence of passive areas of spatial charge between drain-source contacts and the gate.

Using of silicon carbide as a base material, which exceeds silicon on major parameters [4]: -wide bandgap, permitted working temperatures, speed of drift of charge carriers ($2{,}5\cdot10^7$cm/s) allows to eliminate those shortcomings [5]. Using of heteroelectronic structures SiC/Si broadens the functional capabilities of the elements and allows technological integration of them with elements of integrated circuits [6].

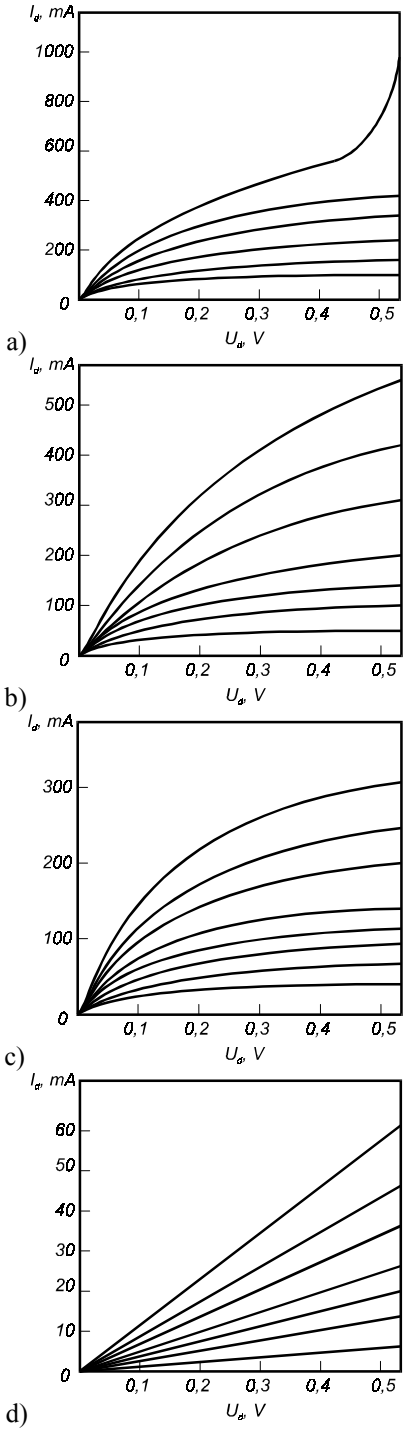

Fig. 2. Volt-ampere characteristics of ShFET with different length of channel

The technology of forming of silicon carbide structures on the silicon doesn't differ in principle from processes of forming of silicon films and is carried out on the typical equipment [7, 8].

Heteroepitaxial layers were grown-up by the method of vapor-phase epitaxy in the open system: diffusion technology in two-zone oven was used. Hydrogen was used as gas-carrier: in first zone the free carbon is associated with hydrogen and is carried to the zone of growth of semiconductor film. The temperature of carbidized pedestal at which hydrocarbons become decomposed and the silicon substrate is carbidized is equal to 1360-1380 °C.

Ohmic contacts for SiC films were formed by method of thermal deposition of nickel by further pulse type thermo-processing by non- coherent IR radiation on the technology described in [9].

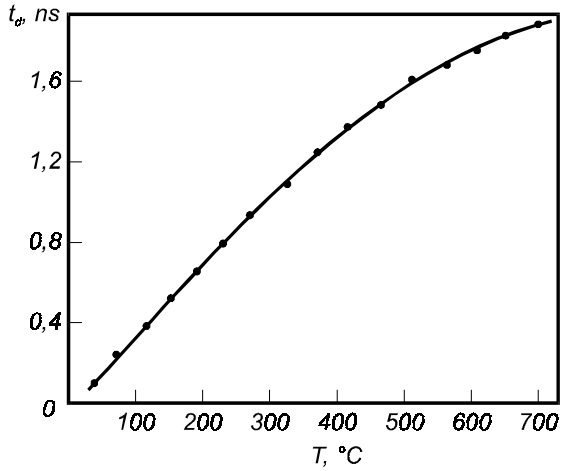

Fig. 3. Dependence of ShFET logic elements switching delay time on the temperature.

Output characteristics of depleted ShFET with space charge limited current (SCLC), made on the basis of silicon carbide with -type channel for values of the channel length L=30 nm (fig. 2a), L=40 nm (fig. 2b), L=100nm (fig. 2c) and L=250 nm (fig. 2d) are given in fig. 2. The results of measures have shown, that on channels length equal to 30-100 nm, V-A characteristics has a pentode but by increase of the channel's length up to 250 nm, these characteristics become near to linear type ones (fig. 2d). Sharp increase of the drain's current on L=30 nm (fig. 2a) is conditioned by the tunnel effect, occurred under minimal length of the channel.

Dependence of time delay of switching of integrated logic element made on the basis of complementary ShFET with SCLC from temperature by voltage source U_s=0,2 V is given in fig. 3. Increase of switching delay is connected to the temperature dependence of the carrier's mobility.

In order to increase fast-response and to widen the temperature band of elements made at the basis of ShFET the thermocorrelated supply have been used. This means, that in the process of functioning of IC, the supply voltage was decreased in proportion to the temperature change of height of potential barrier of source-drain. This makes it possible to curtail the time delay of logic elements switching made on the basis of ShFET down to parts of nanoseconds, i.e. more, than 5 times (fig. 4).

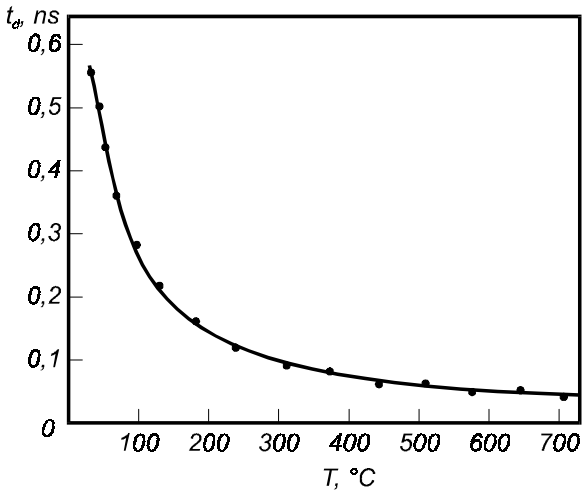

Fig. 4. Dependence of delay time on temperature under thermo correlative supply voltage

As a result, the pentode character of V-A characteristics, the high steepness of transistors, the low values of time delays allow to design super high fast action IC on the basis of field transistors with controlling Shottky type junctions.

[1] *Yu.K. Pojela*. Fizika bistrodeystvuyuschix tranzistorov. Vilnyus: Mokslas, 1989, 261s.

[2] *M. Shur*. Sovremennie pribori na osnove arsenide galliya. Per. s angl. M.: Mir, 1991, 632s.

[3] *E.A. Ryndin, B.G. Konoplev*. Submikronnie integralnie sxemi: elementnaya baza i proektirovanie. Taganrog: TRTU, 2001, 147s.

[4] *A.V. Afanasyev, V.A. Ilyin, A.A. Petrov*. Visokotemperaturnie diodi Shottki na osnove SiC. Peterburgskiy jurnal elektroniki, 2000, №3-4, s.12-20.

[5] *F.D. Kasimov, A.A. Mamedov*. Sverxbistrodeystvuyuschie IS na osnove tranzistorov so staticheskoy induktsiey. Tezisi dokladov Respublikanskoy konferensii «Rol nauki I obrazovaniya v reshenii sovremennix problem grajdanskoy aviatsii», NAA, Baku, 2002, s.130.

[6] *V.I. Osinsky, P.F. Olekseinko, A.V. Palagin i dr*. Problemi integratsii struktur geteroelektroniki s kremnievimi IS. Tehnologiya i konstruirovanie v electronnoy apparature (Odessa), 1999, №1, s.3-17.

[7] *P.A. Ivanov. V.E. Chelnokov*. Poluprovodnikoviy karbid kremniya - tehnologiya i pribori. Fizika i tehnika poluprovodnikov, 1995, t.29, vip.11, s.1921-1943.

[8] *A.N. Komov, V.I. Chepurnov*. SVCH chuvstvitelnie poluprovolnikovie preobrazovateli na strukturakh SiC/Si. Proceeding of Seventh International Conference "Actual Problems of Solid-State Electronics and Microelectronics" Divnomorskoye, Russia, 2000, part 2, p.131-133.

[9] *O.A. Ageev, N.A.Kovalev, A.M.Vasilenko, E.K.Guseynov, S.A. Ismailova*. Vliyanie elektroerozionnoy obrabotki na parametri kontaktov Ni/6H-SiC. Fizika, Baku, 2000, t.6, №4, s.16-18.

F.C.Qasımov, Ə.A.Məmmədov

İFRAT YÜKSƏK CƏLDLİYƏ MALİK ŞOTTKİ SAHƏ TRANZİSTORLARI

Müxtəlif uzunluqlu kanallı SiC/Si əsasında vertikal struktura malik idarəedici Şottki keçidli sahə tranzistorları tədqiq edilmişdir.

Göstərilmişdir ki, geniş temperatur diapazonunda (700 °S-yə qədər) cəldliyin artırılması, kanalın ifrat kiçik uzunluqlarında (<100 nm) və termokorrelyasiya olunmuş qida gərginlikləri zamanı əldə edilir.

Ф.Д. Касимов, А.А. Мамедов

ПОЛЕВЫЕ ТРАНЗИСТОРЫ ШОТТКИ СО СВЕРХВЫСОКИМ БЫСТРОДЕЙСТВИЕМ

Исследованы полевые транзисторы с управляющим переходом Шоттки вертикальной структуры на основе SiC/Si с различными длинами каналов. Показано, что повышение быстродействия в широком диапазоне темперпатур (до 70°C) достигается при сверхмалых длинах канала (<100 нм) и термокоррелированном напряжении питания.

Received: 09.12.02

THE ZEEMAN SPLITTING IN KANE TYPE SEMICONDUCTOR WIRE

A.M. BABAYEV
Institute of Physics, Azerbaijan National Academy of Sciences,
370143 Baku, Azerbaijan, e-mail: semic@lan.ab.az

The electronic states of a Kane type semiconductor quantum wire with and without magnetic field are theoretically investigated and compared with those of a quantum wire of the same size. The eigenstates and eigenvalues of the Kane's Hamiltonian are obtained. Numerical calculations are performed for a hard-wall confinement potential and electronic states are obtained as functions of the magnetic field. We calculated the size dependence of the effective *g*-values in bare InSb, GaAs and CdSe nanocrystals. It has been seen that the effective *g*-value of the electrons is decreased with the increasing of quantum wires radius.

1. Introduction

In recent years, there have been many studies about optic properties of quantum nanostructures such as quantum dots, quantum wires, quantum wells and others [1-3]. It is known that the application of a magnetic field could provide additional information about the properties of electrons in solids and in nanostructures. Energy spectrum of carriers in quantum dots and quantum wires, were considered theoretically in [4-8]. In [9] in the absence of magnetic field quantum wire energy spectra and wave functions were obtained for two band Kane model in the case of zero spin orbital interaction and zero magnetic field. The electron energy states were investigated in the uniform magnetic field directed along the quantum wire [4]. In this study the free electron model was used. The energy spectrum was determined as a function of a quantum number m for the finite and infinite potential cases from the boundary conditions. The energy spectrum in the dependent of magnetic field is found to have a minimum for the negative values of quantum number m.

Magneto-optical properties of quantum dots in semiconductors have been considered for the model of hard-wall confinement [6] when the real band structure of InSb-type materials (narrow energy gap and strong spin-orbital interaction) was taken into accaunt. The results of [6] are in a good agreement with the magneto-optical experiments in InSb quantum dots [10]. The effect of quantum confinement and the nanocrystal surface on the *g*-factors are studied in [8] for the ground and excited electron states in bare CdSe and ZnO nanocrystals. The calculation was made by using 8x8 and 14x14 band Kane models second-order $\vec{k}\,.\,\vec{p}$ perturbation theory. The spin-orbital interaction and the contribution of the electrons to the *g* factor were presented in details in [11,12]. For the calculation of the electron *g*-values in [11] the eight-band Kane`s model was used where the nonparabolicity of the electron and light-hole bands and the complex structure of the valence bands had been taken into account simultaneously. This model describes the energy band structure around the Γ point of the Brillouin zone very well. The electron *g*-factor values for quantum wires and quantum dots using the parameters of GaAs/Al_x Ga_{1-x} As hetero-system were calculated by perturbation theory[11]. It was obtained that the *g*-factor is anisotropic ($g_{\parallel} \neq g_{\perp}$) for quantum well and isotropic in cylindrical wire [12].

In this work, using three-band Kane`s model including the conduction band, light and spin-orbital hole bands, the electron spectrum with and without magnetic field and electron effective *g*-factor of quantum wire are calculated. In opposite to [11,1available 2] we take the potential of the quantum wire to be infinitive and consequently the wave functions to be zero at the boundary.

In the eight-band Kane's Hamiltonian the valence and conduction bands interaction is taken into account via the unique matrix element *P* (so called Kane's parameter). The system of Kane equations including the nondispersional heavy hole bands have a from [12, 13]:

$$-EC_1 - \frac{Pk_-}{\sqrt{2}}C_3 + \sqrt{\frac{2}{3}}Pk_z C_4 + \frac{Pk_+}{\sqrt{6}}C_5 + \frac{Pk_z}{\sqrt{3}}C_7 + \frac{Pk_+}{\sqrt{3}}C_8 = 0 \quad (1)$$

$$-EC_2 - \frac{Pk_-}{\sqrt{6}}C_4 + \sqrt{\frac{2}{3}}Pk_z C_5 + \frac{Pk_+}{\sqrt{2}}C_6 + \frac{Pk_-}{\sqrt{3}}C_7 - \frac{Pk_z}{\sqrt{3}}C_8 = 0 \quad (2)$$

$$-\frac{Pk_+}{\sqrt{2}}C_1 - (E+E_g)C_3 = 0 \quad (3)$$

$$\sqrt{\frac{2}{3}}Pk_z C_1 - \frac{Pk_+}{\sqrt{6}}C_2 - (E+E_g)C_4 = 0 \quad (4)$$

$$\sqrt{\frac{2}{3}}Pk_z C_2 + \frac{Pk_-}{\sqrt{6}}C_1 - (E+E_g)C_5 = 0 \quad (5)$$

$$\frac{Pk_-}{\sqrt{2}}C_2 - (E+E_g)C_6 = 0 \quad (6)$$

$$\frac{Pk_z}{\sqrt{3}}C_1 + \frac{Pk_+}{\sqrt{3}}C_2 - (\Delta+E+E_g)C_7 = 0 \quad (7)$$

$$\frac{Pk_-}{\sqrt{3}}\cdot C_1 - \frac{Pk_z}{\sqrt{3}}C_2 - (\Delta+E+E_g)C_8 = 0 \quad (8)$$

Here P is the Kane parameter, E_g - is the band gap energy, Δ - is the value of spin-orbital splitting and $k_\pm = k_x \pm ik_y$, $\vec{k} = -i\vec{\nabla}$.

2. Zero magnetic field

Substituting expressions (3)-(8) into formulas (1) and (2) we obtain:

It needs

$$(-E - \frac{P^2}{3}(\frac{2}{E+E_g} + \frac{1}{E+E_g+\Delta})\Delta_3)C_{1,2} = 0 \quad (9)$$

where Δ_3 three dimensional Laplacian.

In cylindrical coordinates the eigenfunction is

$$C_{1,2} = A_{1,2}\, exp(im\phi + ik_z z)R_{1,2}(\rho) \quad (10)$$

where $A_{1,2}$ is a normalization factor and the radial function $R(\rho)$satisfies

$$\left\{\frac{P^2}{3}(\frac{2}{E+E_g} + \frac{1}{E+E_g+\Delta})\left[\frac{d^2}{d\rho^2} + \frac{1}{\rho}\frac{d}{d\rho} - \frac{m^2}{\rho^2} - k_z^2\right] + E\right\}R_{1,2}(\rho) = 0 \quad (11)$$

The Kane's parameter P is connected with effective mass m_n and can be written in a usual way [15].

$$P^2 = \frac{3\hbar^2}{2m_n}\frac{E_g(E_g+\Delta)}{3E_g+2\Delta} \quad (12)$$

After substitution of the values of P^2 from (12), the equation (11) can be rewritten in the form:

$$\left(\frac{d^2}{d\rho^2} + \frac{1}{\rho}\frac{d}{d\rho} - \frac{m^2}{\rho^2} + \frac{2m_n}{\hbar^2}E'\right)R_{1,2}(\rho) = 0 \quad (13)$$

where

$$E' = \frac{E(E+E_g)(E+E_g+\Delta)(3E_g+2\Delta)}{E_g(E_g+\Delta)(3E+3E_g+2\Delta)} - \frac{\hbar^2 k_z^2}{2m_n} \quad (14)$$

Equation (13) is Bessel's differential equation [16], with the solution bounded at $\rho=0$ being

$$R_{1,2}(\rho) = CJ_m(\chi\rho) \quad (15)$$

where

$$\chi^2 = \frac{2m_n}{\hbar^2}\left(\frac{E(E+E_g)(E+E_g+\Delta)(3E_g+2\Delta)}{E_g(E_g+\Delta)(3E+3E_g+2\Delta)} - \frac{\hbar^2 k_z^2}{2m_n}\right) \quad (16)$$

For an infinite wall at radius R, the boundary condition is $R_{1,2}(R) = 0$, so the eigenvalue equation is

$$J_m(\chi R) = 0 \quad (17)$$

Equations (16) and (17) together show that the radial eigenvalue spectrum is

$$\frac{E(E+E_g)(E+E_g+\Delta)(3E_g+2\Delta)}{E_g(E_g+\Delta)(3E+3E_g+2\Delta)} = \frac{\hbar^2}{2m_n}\frac{z_{mp}^2}{R^2} + \frac{\hbar^2 k_z^2}{2m_n} \quad (18)$$

where z_{mp} is the p-th root of the m-th Bessel function $J(z)$.

Equation (18) determines the energies of electrons, light holes, and the spin-orbit split-off band of holes. This equation can be useful for analyzing the influence of nonparabolicity on the energy spectrum of electrons in a quantum wire.

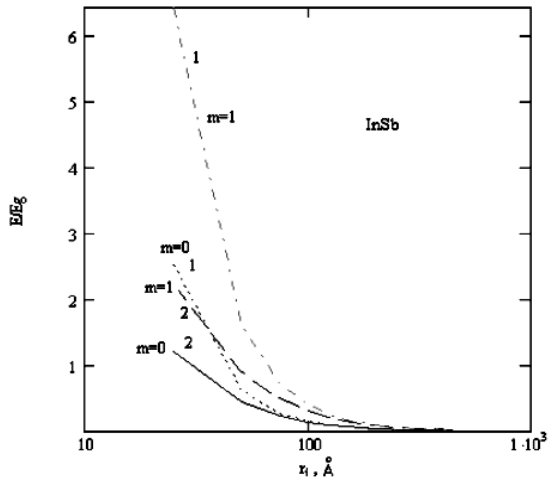

Fig.1. The dependence of the lowest quantum size levels in InSb quantum wire as function of the quantum wire radius. (1) for parabolic dispersion law. (2) for Kane's dispersion law.

In fig.1, the dependencies $E(R)$ for two cases are presented: a) electrons with parabolic dispersion law, b) electrons with Kane's dispersion law for InSb quantum wire. According to this figure, with increase of R, the electron energy levels in both cases are close to each other. At rather small sizes of R, the variance electron dispersion laws become more and more important and therefore, the curves for $E(R)$ keep away from each other.

3. Applied magnetic field, infinite step

The atomic Zeeman splitting is incorporated by adding the terms $\pm\frac{1}{2}g_0\mu_B H$ the diagonal of Kane's Hamiltonian,

μ_B is the Bohr magneton, g_0 is the Lande effective factor. For a uniform magnetic field, H directed along the z axis, the vector potential may be choosen in the form

$$\vec{A} = \frac{1}{2}\left[\vec{H} \times \vec{r}\right] = \left(-\frac{H_y}{2}, \frac{H_x}{2}, 0 \right) \tag{19}$$

and $k_\pm$ have the forms

$$k_\pm \to k_\pm \pm i\frac{1}{2}\lambda_H r_\pm \tag{20}$$

where

$$r_\pm = x \pm iy, \ \lambda_H = \frac{eH}{\hbar c} \tag{21}$$

Substituting expressions (3)-(8) into formulas (1) and (2), and using the (20), (21) relations we obtain:

$$\left(-E_1 + \frac{P^2}{3}\left(\frac{2}{E_1 + E_g} + \frac{1}{E_1 + E_g + \Delta}\right)\left(-\nabla^2 + \lambda_H L_z + \frac{1}{4}\lambda_H^2 \rho^2\right) \pm \frac{P^2 \lambda_H}{3}\left(\frac{1}{E_1 + E_g} - \frac{1}{E_1 + E_g + \Delta}\right) \right) C_{1,2} = 0 \tag{22}$$

where L_z is a z component of in angular momentum operator L, $\rho^2 = x^2 + y^2$ and $E_1 = E \mp \frac{1}{2} g_0 \mu_B H$.

If one seeks the solution of equation (22) in cylindrical coordinates in the form

$$C_{1,2} = A_{1,2}\, exp(im\varphi + ik_z z) exp\left(-\frac{\xi}{2}\right) \xi^{\frac{|m|}{2}} \Phi_{1,2}(\xi) \tag{23}$$

he obtains for the radial function $\Phi(\xi)$ the following equation

$$\xi \frac{d^2\Phi}{d\xi^2} + \left(|m| + 1 - \xi\right)\frac{d\Phi}{d\xi} - \alpha_{1,2}\Phi = 0 \tag{24}$$

Equation (24) is the canonical form of Kummer's equation for the confluent hypergeometric function. In (23) $\xi = \frac{\rho^2}{2l_H^2}$ is the dimensionless variable. The solution of (24) that is bounded at $\rho = 0$ is

$$\Phi(\xi) = M(\alpha_{1,2}, b, \xi) \tag{25}$$

where

$$\alpha_{1,2} = \frac{1}{2} + \frac{m}{2} + \frac{|m|}{2} + \frac{1}{2}k_z^2 l_H^2 - \frac{E_1}{\hbar\omega_c}\frac{(E_1 + E_g)(E_1 + E_g + \Delta)(3E_g + 2\Delta)}{E_g(E_g + \Delta)(3E_1 + 3E_g + 2\Delta)} \pm \frac{\Delta}{2(3E_1 + 3E_g + 2\Delta)} \tag{26}$$

$\omega_c = \frac{eH}{m_n c}$ is the cyclotron frequency, $l_H = \sqrt{\frac{\hbar c}{eH}}$ is the magnetic length and

$$b = |m| + 1 \tag{27}$$

are the parameters of the Kummer function in standard notation. The boundary conditions which correspond to the infinite potential at $\rho = R$ are $C_{1,2} = 0$. These lead to the eigenvalue equations

$$M(\alpha_{1,2}, b, \frac{R^2}{2l_H^2}) = 0 \tag{28}$$

We can find the energy spectrum $E(R, m, l_H, k_z)$ from equation (26). It is necessary for this to find α_1 and α_2 from equation (28) for a given R, azimuthal quantum number m and l_H, and then to substitute them into equation (26). For an infinite medium, $R \to \infty$, equation (28) is replaced by the requirement that M be bounded as $\frac{R^2}{2l_H^2} \to \infty$. This simply means that $\alpha_{1,2}$ is a negative integer [16],

$$\alpha_{1,2} = -l, \ l = 0,1,2,... \tag{29}$$

leading to the result

$$\frac{E_1(E_1 + E_g)(E_1 + E_g + \Delta)(3E_g + 2\Delta)}{E_g(E_g + \Delta)(3E_1 + 3E_g + 2\Delta)} = \left(n + \frac{1}{2}\right)\hbar\omega_c \pm \frac{\Delta}{2(3E_1 + 3E_g + 2\Delta)}\hbar\omega_c + \frac{1}{2}k_z^2 l_H^2 \hbar\omega_c \tag{30}$$

with

$$n = l + m \quad \text{for } m > 0 \tag{31}$$

$$n = l \quad \text{for } m \le 0 . \tag{32}$$

The expression (30) is the same as the expression of the energy spectrums of carriers of bulk Kane type semiconductors in the magnetic field [15].

The magnetic field dependencies of electrons energy spectrum for the lowest sequences of m at the subbands bottom $(k_z=0)$ for InSb quantum wire with R=300Å, in which

the non-parabolicity was taken into account, are shown in Fig.2 (for $g_0=0$).

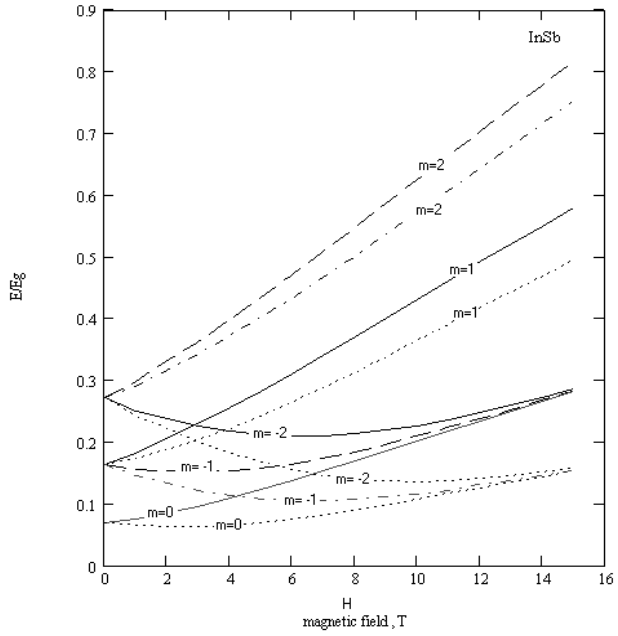

Fig.2. Lowest part of the energy spectrum of electrons as a function of the magnetic field in cylindrical quantum wires for the InSb.

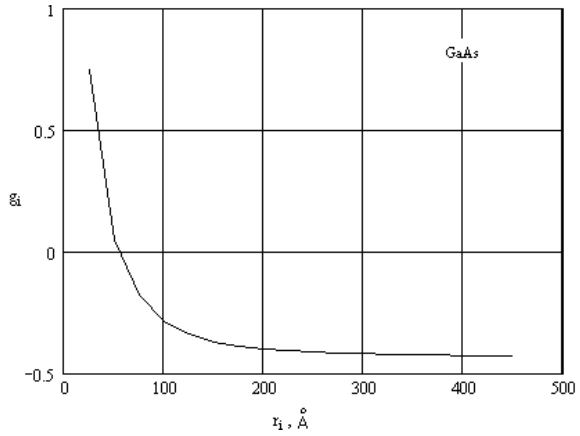

Fig.3. The electron *g* factor calculated as a function of the radius in cylindrical quantum wires for GaAs.

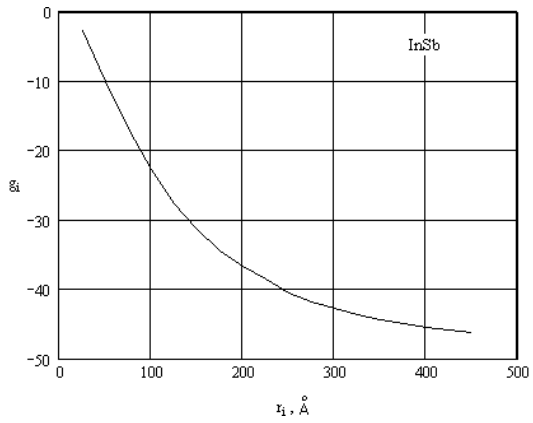

Fig.4. The electron g factor calculated as a function of the radius in cylindrical quantum wires for InSb.

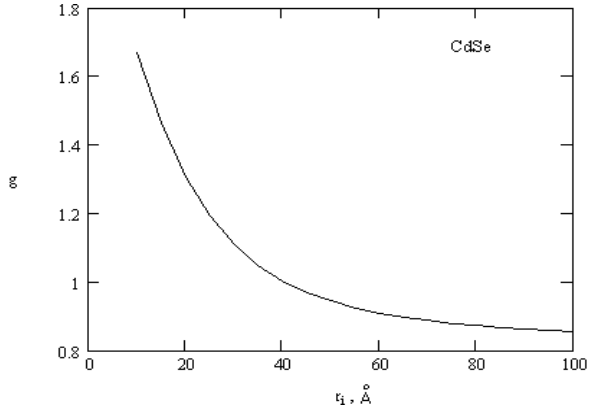

Fig.5. The electron *g* factor calculated as a function of the radius in cylindrical quantum wires for CdSe.

The light hole and spin-orbital splitting subbands can be obtained by the same way for two other roots of equation (26). As it is seen from fig.1 the magnetic field dependence of energy has a minimum only for subbands with the negative *m*. These results are in good agreement with those given in [4].

Note that for the quantum wire with the finite length *d*

$$k_z = \frac{\pi}{d} l \ , l=1,2,3,... \qquad (33)$$

and the minimal value for k_z must be taken as $\frac{\pi}{d}$.

The expression for the *g*-factor obtained in the second order of $\vec{k}.\vec{p}$ perturbation theory has the form [15]

$$g(E) = 2\left[1 + (1 - \frac{m_0}{m_n})\frac{\Delta}{3E + 3E_g + 2\Delta}\right] \qquad (34)$$

But in magneto-optical experiments, transitions from the bottom of the subbands take place and the effective *g*-factor can be determined from the Zeeman splitting of subbands

$$g(E) = \frac{E_\uparrow - E_\downarrow}{\mu_B H} \qquad (35)$$

Here $E_\uparrow$ and $E_\downarrow$ are the electron energy for spin $+z$ and $-z$ directions, respectively. Note that the *g*-factor determined by the equations (34) and (35) are the same if one considers the bottom of the lowest subband.

Figures 3, 4 and 5 show the electron g-factor dependence on *R* calculated by the equation (35) for GaAs, InSb and CdSe quantum wires for the fixed magnetic field value *H=0.5T*, respectively. As seen from fig.3 in GaAs quantum wire, the electron *g* factor value changes its sign with a radius. The following band parameters have been used for GaAs $E_g = 1.52$ *eV*, $\Delta = 0.34$ *eV*, $2p_{cv}^2/m_0 = 28.9$ *eV* (here $p_{cv}=m_0P/\hbar$, m_0 is the free-electron mass) [11]. The contribution of remote bands is taken into account by adding the constant $\Delta g = -0.12$ to the Kane's model values of *g* [12]. This result is also found in [11] for $GaAs/Al_{0.35}Ga_{0.65}$ as structures in the finite barrier case. It is obvious that the same will occur in the case of fixed R with increasing of magnetic field. The figure which shows the *g*-factor dependence on *R*

for CdSe (figure 5) is in good agreement with the reference [8].

It should be noted that the obtained results can be applied to quantum wires of InAs and zero-gap semiconductor HgTe and narrow-gap semiconductor Cd_{1-x} Hg_xTe also.

4. Conclusion

In this work using the eight band Kane's model the electron spectrum with and without magnetic field and electron effective *g*-factor for quantum wire is calculated. It was shown that the effective *g*-factor of electrons decreases with increasing of quantum wires radius and changes its sign for GaAs quantum wires.

The size dependence of the spectra of electrons in A^3B^5 and A^2B^6-type semiconductor cylindrical quantum wires was studied. It was taken into account the nonparabolicity of the spectrum of light holes, electrons and spin-orbit splitting valence band.

[1] *J.I.Alferov*.FTP N1,32, 1, p.3-18, (1998).
[2] *J.I.Alferov*. FTP N4, 32, 1, p.385-410, (1998).
[3] *M.Masale*. Physica E 5 98-107, (1999).
[4] *N.C.Constantinou, M.Masale and D.R.Tiley*. J. Phys:Condens.Matter 4 , 4499-4508, (1992).
[5] *N.C.Constantinou and M.Masale.* Phys. Rev. B 48, 11, 128, (1993).
[6] *W.Zawadski and M.Kubisa*. Semicond.Sci. Technol. 8 , S240-S242, (1993).
[7] *A.Garcia-Cristobal, V.M. Fomin and J.T.Devreese*. Physica B 256-258 190-193, (1998).
[8] *A.V. Rodina, Ai.L. Efros, M. Rosen, B.K. Meyer.* Material Science and Engineering C 19 435-438 (2002).
[9] *Chhi-Chong Wu and Chau-Ju Lin*. J.Appl.Phys 83 (3), 1390-1395, (1998).
[10] *Ch. Sikorski and V. Merkt*. Phys.Rev.Lett 62 ,2164, (1989).
[11] *A.A.Kiselev, E.L. Ivchenko*. Pismo v JETF 67, 1,41-45, (1996).
[12] *A.A.Kiselev, E.L. Ivchenko U.Rössler*. Phys. Rev. B58, 24, 16353-15359, (1998).
[13] *B.M. Askerov*. Kinetic Effects in Semiconductors (Nauka, Leningrad, 1970).
[14] *A.I. Anselm*. Introduction to Semiconductor Theory (Nauka, Moscow, 1978; Prentice-Hall, Englewood.
[15] *B.M. Askerov.* Electron Transport Phenomena in Semiconductors (World Scientific, 1994, Singapur).
[16] *V.M. Galitskii, B.M. Karnakov, V.I. Kogan.* A collection of problems Quantum mechanics Science, Moscow, 1981 (in Russian).
[17] *L.D.Landau and E.M.Lifshitz.* Quantum Mechanics, 1977 Pergamon press Cliffs.

A.M. Babayev

KEYN TİPLİ YARIMKEÇİRİCİ KVANT MƏFTİLLƏRDƏ ZEYMAN PARÇALANMASI

Keyn tipli yarımkeçrici kvant məftillərdə maqnit sahəsində və sahənin sıfır qiymətində elektron halları tapılmış və eyni ölçülü yarımkeçrici kvant məftillin elektron halları ilə müqayisə edilmişdir. Keyn hamiltonianı üçün məxsusi qiymətlər və dalğa funksiyaları tapılmışdır. Ədədi hesablamalarla sonsuz məhdudlaşdırıcı potensial üçün elektronun enerjisinin maqnit sahəsindən asılılığı tapılmışdır. İnSb, GaAs və CdSe nanokristalları üçün elektronların effektiv *g*-faktorunun sistemin ölçüsündən asılılığı hesablanmışdır. Göstərilmişdir ki, ölçü kiçildikcə *g*-faktorun qiyməti artır.

А. М. Бабаев

ЗЕЕМАНОВСКОЕ РАСЩЕПЛЕНИЕ В КЕЙНОВСКИХ ПОЛУПРОВОДНИКОВЫХ КВАНТОВЫХ ПРОВОЛОКАХ

Найдены электронные состояния в кейновских полупроводниковых квантовых проволоках в магнитном поле и в отсутствии поля. Проведены сравнения с обычной полупроводниковой квантовой проволокой того же размера. Получены собственные значения и собственные функции кейновского гамильтониана. Проведены численные расчеты для бесконечного ограничивающего потенциала и найдены электронные состояния в зависимости от магнитного поля. Рассчитаны величины электронного эффективного *g*-фактора в зависимости от размера в наноструктурах полупроводников InSb, GaAs, и CdSe. Показано, что значение эффективного *g*-фактора растет с уменьшением размера квантовой проволоки.

Received: 30.10.12

PRESSURE AND TEMPERATURE EFFECTS ON ELECTRONIC SPECTRA OF $TlGaSe_2$ TYPE CRYSTALS

K.R. ALLAKHVERDIYEV, T.G. MAMMADOV, R.A. SULEYMANOV, N.Z. GASANOV
Institute of Physics of the Azerbaijan National Academy of Sciences
H. Javid ave. 33, Baku, 370143

The deformation effects in electronic spectra of ternary layered $TlGaS_2$, $TlGaSe_2$ and $TlInS_2$ semiconductors are considered. It is shown that the influence of hydrostatic pressure, thermal expansion, variation of composition in solid solutions on the band gap of investigated crystals can be described in the framework of one common model of deformation potentials.

This model is close to that in layered semiconductors of A_3B_6 group and testifies the fact that the main principles of formation of band structure in these two groups of layered crystals are the same.

1. Introduction

The ternary $TlGaS_2$, $TlGaSe_2$ and $TlInS_2$ semiconductors have layered crystalline structure and according to existing data [1-5] all three compounds crystallize to the same monoclinic structure. It's shown that monoclinic structure of these crystals is very close to tetragonal, and due to absence of anisotropy in the layers plane elastic and thermal properties can be treated even in the framework of hexagonal structure [6, 7].

The great number of investigations of ternary compounds concentrates on the phase transitions, which are observed obviously at least in $TlGaSe_2$ and $TlInS_2$ [5, 8]. It's known, that both of these crystals undergo a phase transitions with lowering the temperature from paraelectric phase to incommensurate phase (T_i=216K in $TlInS_2$ and T_i=120K in $TlGaSe_2$) and then to ferroelectric phase (T_c=202K in $TlInS_2$ and T_c=107K in $TlGaSe_2$) with quadrupling of unit cell along the "C" axes.

The influence of phase transitions on different physical properties in particular on the electronic spectra near the absorption edge is studied in various works [8-10]. However, it's difficult to interpret the obtained results because of lack of the model explaining the deformation effects in ternary layered semiconductors (TLS). The construction of such a model is a main goal of present work.

2. The model of deformation potential in ternary layered $TlGaS_2$, $TlGaSe_2$ and $TlInS_2$ semiconductors.

First of all the results of investigations of deformation effects in TLS are summarized below.

1. In [11] the unusual behavior of exciton absorption peak with temperature was observed in $TlGaS_2$: the energy position of exciton peak (E_{exc}) was shifted to the higher energies with increasing temperature in 4,2÷200K range in which exciton absorption peak was observed (fig.1).

Because of lack of appropriate deformation potentials it was not possible to evaluate the contribution of lattice deformation to the temperature dependence of energy gap (E_g) in $TlGaS_2$. In figs. 1 and 2 the temperature dependences of exciton positions in $TlGaSe_2$, $TlGaS_2$ [11], $TlInS_2$ [10], which reflect the E_g *(T)* dependences, and linear expansion coefficients parallel ($\alpha_\parallel$) and perpendicular ($\alpha_\perp$) to the layers plane for all three crystals [7, 12, 13] are shown. As it is seen from fig.1 the E_{exc} *(T)* dependences in $TlGaSe_2$ and $TlInS_2$ are quite different from that in $TlGaS_2$. At the same time the $\alpha_\parallel(T)$ and $\alpha_\perp(T)$ dependences are very close, for example, in $TlGaS_2$ and $TlInS_2$ in the temperature region far from phase transition point in $TlInS_2$ (fig.2).

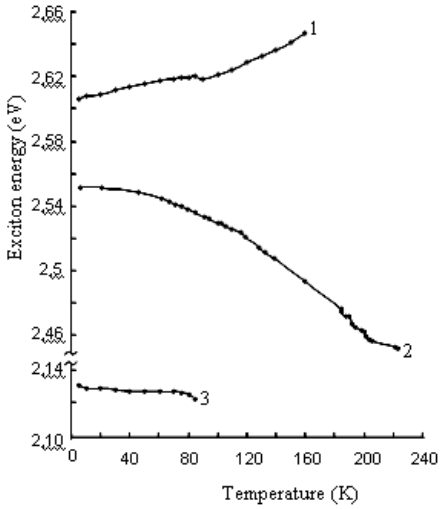

Fig.1. Temperature dependences of exciton energies in $TlGaS_2$ (1) [11], $TlInS_2$ (2) [10] and $TlGaSe_2$ (3) [11].

2. In [8] the influence of hydrostatic pressure on the absorption edge of all three TLS was investigated at room temperature – the results are presented in fig.3. At small pressures (P≤ 0,5GPa) the behavior of band gap with pressure is the same in all crystals: baric coefficient, dE_g/dP, is negative, which is typical for almost all semiconductors with layered structure [14]. With increasing of pressure, however, the behavior of baric coefficients in TLS becomes different.

In $TlInS_2$ dE_g/dP changes the sign at pressures P≥0,59 GPa and remains positive up to P~0,9 GPa. At higher pressures dE_g/dP in $TlInS_2$ again changes the sign and becomes negative but the absolute value of dE_g/dP increases: $dE_g/dP\approx -22\times10^{-11}$ eV×Pa^{-1} ($dE_g/dP=-8{,}5\times10^{-11}$ eV×Pa^{-1} at P<0,59GPa). It's shown in [13, 14], that phase transitions take place in $TlInS_2$ at pressures P~0,59 GPa and P~1,0 GPa.

In $TlGaSe_2$ baric coefficient remains negative up to P~0,92 GPa, $dE_g/dP=-12{,}5\times10^{-11}$ eV×Pa^{-1} . At P>0,92 GPa dE_g/dP stays negative, but $|dE_g/dP|$ increases drastically, $dE_g/dP= -20\times10^{-11}$ eV×Pa^{-1} .

In $TlGaS_2$ $dE_g/dP\approx -7{,}2\times10^{-11}$eV×Pa^{-1} and remains practically unchanged in all investigated range of pressures.

Again, because of lack of deformation potentials it was not possible to interpret the common and different features of baric coefficients behavior in TLS.

3. In [17] the influence of uniaxial, perpendicular to the layers plane, pressure on the exciton absorption peak position in $TlGaS_2$ and $TlGaSe_2$ were investigated at low temperatures, 4,2K<T<100K. Baric coefficients were appeared to be approximately the same in both crystals: $dE_g/dP \approx -3\times10^{-11}$eV×Pa^{-1} in the investigated range of temperatures.

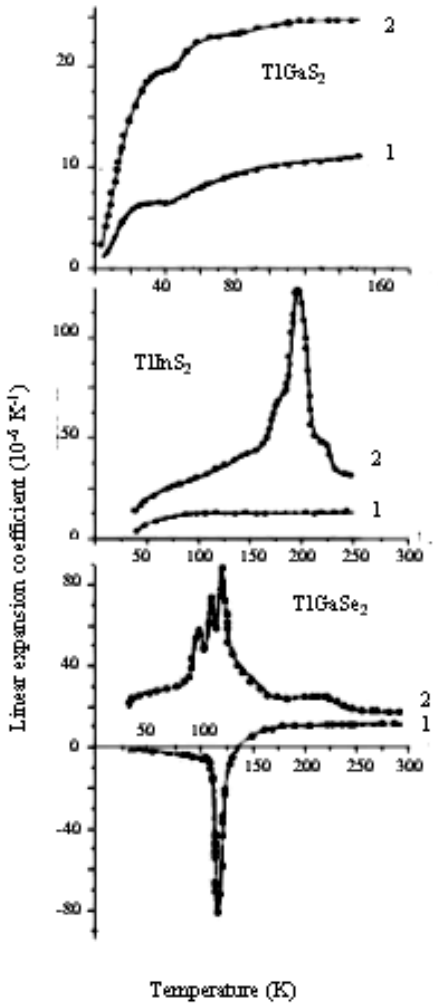

Fig.2. Linear expansion coefficients for $TlGaS_2$, $TlGaSe_2$ and, $TlInS_2$ parallel (1) and perpendicular (2) to the layers plane [7, 12, 13].

We tried to explain all results described above on the basis of a simple model, introducing two deformation potentials $D_\perp$ and $D_\parallel$. In this model the dependence of E_g on deformation is: $\Delta E_g = D_\perp U_\perp + 2D_\parallel U_\parallel$, where $U_\parallel$ and $U_\perp$ deformations in the layers plane and in the perpendicular direction, respectively. Such a model allowed explanation of all types of deformation phenomena in layered semiconductors of A_3B_6 group [14].

For determining the deformation potentials $D_\perp$ and $D_\parallel$ the results of at least two independent deformation experiments are needed. We have chosen the results of influence of hydrostatic pressure on the optical absorption spectra (fig.3). The results of uniaxial deformation experiments which are known for $TlGaS_2$ and $TlGaSe_2$ at low temperatures can not be used because, as it was shown in A_3B_6 group layered crystals, the deformation potential $D_\perp$, may depend strongly on temperature and pressure.

Supposing that $TlInS_2$, $TlGaSe_2$ and $TlGaS_2$ have close deformation potentials and using the results of hydrostatic pressure influence on E_g at low pressures ($P \leq 0{,}5$GPa) the deformation potentials, $D_\parallel$ and $D_\perp$, were obtained. The data for $TlInS_2$ and $TlGaSe_2$ were used because only for these crystals the values of elastic constants are known [6] (table 1). By calculating $D_\parallel$ and $D_\perp$ in $TlInS_2$ and $TlGaSe_2$ we used the value of elastic constant $C_{13}=1{,}5\text{x}10^{10}$ Pa which is almost the same in the majority of layered crystals [14]. This elastic constant was not measured in $TlInS_2$ and $TlGaSe_2$ because of significant experimental difficulties that always appear measuring this elastic constant in layered crystals. Simple calculations [14] give the values: $D_\parallel$=-7,3eV and $D_\perp$=11,9eV. Below we'll explain the results of other deformation experiments on the basis of obtained values of $D_\parallel$ and $D_\perp$.

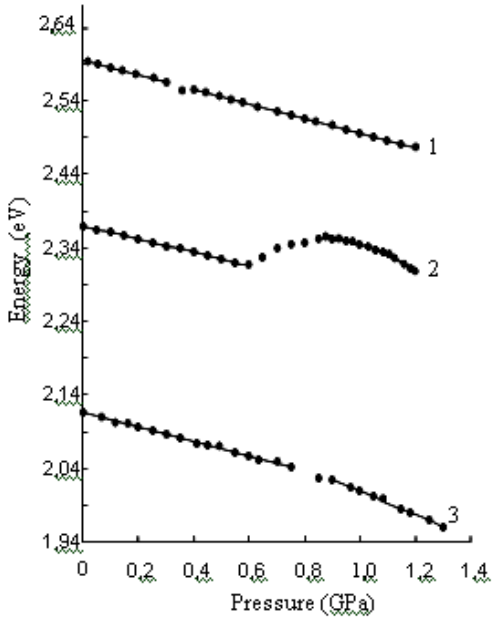

Fig.3. Pressure dependences of energy gaps obtained from absorption edge behavior with pressure at 300K in $TlGaS_2$ (1), $TlInS_2$ (2) and $TlGaSe_2$ (3) [8].

Using the thermal expansion curves (fig.2) the contribution of thermal expansion to $E_g(T)$ dependences can be obtained for all three crystals:

a) in $TlGaS_2$ this contribution gives $\Delta E_g \approx +20$meV in 4.2÷100K temperature range;

b) in $TlGaSe_2$ this contribution must lead to ΔE_g=+25meV due to small linear expansion in the layers plane, $\alpha_\parallel$;

c) the positive shifts of ΔE_g =+25meV with temperature must be in $TlInS_2$ in the same temperature region.

As it is seen from experimentally measured E_{exc} dependences (fig.1) the results of calculations are appeared to be true only for $TlGaS_2$ - in $TlGaSe_2$ and $TlInS_2$ E_{exc} decreases with temperature. However, it can be shown, that this discrepancy between calculations and experiment are not due to the method used for the calculation of $D_\parallel$ and $D_\perp$. Really, as it was noted above, unlike $TlGaS_2$, both $TlGaSe_2$ and $TlInS_2$ are in ferroelectric phase at 4,2-100K due to phase transitions, which they underwent when temperature became lower. It is shown in [11] that addition of sulfur into $TlGaSe_2$ in $TlGaSe_{2(1-x)}S_{2x}$ solid solutions leads to $E_g(T)$ dependences which are typical for $TlGaS_2$ beginning from x=0,1. At the same time there are no evidences of phase transition typical for $TlGaSe_2$ in solid solutions $TlGaSe_{2\,(1-x)}\,S_{2x}$ at x≥0,25 [18].

Thus, unusual behavior of $E_g(T)$ in $TlGaS_2$ and $TlGaSe_{2(1-x)}S_{2x}$ with $x \geq 0,1$ are typical for crystals without phase transitions and deformation potentials $D_{\|}$ and $D_{\perp}$ obtained above are true for $TlGaS_2$ and paraelectric phases of $TlInS_2$ and $TlGaSe_2$.

The other type of deformation effects is the change of band gap in $TlGaSe_{2(1-x)}S_{2x}$ solid solutions, where the changing of lattice parameters can be interpreted as effective lattice deformation. Using the lattice parameters of $TlGaSe_2$ and $TlGaS_2$ (table 1) and deformation potentials $D_{\|}$ and $D_{\perp}$ the change of E_g very close to experimental value can be found: ΔE_g=450meV. Thus, deformation potentials $D_{\|}$ and $D_{\perp}$, obtained above, can describe the results of at least four independent deformation experiments.

Table 1.
Lattice parameters and elastic constants in $TlGaS_2$, $TlGaSe_2$ and $TlInS_2$.

Crystals	Lattice parameters, Å [1-3]			Values of elastic constants, 10^{10}Pa [6]			
	a	b	c	C_{11}	C_{12}	C_{33}	C_{44}
$TlGaS_2$	10,29	10,29	15,28	-	-	-	-
$TlGaSe_2$	10,77	10,77	15,64	6,42	3,88	4,37	0,5
$TlInS_2$	10,95	10,95	15,14	4,49	3,05	3,99	0,5

As it was shown in [14] the deformation potentials obtained at room temperatures and low pressures cannot be used determining the energy shifts at low temperatures, and high pressures in layered crystals of A_3B_6 group. The same seems to be true also for TLS. For example, using the $D_{\|}$ and $D_{\perp}$obtained above the values $dE_g/dP \approx 34\times10^{-11}$eV×Pa^{-1} for $TlGaSe_2$ and $dEg/dP \approx -41\times10^{-11}$eV×Pa^{-1} for $TlInS_2$ are obtained for uniaxial perpendicular to the layers plane pressures instead of experimentally obtained value $dE_g/dP \approx -3\times10^{-11}$eV×Pa^{-1} for low temperatures. To explain the significant changes of baric coefficients with pressure in $TlInS_2$ and $TlGaSe_2$ one must also suppose that deformation potentials strongly depend on pressure. As in the case of layered crystals of A_3B_6 group to explain the discrepancy between experimental results and calculations, it should be assumed that deformation potential $D_{\perp}$, describing the energy shifts at deformations perpendicular to the layers plane decreases (or even changes its sign from positive to negative) with the lowering of the temperature or pressure increasing.

The nature of such a behavior of deformation potential $D_{\perp}$ is due to peculiarities of the band structure of layered crystals of A_3B_6 group. According to band structure calculations [14] interlayer interaction leads to splitting of the top of valence band and bottom of conduction band of layer crystal. Under deformation when interlayer distances decrease, splitting increases and leads to decrease of E_g. On the other hand the compression of layers in both directions leads to increase of E_g. Thus the final change of band gap depends on two competitive parts having opposite signs. Since the interlayer forces increase faster than intralayer ones with temperature lowering or pressure increasing the baric coefficient may decrease by absolute value or even change the sign from negative to positive with temperature or pressure. For example, the baric coefficients for direct gaps in A_3B_6 group layered crystals change the signs from negative to positive with temperature lowering ($T \leq 77$K) and pressure increasing ($P \geq 0,5$GPa). At the same time the baric coefficients for indirect gaps in A_3B_6 group crystals do not change the signs and remain negative but the absolute values of baric coefficients decrease significantly as described above for TLS for uniaxial pressures at low temperatures. So, as it's seen from obtained results the deformation phenomena in TLS and layered crystals of A_3B_6 group have many common features.

3. Conclusion

The deformation potentials $D_{\|}$ and $D_{\perp}$ obtained above for TLS $TlGaSe_2$, $TlInS_2$ and $TlGaS_2$ have allowed making following conclusions:

1. Deformation effects in TLS are very close to that observed in layered semiconductors of A_3B_6 group:

a) deformation potentials $D_{\|}$ and $D_{\perp}$ have the opposite signs, and behavior of band gap E_g under pressure depends on two competitive contributions: positive one due to contraction of layers and negative one due to contraction of interlayer distances ;

b) deformation potential $D_{\perp}$ depends on pressure and temperature due to different behavior of elastic constants determining the deformation of layered crystals parallel and perpendicular to the layers plane.

The similarity of deformation effects in TLS and A_3B_6 group crystals leads to the conclusion that the band structures of these two types of crystals have the following common feature: E_g decreases when the interlayer distances decrease and E_g increases when intralayer distances decreases.

2. At low pressures (P<0,5 GPa) and room temperature all three investigated crystals have the close band structures and deformation potentials. The differences in contribution of thermal expansion to $E_g(T)$ dependences in $TlInS_2$ and $TlGaSe_2$ on one hand, and in $TlGaS_2$ on the other hand are due to phase transitions, which take place in $TlInS_2$ and $TlGaSe_2$ with temperature. The different behavior of baric coefficients with pressure may be due to different degree of elastic anisotropy and also to the phase transitions in $TlInS_2$ and $TlGaSe_2$ at high pressures.

3. It was mentioned above in introduction that according to the literature phase transitions that take place with temperature in $TlInS_2$ and $TlGaSe_2$ have the same natures. However, as it can be seen from fig.2 the deformation of lattices with temperature in the layers plane is quite different and phase transitions reveal itself in different way in $TlGaSe_2$ and $TlInS_2$. The analogous conclusion was made in [19] investigating the temperature dependences of elastic constants in $TlGaSe_2$ and $TlInS_2$: near phase transition points the elastic constants in $TlInS_2$ and $TlGaSe_2$ behave in somewhat different way. The pressure dependences of baric coefficients in $TlGaSe_2$ and $TlInS_2$ also demonstrate differences at pressures when phase transitions in both crystals take place. Though it's difficult to interpret the nature of such differences, one can conclude that baric coefficients behavior with pressure also testifies the differences in the nature of phase transitions in $TlInS_2$ and $TlGaSe_2$.

[1] *D. Muller, F.E. Poltmann, H. Hahn*. Naturforschung, 1974, v.29B, pp.117-118.

[2] *D. Muller, H. Hahn.* Anorg. Allg. Chem., 1978, v.43B, N1, pp.258-272.

[3] *K.R. Allakhverdiev, T.G. Mamedov, B.G. Akinoglu, Sh.S. Ellialtioglu*. Turkish J. of Phys., 1994, v.18, N1, pp.1-66.
[4] *W. Henkel, H.D. Hochheimer, C. Carlone, A. Werner, S. Ves, H.G. Schnering.* Phys.Rev.B, 1982, v.26, N6, pp.3211-3221.
[5] *K.A. Yee, T.A. Albright*. J. Am. Chem. Soc., 1991, v.113, p.6474.
[6] *R.A. Suleymanov, M.Yu. Seidov, F.M. Salaev*. Sov. Phys. Solid State, 1991, v.33, N6, pp.1797-1800.
[7] *N.A. Abdullayev, T.G. Mamedov, R.A. Suleymanov*. J. Low Temp. Phys, 2001, v.27, p.676.
[8] *K.R. Allakhverdiev, T.G. Mamedov, V.V. Panfilov, M.M. Shukyurov, S.I. Subbotin*. Phys. Status Solidi b, 1985, v.131, pp.k23-k28.
[9] *K.R. Allakhverdiev, M.A. Aldzanov, T.G. Mamedov, E.Yu. Salaev*. Solid State Commun., 1986, v.58, N5, pp.295-297.
[10] *K.R. Allakhverdiev, S.S. Babayev, N.A. Bakhyshov, T.G. Mamedov, E.Yu. Salaev*. Sov. Phys. Semicond, 1984, v.18, p.1307.
[11] *S.G. Abdullayeva, G.L. Belenkii, N.T. Mamedov*. Phys. Status Solidi b, 1980, v.102, p.19.
[12] *G.L. Belenkii, S.G. Abdullayeva, A.V. Solodukhin, R.A. Suleymanov*. Solid State Commun., 1982, v.44, p.1613.
[13] G.*L. Belenkii, T.G. Mamedov, N.A. Abdullayev, K.R. Allakhverdiev, R.A. Suleymanov, Ya.N. Sharifov*. Solid State Commun., 1985, v.53, p.601.
[14] *G.L. Belenkii, E.Yu. Salaev, R.A. Suleymanov*. Sov. Phys.- Uspekhi, 1988, v.155, p.89.
[15] *K.R. Allakhverdiev, A.I.Baranov, T.G.Mamedov,V.A.Sandler, Ya.N. Sharifov*. Sov. Phys. Solid State, 1988, v.30, 751.
[16] *E. Bairamova, K.R. Allakhverdiev, B.G. Akinoglu, T. Arai, T.G. Mamedov*. Turkish J. of Phys., 1994, v.18, p.497.
[17] *S.G. Guseynov, G.D. Guseynov, N.Z. Gasanov, S.B. Kyazimov*. Phys. Status Solidi (b), 1986, v.133, N1, pp.k25-k30.
[18] *A.A. Volkov, Yu.B. Goncharov, G.V. Kozlov, K.R. Allakhverdiev, R.M. Sardarly*. Sov. Phys – Solidi State, 1984, v.26, p.2754.
[19] *Yu.V. Ilisavskii, V.M. Sternin, R.A. Suleymanov, F.M. Salaev, M.Yu. Seyidov*. Sov. Phys.- Solidi State, 1991, v.33, N1, pp.104-109.

K.R. Allahverdiyev, T.Q. Məmmədov, R.A. Süleymanov, N.Z. Həsənov

$TlGaSe_2$ TİPLİ KRİSTALLARININ ELEKTRON SPEKTRLƏRİNƏ TƏZYİQ VƏ TEMPERATURUN TƏSİRİ

$TlGaS_2$, $TlGaSe_2$ və $TlInS_2$ üçqat laylı yarımkeçiricilərin elektron spektrlərində deformasiya effektlərinə baxılmış və göstərilmişdir ki, hidrostatik təzyiqin, temperatur genişlənməsinin və bərk məhlulların tərkibinin dəyişilməsinin tədqiq olunan kristalların qadağan olunmuş zonasına təsiri deformasiya potensialının ümumi modeli çərçivəsində təsvir oluna bilər.

Məlum olmuşdur ki, göstərilən model A_3B_6 qrupun laylı yarımkeçiriciləri üçün deformasiya potensialları modelinə yaxındır. Bu isə onu göstərir ki, hər iki qrup laylı kristalların zona strukturlarının əsas formalaşması prinsipləri eynidir.

К.Р. Аллахвердиев, Т.Г. Мамедов, Р.А. Сулейманов, Н.З. Гасанов

ВЛИЯНИЕ ДАВЛЕНИЯ И ТЕМПЕРАТУРЫ НА ЭЛЕКТРОННЫЕ СПЕКТРЫ КРИСТАЛЛОВ ТИПА $TlGaSe_2$

Рассмотрены деформационные эффекты в электронных спектрах тройных слоистых полупроводников $TlGaS_2$, $TlGaSe_2$ и $TlInS_2$. Показано, что влияние гидростатического давления, температурного расширения, изменения состава твердых растворов на ширину запрещенной зоны исследуемых кристаллов может быть описано в рамках общей модели деформационных потенциалов.

Оказалось, что указанная модель близка к модели деформационных потенциалов для слоистых полупроводников группы A_3B_6. Это свидетельствует о том, что основные принципы формирования зонной структуры этих двух групп слоистых кристаллов одни и те же.

Received: 27.12.02.

RESONANT INTERACTION OF ULTRASOUND WAVE WITH ELECTRONS IN QUANTUM WIRE

G.B. IBRAGIMOV
Institute of Physics of the Azerbaijan National Academy of Sciences
H. Javid av. 33, Baku, 370143

The effects of possible resonance interaction ultrasound wave with electrons in the parabolic quantum well wires have been studied. The intersubband transition probability of electrons under the influence of the sound wave have been calculated.

In the ultra-thin semiconducting wires (submicron dimensions) usually called quantum well wires, carriers are quantized in two transverse directions and move only along the wire and they behave as a quasi-one-dimensional (Q1D) electron gas. Size quantization of levels of electrons and holes brings about the splitting of conduction band and valence band into the subbands separated by energies of the dimensional quantization. Due to such splitting a number of physical properties of a Q1D electron gas differ from the property of its three-dimensional analog [1-7]. Magnetophonon resonances [2] and effects of resonant intersubband optical-phonon scattering [3] in Q1D systems is well developed.

In this communication we present the effects of possible of resonant interaction of ultrasound wave with electrons of a quantum wire with parabolic wells. We consider a Q1D electron gas confined in a wire of sizes L_x=L, L_y,L_z. The lateral restriction in the y direction is modeled by parabolic potential of frequency ω and that in the Z direction with a triangular well. We will consider electron densities such that only the lowest subband with energy E_z^0 is occupied in the Z direction. The corresponding wave function is denoted by $\Psi_0(z)$. The electrons are free in the wire direction.

Electron wavefunction depending on time in quantum wire in the presence of the sound field satisfies the Schrödinger equation

$$i\hbar\frac{\partial\psi(r,t)}{\partial t}=(H_0+H_1)\psi(r,t) \tag{1}$$

with

$$H_0=\frac{p^2}{2m^*}+\frac{m^*\omega^2y^2}{2}+H(z),$$

$$H_1=\frac{1}{2}V_c\left[e^{iqx}e^{-i\omega t}+e^{-iqx}e^{i\omega t}\right],\quad V_c^2=\frac{2IE_c^2}{\rho_0\upsilon_s^3} \tag{2}$$

Where H_0 is an unperturbed Hamiltonian of electron in the quantum wires, ω is a frequency of the parabolic potential, E_d is the deformation potential, I is sound wave intensity, ρ is a crystal density, $\omega_q=q\upsilon_s$, where q, υ_s are wave number and velocity of the sound wave, respectively.

We assume that, the sound wave can cause the transition of an electron between the first subband (n=1) and the second subband (n=2). Therefore, in the resonant approximation the eigenfunctions $\Psi(r,t)$ of Hamiltonian H_0+H_1 can be expressed as a superposition of wave function for n=1 and n=2 subband [8]

$$\psi(t)=\sum_k[a_2(k,t)\psi_2\exp(-\frac{iE_2t}{\hbar})+a_1(k,t)\psi_1\exp(-\frac{iE_1t}{\hbar})] \tag{3}$$

where electron wave function Ψ_n and energy eigenvalue E_n in the case of parabolic quantum well wires are well-known [1]

$$E_n=\hbar\omega(n+\frac{1}{2})+\frac{\hbar^2k^2}{2m^*}+E_z^0,$$
$$\psi_n=\sqrt{1/L}H_n(y)e^{ikx}\psi_0(z), \tag{4}$$
$$n=1,2,...,$$

$$\psi_0(z)=z(b_0^3/2)^{1/2}\exp(-b_0z/2),$$
$$\langle L_z\rangle=3/b_0$$

Here $|a_1|^2$ and $|a_2|^2$ are probability of finding electrons in n=1 and n=2 subbands, respectively, $H_n(y)$ is a Hermite polynomial. Inserting Eq.(3) into Eq.(1), we obtain the following equations for a_1 и a_2:

$$i\hbar\frac{\partial a_2}{\partial t}=\lambda a_1(k-q_x)\exp[\frac{i}{\hbar}2\xi(k)t]$$
$$i\hbar\frac{\partial a_1}{\partial t}=\lambda^* a_2(k+q_x)\exp[-\frac{i}{\hbar}2\xi(k+q_x)] \tag{5}$$

with

$$2\xi(k)=\hbar(\omega-\omega_q)+\frac{\hbar^2k^2}{2m^*}-\frac{\hbar^2(k-q_x)^2}{2m^*} \tag{6}$$

$$\lambda^2=\frac{u^{1/2}IE_c^2e^{-u}[L_1^l(u)]^2}{4\rho_0\upsilon_s^3}. \tag{7}$$

where $u = q_y^2 l_\omega^2 / 2$, $l_\omega^2 = \hbar / m^* \omega$, L_n^p – Laguerra polynomial.

Passing in (5), to new variables α_1 and α_2 by the formulae.

$$a_2 = \alpha_2 \exp(\frac{i}{\hbar}\xi t) \qquad a_1 = \alpha_1 \exp(-\frac{i}{\hbar}\xi t) \tag{8}$$

we receive a system of he equations.

$$i\hbar\frac{\partial\alpha_1}{\partial t} + \alpha_1\xi = \lambda^*\alpha_2 \qquad i\hbar\frac{\partial\alpha_2}{\partial t} - \alpha_2\xi = \lambda\alpha_1 \tag{9}$$

From (9) it follow [8], that if at t=0, electron was in n=1 subband, probability of the transition to the n=2 subband oscillates with time by the formula

$$|\alpha_2|^2 = \frac{|\lambda|^2}{|\varepsilon|^2} sin^2[\frac{\varepsilon t}{\hbar}] \tag{10}$$

where $\varepsilon = \sqrt{\xi^2 + \lambda^2}$. Thus, $|a_2|^2$ is a periodic function of time varying from zero up to λ^2/ε^2 with frequency $\varepsilon/\hbar$. It means, that in a strong sound field electron makes the transition between the next subband with frequency $\varepsilon/\hbar$. Notice that the at ξ =0 (exact resonance) the transition probability

$$|\alpha_2|^2 = \sin^2[\frac{\lambda t}{\hbar}] \tag{11}$$

varies from zero up to unit with frequency $\lambda/\hbar$. Such character of transitions reflects coherency of interaction of electrons with a sound field, which shows itself under the condition that, if the frequency of transitions λ surpasses frequency of collisions electrons $1/\tau$, i.e. $\lambda\tau/\hbar >> 1$.

For a quantum wire such as GaAs/AlGaAs: E_c=7 eV, ρ_0=5.37 g/cm^3, υ_s=5.3·10^5 cm/c, q_x=10^{6}cm^{-1}, at I=1Вт/cm^2 (quite achievable meaning of sound energy flow [9]) we receive λ= 3·10^{-3} eV . Thus, coherency of interaction of electrons with a sound can expose itself at

$\tau \geq$ 10^{-12}c, that is quite real.

Acknowledgements: The author would like to thank M.I.Aliev and F.M. Gashimzade for helpful discussions.

[1] *P.Vasilopoulos, F.M. Peeters.* Phys.Rev.B v.40, p.10079-10087, (1989).
[2] *P.Vasilopoulos, P.Warmenbol, F.M. Peeters, and J.T. Devrese.* Phys.Rev.B v.40, p.1810-1816, (1989).
[3] *D. Jovanovic, S. Briggs, and J.P. Leburton.* Phys.Rev.B v.42, p.11108-11113, (1990).
[4] *V.D. Shadrin and F.E. Kistenev* J. Appl.Phys., v.75, p.985-988, (1994).
[5] *C.C. Wu and C.J.Lin.* J.Appl.Phys.83, p.1390, (1998).
[6] *G.B. Ibragimov.* J.Phys.: Condens.Matter, v.14, p.8145-8152, (2002)
[7] *G.B. Ibragimov.* Phys. Stat. Sol.(b), v. 235, (2003).
[8] *V. M. Galickiy, V.F. Elesin*. Resonant interaction of electromagnetic fields with semiconductors. M., 1986, p.192.
[9] *A.A. Abricosov.* Basis of the theory of metals M., 1987. p.520.

H.B. İbrahimov

ULTRASƏS DALĞALARI İLƏ KVANT NAQİLİN ELEKTRONLARININ REZONANS QARŞILIQLI TƏSİRİ

Ultrasəs dalğaları ilə parabolik çuxurlu kvant naqilin elektronlarının rezonans qarşılıqlı təsirinin mümkünlüyü göstərilmişdir. Güclü səs dalğaları sahəsində elektronların qonşu altzonalar arası keçidin ehtimalı hesablanmışdır.

Г.Б. Ибрагимов

РЕЗОНАНСНОЕ ВЗАИМОДЕЙСТВИЕ УЛЬТРАЗВУКА С ЭЛЕКТРОНАМИ КВАНТОВОЙ ПРОВОЛОКИ

Показана возможность резонансного взаимодействия ультразвука с электронами квантовой проволоки с параболическими ямами. В сильном звуковом поле вычислена вероятность перехода электронов между соседними подзонами.

Received: 27.12.02

OPTICAL PROPERTIES OF $LiNbO_3$. PART ONE.

TALAT R. MEHDIYEV
Institute of Physics, National Academy of Sciences of Azerbaijan
370143, Baku, pr. H. Javid, 33

Optical spectrum and spectrum of scattering of lithium niobate of doped 0.03 % by impurity Fe in requirements of impulse excitation by the second harmonic of radiation (532 nm) the laser are observationally investigated YAG:Nd with the continuous illumination from He-Ne the laser (632.8 nm). Presumable theoretical interpretation of the obtained experimental outcomes is given.

1. Introduction

Lithium niobate remains one of most attractive materials with wide spectrum importance technical applications: holographic storage systems, optic components and devices for telecommunications, conversations and processing information, for integrated optics. These applications depend on the photorefractive effects, that are related to the occurrence of some impurities or structural defects acting as donors or acceptors, another words, composition of lithium niobate has contain large deflection from stoichiometry in the direction of deficit Li, that lead to increase thermo-, photorefractive effects. For example, thermal expansions, band gap, UV-luminescence, OH^--vibrational bands in H-doped crystals and etc. have been found to depend from Li/Nb ratio. In present time, wide propagation received "Li – vacancies" and "Nb – vacancies" models, but more experimental results show, that "Li – vacancies" model is more preferable.

The photorefractive effect in $LiNbO_3$ can drastically to enhance by doping with transition metals (for example Fe and Cu being the most widely used ones). While the leading role of these dopants in this as well as the dominance of photovoltaic currents over diffusion and drift processes has been studied intensively, for example in the publications [1]. A detailed description of microscopic mechanisms steering the photorefractive effect is still pending.

The ground limitation for using of lithium niobate crystals in holography bound up with lifetime holograms after process of thermal fixing. In [2,3] was assumed probable methods optimization parameters of process for crystals with concrete ionic concentrations and their ratio to receive maximal values lifetime for high diffraction efficiencies holograms.

In generally, model of process can be describing so: electrons are exciting with light in the determine regions of crystal's volume can be capture on the deep energies levels, so that in process of recording hologram will have been fixing the periodic distribution of intensities interference of waves. We will be receiving "sinusoidal relief" of the occupation the traps, i.e. so name electronic matrix". Following step is process of thermal fixing hologram. It is bound up with thermal heating of crystal, ion current is began dominant, screening of "electronic matrix" and arise non-photosensitive "ionic matrix". Following cooling of crystal to initial temperature and illumination with equipartition intensity light are leaded the process to equalize electronic occupation.

The problem of gratings dynamics extensively considered in [4-5]. However, more questions remain now as before unsolved problems.

The crystal structure of lithium niobate was study in [6-7]. It was determined space group symmetry – *R3c*, hexagonal cell contain six formulas of units and parameters of low-level cell of crystal: c=13.836±0.0004*Å*; a = 5.14829±0.00002*Å*.

A model of the transition of lithium niobate from paraelectric to ferroelectric phase was proposed by [6-8]. In the phase transition, the sublattices of positive ions of Li and Nb displaced relative to the sublattice of oxygen anions. The direction of the displacement of the cations determines the direction of the spontaneous polarization vector, in the ferroelectric phase [0001]. In [8] authors have pointed out that it is position of the metal ions in the structure of the ferroelectric phase that gives rise to dipole moment. At temperature Curie point, where may occur two opposite directions of displacement for metal ions, which correspond to 180° electrical domains. It has been suggested that between the positive and negative ends of crystal by means of etching or from the intensity x-ray reflections. The negative end its x-ray reflection is less distinct. In order to change the polarization of single-domain crystals it is necessary to allow the ions of niobium and lithium to pass through the oxygen layers. At high (1423) this distance is larger than the sum of radii of the ions Li and O.

Composition of lithium niobate crystal can be to represent in form: $(LiNbO_3)_{0.941}(Nb_{Li}NbO_3)_{0.0118}(V_{Li}NbO_3)_{0.0472}$, where first component is usual lithium niobate, second – antisite defects and third – cation vacancies. Usually, lithium niobate crystals are grown with congruent composition Li/Nb ~0.94. Lattice defects stern from non-stoichiometry composition of the crystal and caused occupation Li-locations with Nb and others atoms. Nb_{Li} are most probable electron shallow traps and V_{Li} – are probably hole traps.

One of very importance singularity lithium niobate, which determine optical properties of crystal, is fact, that bounds (O^{2-}-Nb^{5+}) has mainly covalent and (O^{2-}-Li^{+}) - ionic characters. Radii of ions Nb^{5+} and Li^{+} are practically equal. All current models of defects as-grown agree that part of the Li - sites are filled up by excess Nb^{5+} ions accommodate Li deficiency. In original models [15] each Nb_{Li} antisite compensated by four Li vacancies, which are potential hole traps.

Defects of type (Nb_{Li} - Nb_{NB}) with $d \sim 3$*Å* are placed in direction along C_3 – axis. Concentration of defects is approximately 2 10^{20}cm^{-3} and $c_{V_{Li}}$ ~$8\cdot10^{20}$cm^{-3}. Capture one of electrons on (Nb_{Li} - Nb_{NB}) defects (one-electron localization) make "small" polaron (Nb_{Li}^{4+} - Nb_{Nb}^{5+}) with optical band absorption near 1.64 eV. Accordingly, capture two electrons on this defect make Gaitler-London's bipolaron with optical band absorption from 1.7 to 4 eV. Authors of publication showed, that for description optical spectra's of absorption in the interval energies higher than 2.5 eV also need assumption defects of type (Nb_{Li} - Nb_{Li}), minimal

distance is 3.76 *Å*, concentration of defects is ~$6\cdot10^{18}$cm^{-3}. However, computer simulation of bipolaron state (Nb_{Li}^{4+} - Nb_{Li}^{4+}) showed, that this defects do not contribute into optical spectrum for energies high 2.3 eV. In other side, four-electron defect $\begin{pmatrix} Nb_{Nb}^{4+} - Nb_{Nb}^{4+} \\ Nb_{Li}^{4+} - Nb_{Li}^{4+} \end{pmatrix}$, in which on each ions Nb accordance one non-degeneration level and Hamiltonian describe through "four nodes Hamiltonian" in four-electron basis, well explain and describe singularities optical spectrum of lithium niobate crystal for energies high 2.5 eV (model Q-polaron). [19]

Follow type of defects bound up with OH^-, which in $LiNbO_3$ may have two forms: impurity complex and molecular ion. The OH- absorption and Raman-scattering spectrums of congruent, pure and nearly stoichiometric $LiNbO_3$ crystals investigated in publications [16]. Maximum by the 3466 cm^{-1} considered to relate to the stretching vibration of OH^- for protons directly substituted for Li^+ ions and located at 3.36Å (O-O) bonds in oxygen triangles nearest to the Li –site. Maximums by the 3481cm^{-1} and 3486 cm^{-1} are also due to OH^- in 3.36Å (O-O) bonds, but protons suggested occupying V_{Li}^- near Nb_{Li}^{5+}. Two different ions environment around V_{Li}^- are cause these two absorption maximums. Distance (O-H) is near 0.9896Å, concentration c_{OH^-} is approximately $10^{16}\div10^{18}$ cm^{-3}, energy of thermal activation is 1.23 eV for $LiNbO_3$ and 1.17 eV for $LiNbO_3$: Fe. [20]

The transport properties in crystal $LiNbO_3$ are of major relevance in connection with the hydrogen doping processes, ionic conductivity, photorefractive fixing etc. Although proposal was first made about possible OH^--molecular migration to explain proton diffusion, in [17] had found a strict proportionality between the proton concentration and conductivity up a similar temperature. H^+ ions are occupying Li-vacancies.

Role donors and traps of electrons in $LiNbO_3$: Fe is ions Fe^{2+} and Fe^{3+}, respectively, [18] and they are deeper then Nb_{Li}^{4+} and Nb_{Li}^{5+} with respect to condition band edge.

Summarizing the XSW measurements, the lattice position for an assumed single – site occupancy of Fe atoms in $LiNbO_3$ structure is determined to be (0.18±0.07) Å above the ferroelectric Li –site in direction of "c" axis of crystal. However, due to the systematic differences in coherent fractions for $(00\bar{6})$ and $(1\bar{1}4)$measurements, spread of positions in range up to ±0.7Å is conceivable.

Thermal reduction of lithium niobate with iron used to change the charge state of the impurity and so adjust the ration between concentrations Fe^{2+} and Fe^{3+} states. Usually ratio is $c_{Fe^{2+}}/c_{Fe^{3+}} \approx 0.05$ for case $c_{Fe} \approx 56\cdot10^{18}$cm^{-3} and $c_{Fe^{2+}} \approx 2.5\cdot10^{18}$cm^{-3}, where $c_{Fe} = c_{Fe^{2+}} + c_{Fe^{3+}}$.

2. Optical spectra and spectra of scattering.

Experimental researches of optical spectra of absorption $LiNbO_3$ published in many works. On fig. 1 our experimental results are shown only in connection with a context of article. We shall notice only, that in spectral area in which our researches (is area of a transmission of a crystal) were carried out, values of factor of absorption are small.

On fig. 2 plotted spectral dependence of volume photogalvanic current for $LiNbO_3$.

Curves of two-refraction Δn changes on diameter of the area of a crystal covered by light given on fig. 3. With increase of time of an exposition, the area of changes Δn grows.

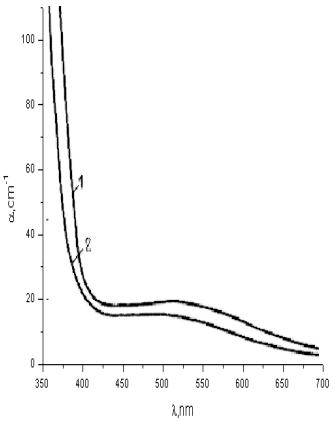

Fig. 1 Optical spectra of absorption $LiNbO_3$ for two polarizations: 1- $E_{light}\perp$c and 2- $E_{light}\|$c.

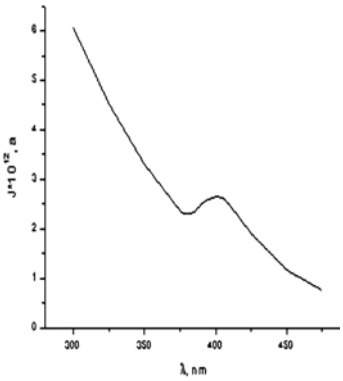

Fig. 2 Spectral dependence of volume photogalvanic current for $LiNbO_3$

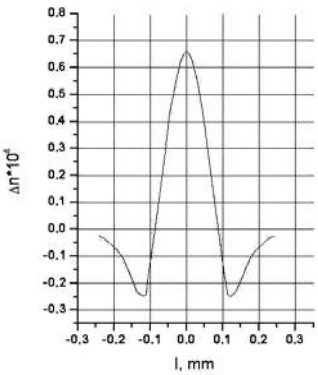

Fig.3. Optically induced changes of factor refraction Δn on diameter of the covered area of a crystal.

At achievement of some critical size $\Delta n\approx1.7\cdot10^{-3}$ on dependence Δn (fig. 4) are observed "jumps" (effect partial polarization reversal) which quantity is defined by density of capacity (~8 W/cm^2).

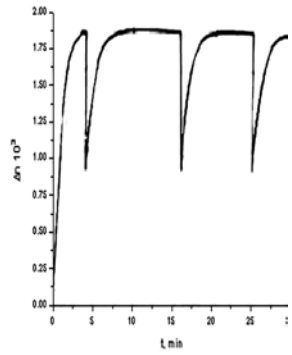

Fig.4 "Jumps" Δn in $LiNbO_3$+Fe.

This result earlier published in article [10] and explained in authors of paper [14].

Investigations of spectral dependences of Raman-scattering by frequency ω scattering cross-sections, allow studying time-development of process. As well known, parameter of line width directly connected with time-delay between processes absorption and radiation photons. The scattering cross-section defines from expression:

$$d_1\sigma(k_1\lambda_1;\Theta\lambda_2) = \left(\frac{\left|M_{fi}M_{i0}\right|^2}{\hbar^2\left[(\omega_1-\omega_i)^2+\gamma_i^2\right]}\right)\left(\hbar\omega_1-E_f\right)^2\frac{d\Omega}{\left(4\pi^2\hbar^4c^4\right)}.$$

M_{fi} and M_{i0} are matrix elements and $\tau_i=1/\gamma_i$.
Therefore, we have two cases: slow $|\omega_1-\omega_i|<<\gamma_i$ (depend on lifetimes) and fast $|\omega_1-\omega_i|>>\gamma_i$ (depend on experimental conditions) processes. For slow processes:

$$I(t)\sim\begin{cases}\gamma_i^2\left\{1-\exp\left(-\frac{\gamma_i}{2}t\right)\right\}^2 & t<T_L\\ I(T_L)\exp\left[-\gamma_i\left(t-T_L\right)\right] & t>T_L\end{cases}$$

For fast processes:

$$I(t)\sim\begin{cases}\left(\Delta\omega_i\right)^{-2}\left\{1-\exp\left(-\frac{t}{\tau_L}\right)\right\}^2 & t<T_L\\ I(T_L)\exp\left[-2\frac{\left(t-T_L\right)}{\tau_L}\right] & t>T_L\end{cases}$$

Here t=0 and $t=T_L$ are leading edge and trailing edge of impulse, correspondingly.

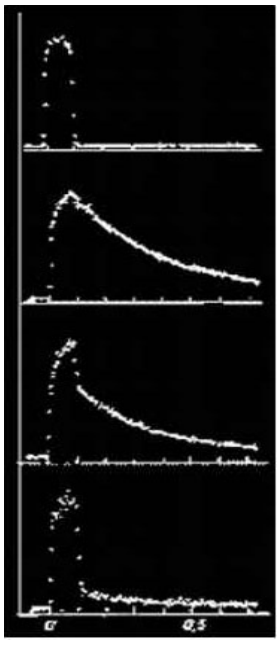

Fig. 5 Study lifetime of states in $LiNbO_3$ (here x-axis is t, μs):
Impulse of laser:
a. λ=532 nm, 100 ns

b. Case $\omega_1=\omega_i$

c. Case $\omega_1=\omega_0+1.2$ GHz

d. Case $\omega_1=\omega_0+2.2$ GHz

The received results show, that at a resonance with a line of absorption (case "*b*") intensity of radiated light slowly grows (an interval $0\le t\le T_L$) and then (in an interval $t>T_L$) slowly decreases with time of attenuation about ~14 μs.

In cases "*c*" and "*d*" in intensity of radiated light "slow" and "fast" components, and amplitude slow components are well observed is less, than in a case "*b*".

Time-delay between processes of absorption and radiation of photons are approximately ten nanoseconds.

These investigations will well be coordinated with relaxation changes of factor of the absorption, in this case reflecting recombination processes (see fig. 6). The received experimental results easily can be approximated function $\alpha(t)=\alpha_1(0)\exp(t/\tau_1)+\alpha_2(0)\exp(t/\tau_2)+\alpha_3(0)\exp(t/\tau_3)$ with parameters $\alpha_1(0)$=4.13, τ_1=0.016 ms; $\alpha_2(0)$=0.972, τ_2=0.95 ms; $\alpha_3(0)$=2.19 and τ_3 =0.144ms (see fig. 6a). They also can be approximated with function $\alpha(t)=\alpha_1(0)\exp(t/\tau_1)+\alpha_2(0)\exp(t/\tau_2)$ with parameters $\alpha_1(0)$=2.536, τ_1=0.3 ms, $\alpha_2(0)$=4.848 and τ_2=0.016 ms (see fig. 6b). Points give experimental data.

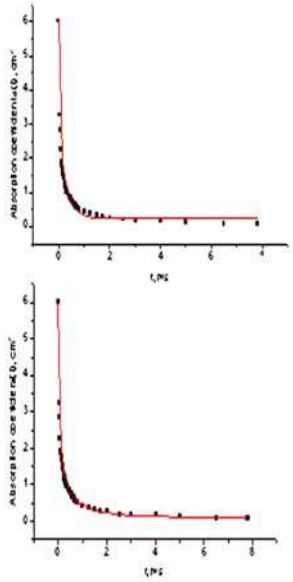

Fig. 6 (See comments in the text)

a

b

On fig. 6 results of adjustment in experimental dependence relaxation processes which estimate on change of factor of absorption, which will be coordinated to results of work [11] is given. Want to remind, that in [11] was defined light-induced absorption changes vs time. In same work it is possible to find the data on dependence of maximum α_{li}^{max} of light-induce absorption, lifetime τ, stretching factor β changes from intensity of pump light (see also [12]), and, for excellent description of the complete evolution of $\alpha_{li}(t)$ is obtained by function $\alpha_{li}(t)=\alpha_1(t=0)\exp[(t/\tau)^{\beta}]$. Here $f_{KWW}(t)=\exp[(t/\tau_{KWW})^{\beta}]$ is "stretched" exponential function, known as the Kohlrausch-Williams-Watts relaxation function [13]. This function applicable only for times long compared molecular vibration periods. Laplace transform resolves $f_{KWW}(t)$ into a linear superposition of simple exponentials $(A(\tau)\ge0)$: $f_{KWW}=\int_0^{\infty}A_{\beta}(\tau)\exp\left(-\frac{t}{\tau}\right)d\tau$. Each dynamical region has a simple exponential relaxation (approximately) with its own characteristic time scale for relaxation. Boundaries and contents of dynamically distinct regions change with passage of time. As known, that value of β

usually decreases from "≈1" to "≈1/3". Use by authors [11] these functions is connected with made by them the assumption, that during absorption and recombination of electrons in $LiNbO_3$:Fe properties small polaron are badly taken into account and dependence of optical absorption should not have simple monoexponential form. The investigation of the dynamics of the light-induced absorption changes in $LiNbO_3$ crystals reveals: the recombination of electrons from small polarons (Nb_{Li}^{4+}) with deep traps (e.g., Fe^{3+}) follows a stretched-exponential behavior (this result from the fact that lifetime of an individual polaron depends on the distance to the next deep trap) and, thus, for all polarons together, a spectrum of lifetimes instead of a single time constant is obtained [11].

Excitation and recombination of the electrons for $LiNbO_3$:Fe can be described by the two-center charge model, which introduced in [15, 18]. Electrons can be excited from Fe^{2+} by light either into the conduction band or into Nb_{Li}^{5+} forming Nb_{Li}^{4+}. Direct excitation into Nb_{Li} centers requires that there are always some these centers close to each Fe^{2+}. In this case, because Nb_{Li} is an intrinsic defect that occurs in a very high concentration [16, 17]. The electrons in the Nb_{Li}^{4+} traps can be excited to the conduction band by light or thermally. The conduction-band electrons can be recombine either with Fe^{3+} or Nb_{Li}^{5+}.

Completely in this model, excitation and recombination of the electrons describe by the equations:

$$\frac{\partial c_{Fe^{2+}}}{\partial t} = -\left[q^{s}_{Fe^{2+}\to cb} + q^{s}_{Fe^{2+}\to Nb_{Li}^{4+}}\left(c_{Nb_{Li}} - c_{Nb_{Li}^{4+}}\right)\right]\cdot I_L c_{Fe^{2+}} + \left(\gamma_{cb\to Fe^{2+}} n + \gamma_{Fe^{2+}\to Nb_{Li}^{4+}} c_{Nb_{Li}^{4+}}\right)\left(c_{Fe} - c_{Fe^{2+}}\right)$$

$$\frac{\partial c_{Nb_{Li}^{4+}}}{\partial t} = -\left[\beta_{Nb_{Li}^{4+}\to cb} + q^{s}_{Nb_{Li}^{4+}\to cb} I_L + \gamma_{Nb_{Li}^{4+}\to Fe^{3+}}\left(c_{Fe} - c_{Fe^{2+}}\right)\right]\cdot c_{Nb_{Li}^{4+}} + \left(\gamma_{cb\to Nb_{Li}^{5+}} n + q^{s}_{Fe^{2+}\to Nb_{Li}^{4+}} I_L c_{Fe^{2+}}\right)\left(c_{Nb_{Li}} - c_{Nb_{Li}^{4+}}\right)$$

Here: $q^{s}_{Fe^{2+}\to cb}$, $q^{s}_{Fe^{2+}\to Nb_{Li}^{4+}}$ - absorption cross-section of Fe^{2+} for absorption and excitation of an electron from Fe^{2+} into conduction band (cb) and Nb_{Li}^{4+}, correspondingly; $q^{s}_{Nb_{Li}^{4+}\to cb}$ - absorption cross-section of Nb_{Li}^{4+} for absorption and excitation of an electron from Nb_{Li}^{4+} into conduction zone; c_{Fe}, $c_{Nb_{Li}}$ – are total concentration of Fe and Nb_{Li}, correspondingly; $c_{Fe^{2+}}$ and $c_{Nb_{Li}^{4+}}$ - concentration of Fe^{2+} and Nb_{Li}^{4+}, correspondingly. I_L – intensity of the spatially homogeneous light; $\gamma_{cb\to Fe^{2+}}$ - coefficient of recombination of conduction band electrons with Fe^{2+}; $\gamma_{cb\to Nb_{Li}^{5+}}$ - coefficient of recombination of conduction band electrons with Nb_{Li}^{5+}; $\gamma_{Nb_{Li}^{4+}\to Fe^{3+}}$ - coefficient of recombination of electrons from Nb_{Li}^{4+} with Fe^{3+}.; n – density of free electrons in the conduction band; $\beta_{Nb_{Li}^{4+}\to cb}$ -rate of thermal excitation of electrons from Nb_{Li}^{4+} into the conduction band. It is impossible to forget, that in real crystals $LiNbO_3$:Fe as it was specified above, always there is a concentration of ions Fe^{3+} and Nb_{Li}^{5+}. In table 1 the experimental values published in paper [15] which are used quality of initial calculations given for carrying out have been reduced.

Table 1

Quality, unit	Value	Notes
$q^{s}_{Fe^{2+}\to cb}$, m^2/J	1.0×10^{-5}	Light wavelength 532 nm
	0	Light wavelength 632.8 nm
$q^{s}_{Nb_{Li}^{4+}\to cb}$, m^2/J	5.0×10^{-5}	Light wavelength 532 nm
	5.2×10^{-5}	Light wavelength 632.8 nm
$q^{s}_{Fe^{2+}\to Nb_{Li}^{4+}}$, m^5/J	3.22×10^{-30}	Light wavelength 532 nm, 632.8 nm
c_{Fe}, m^{-3}	1.2×10^{25} or 5.6×10^{25}	$c_{Fe} = c_{Fe^{2+}} + c_{Fe^{3+}}$
$c_{Nb_{Li}}$, m^{-3}	1.0×10^{26}	
$c_{Fe^{2+}}$, m^{-3}	Variable; initial data 2.5×10^{24} for $c_{Fe} = 5.6 \times 10^{25}$	published in paper [1]
$c_{Fe^{2+}} / c_{Fe^{3+}}$	Variable; initial data ≈0.05 for $c_{Fe} = 5.6 \times 10^{25}$	Typically ratios in the range from 0.01 to 1
$c_{Nb_{Li}^{4+}}$, m^{-3}	variable	
I_L, W/m^2	Variable	$I_{YAG:Nd}$; $I_{He\text{-}Ne}$ to 3×10^4 ($I_{YAG:Nd}$)
$\gamma_{cb\to Fe^{2+}}$, m^3/s	1.65×10^{-14}	
$\gamma_{cb\to Nb_{Li}^{5+}}$ m^3/s	0	
$\gamma_{Nb_{Li}^{4+}\to Fe^{3+}}$ m^3/s	1.14×10^{-21}	
$\gamma_{Nb_{Li}^{4+}\to Fe^{3+}}$ m^3/s	1.14×10^{-21}	
n, m^{-3}	variable	
$\beta_{Nb_{Li}^{4+}\to cb}$, s^{-1}	0	
μ, m^2/Vs	$\approx 7.4\ 10^{-5}$	Very small value of mobility of electrons specifies that fact, that electrons in this case cannot be considered as the free particles.
r_{13}, m/V	10.9×10^{-12}	Electrooptic coefficient, Light wavelength 632.8 nm
ε	28	Dielectric coefficient
n_0	2.286	Refractive index. Light wavelength 632.8 nm

First of all we shall remark, that in this case experiments were carried out in geometry when impulse radiation from YAG:Nd with a wave length 532 nm and intensity $I_{YAG:Nd}$ was guided under an angle 20° to a surface of a crystal while

radiation from He-Ne the laser with a wave length 638,8 nm and intensity I_{He-Ne} has been oriented perpendicularly to the same surface.

Such experiment allowed observing of a modification of absorption stipulated by absorption of transitions $Fe^{2+} \rightarrow Nb_{Li}^{4+}$, $Nb_{Li}^{4+} \rightarrow cb$ and a recombination of electrons from a conduction band on levels Nb_{Li}^{4+} and Fe^{2+}.

Measuring optically induced modifications of a refractivity in $LiNbO_3$:Fe at use He-Ne of the laser such as ЛГ-31 with wave length of radiation 632,8 nm have shown, that magnification of exposure time results in propagation of a refractivity (in particular, see a fig.3. The more a power density the more strongly a steepness of effect. This outcome is not new and early described in [10], [14]).

After light transformations, we can write out the kinetic equations for both cases. However, two-center charge model basically be not capable to explain the modifications of absorption factor observed in experiments (for example, [11]). In paper [21] the data on formation of an electric field in earlier shined field which magnitude as appeared can exceed 10^5 V·cm are published. Such field can reduce in an electrical breakdown and should be taken into account at interpretation, for example optical, experiments. The estimation of a field of a photorefraction on observationally observable values of a modification of a two-refraction with the equation of electrooptical effect gives 680 V/cm for $\delta\Delta n = 5\ 10^{-5}$ and T=300K.

In ferroelectric materials - photoconductors on boundaries of uniformly irradiated field the space charge is formed. The modification of spontaneous polarization at illumination of the crystal, happening as a result of a modification of concentration of the free carriers [22], calls occurrence of a depolarization electric field. Due to photoconductivity this field screens, that is at enough long-lived illumination the field in the field of a light stain is close to null. Magnitude Δn in the field of a light stain, in this case, is determined by the formula [23]. After removal of illumination there can be rather fast relaxation of excited states of impurities therefore, magnitude of spontaneous polarization is returned to an equilibrium value. Thus there is a modification and magnitudes Δn which, however, does not tend to zero. The space charge on boundaries of irradiated area can be maintained long enough and after a relaxation of spontaneous polarization. Therefore, after lockout of light, in earlier irradiated field there is a built-in field which defines a quantity Δn, maintained long enough. This magnitude essentially depends on the shape of a stain. The modification Δn is easy for finding from the equation of electro-optical effect:

$$\Delta n = \frac{n^3}{2}(m + 2MP_S)\left[\frac{(\alpha^* f^2 - g)c}{4\pi(c+g)}P_S + \alpha^* f P_S\right]N^0 + \frac{2\pi N^0 \alpha_0}{n} \quad (1)$$

$$\Delta n = \frac{n^3}{2}(m + 2MP_S)\frac{\varepsilon - 1}{\varepsilon}\left[\frac{(\alpha^* f^2 - g)c}{4\pi(c+g)}P_S + \alpha^* f P_S\right]N^0 \quad (2)$$

where m - the linear electrooptical coefficient, P_s - spontaneous polarization, N – concentration of impurities, α - polarizability, f–Lorenz's factor, M – electrooptical coefficient, g – coefficient of deformation potential.

Presence of two relaxation times Δn, the reference for the given mechanism photorefractive effect, is well-known from operations [21, 24-26,]. In the beginning of illumination for small time, restricted only the velocity of a photo-ionization of an impurity, mounts magnitude Δn, defined by expression:

$$\Delta n = \frac{n^3}{2}(m + 2MP_S)\left[\frac{(\alpha^* f^2 - g)c}{4\pi(c+g)}P_S + \alpha^* f P_S\frac{1-\varepsilon}{\varepsilon}\right]N^0 + \frac{2\pi N^0 \alpha_0}{n}$$

Association n from $\Phi(x)$ - allocation of light intensity and T - temperatures is determined by the concrete mechanism of drive of impurities. If under an operation of light there is a recharge of impurities this association is given by formulas:

$$N^0 = S\Phi N\{(S + S_i')\Phi + [WN_c\ exp(-I/kT)N_i^{-1} + W_{00}]N_0'\}^{-1}$$

where $S_i' = S_i W / W_i$ и

$$N^0 = 2(S\Phi)^{1/2} NN_i\{(N_i + N)(S\Phi)^{1/2} + \{(N_i - N)^2 S\Phi + 4N_i N[S_i'\Phi + WN_c\ exp(-I/kT) + W_{00}N_i]\}^{1/2}\}^{-1}$$

The relaxation time of an excited state is not enough at major impurity concentrations. Shelf time of space charge, defined a thermal ejection of electrons from traps and the pickup on them of the free carriers, is determined by expression:

$$\tau_s^{-1} \approx W_i N_c\ exp(-I/kT) + Wn_0 \quad (3)$$

When the photoexcitation of an impurity does not reduce in ionization, concentration of the excited centers in stationary state can be spotted expression:

$$N^0 = \frac{N\tau\ S\Phi}{1 + \tau\ S\Phi}$$

As a rule, the relaxation time of an excited state is not enough. A unique reason of effect of a photorefraction in this case is formation of space charge which time of maintenance is determined by expression (3).

Let's estimate a reference length of shielding of a field l that is thickness of a stratum of a space charge. Division of charges happens due to ionization of impurity centers, the subsequent electron drift in an electric field and their capture on the free trap. The area in which the electric field is distinct from zero less, the energetically more favorable is the relevant condition. Therefore in the field of the positive space charge there is the complete ionization of deep impurity centers, and in the field of the negative - the complete recharge of traps. Thus, we have $\rho = eN$ and $\sigma = eNl$. Guessing, that the light stain has the homogeneous allocation of illumination and estimating P as we shall discover, that on an order of magnitude $l = \Delta P_s / eN = \alpha^* f d^{-2} \approx 10^{-6} cm$.

It is obvious, that allocation $\Delta n(x)$ during illumination noticeably differs from $\Delta n(x)$ after removal of illumination, more precisely, after relaxation of excited states of impurities. Besides from model follows, that sensitivity induction of photorefraction should have spectral maxima. For $LiNbO_3$:Fe such association has been found out in [27].

As well known, small polarons and bipolarons absorb radiation when a self-trapped carrier is exited from severely localized state to another well-localized state at an adjacent site. The widths of the absorption spectra of small polarons and bipolarons are due to variations of the energy differences between these well-localized states caused by atomic displacements. That is, phonon broadening provides the predominant broadening mechanism for small-polaronic absorption spectra. Therefore, small-polaronic absorption spectra are generally temperature depend. Small-polaronic absorption spectra are generally asymmetric. The absorption on the low-energy side of the peak is greater than that on the high-energy side of the peak.

The absorption coefficient per unit density of small polaron is given by [28, 29]:

$$\frac{\alpha}{n_p} = \frac{2\pi^{3/2}\cdot e^2\cdot t'}{m'\cdot\omega\cdot c\cdot\Delta} exp\left[\frac{-\left(2E_b-\hbar\omega\right)^2}{\Delta^2}\right] \qquad (4)$$

where t' is the intersite electronic transfer energy and the electronic effective mass is defined by relation $t' \equiv \frac{\hbar^2}{2m'a^2}$; $\Delta \equiv \sqrt{8E_bE_{vib}}$. At low temperature E_{vib} is just the zero-point vibrational energy $\frac{\hbar\omega_{ph}}{2}$, at high enough temperatures for the vibrational motion to be treated classically, $E_{vib}=k_BT$. Derivations of (4) presume that $E_b>>\Delta>t'$, this factor reduces the absorption. This reduction factor occurs because the transfer related absorption requires the electronic energies of initial and final sites be within t' of one another while motion broadens the local energy levels by larger amount Δ. The efficacy of the absorption is reduced when the time required for the electronic transfer $\frac{\hbar}{t'}$ is longer than the time interval during which the electronic energies remain coincident, $\frac{\hbar}{\Delta}$. If $E_b>>t'>\Delta$, $\frac{t'}{\Delta}$ should be replace by unity in (4).

For a small bipolaron, two carriers occupy a common site since the depth of electronic well that self-traps the carriers at equilibrium is twice as deep as that for a small polaron, $-4E_b$, rather than $-2E_b$. The electronic energy of the two self-trapped carriers is then $-2(4E_b)+U$, where U is the on-site Coulomb repulsion energy. A small bipolaron is stable with respect to separation into two separated small polarons, if its electronic plus deformational energy, $-4E_b+U$, exceeds that of two separated polarons $-2E_b$. Absorption spectra of small bipolaron are similar to those of small polarons. But energies of the absorption maximums small bipolarons tend to be even higher than those small polarons.

Very small value of mobility of electrons ($\mu\approx 7.4\ 10^{-5} m^2/Vs$) in $LiNbO_3$ specifies that fact, that electrons in this case cannot be considered as the free particles, e.g. polarons are strongly located. Conductivity here carries jump character, i.e. the free length about the lattice constant can exceed time of a recombination essentially 10^{-8} s.

All aforesaid allows making improvements for two-center models:

1. to take into account association of cut of an absorption on an energy of incident photons and on allocation of intensity of light in the field of a light stain;
2. to take into account singularities of recombination processes.

On fig.7 results of calculations of change of absorption after the termination of action of a pulse of light from the YAG:Nd laser (532 nm) on the modified model which show the good consent with experiment (see. Fig.6) are submitted (dashed line is theoretical calculations).

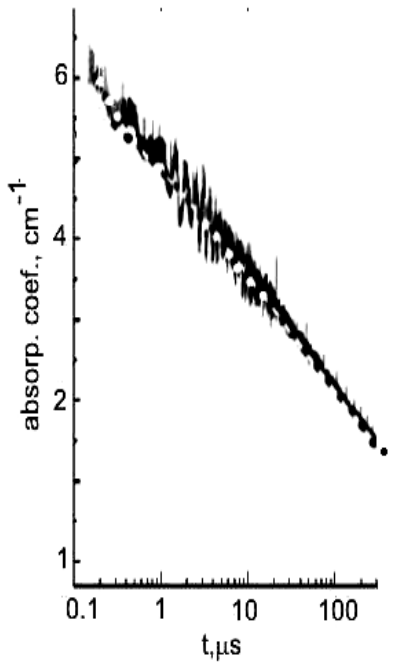

Fig.7

The long-range development of these operations will be submitted in the second part of paper.

[1] *H.Kurz and E.Kratzig, W.Keune, H.Engelman, U.Genzer, B.Discher, A.Rauber* Appl. Phys., 1977, 12, 355

[2] *C.R.Hsieh, S.H.Lin, K.Y.Hsu, T.C.Hsieh, A.Chion, and J. Hong* Appl. Optics, 1999, vol.8, №.29, p.6141

[3] *C.Gu, J.Hong, H.Y.Li, D.Psaltis, and P.Yeh* J.Appl. Phys. 1991, 69, 1167-1172.

[4] *I.Nee, M.Muller, K.Buse* Appl. Phys. B72, 2001,195-200

[5] *M.Carrascosa, F.Aqullo-Lopez* Appl. Optics, 1988, v.27, №14, 2851

[6] *S.C.Abrahams,H.J.Levinstein, J.M.Reddy* J.Phys. Chem. Solids, 1966, 27, 1019
[7] *S.C.Abrahams, P.Marsh* Acta Crystallogr. sect. B 42, 1986, 61
[8] In book "Physics and Chemistry of Crystalline Lithium Niobate" A.M.Prokhorov, IOP Publishing Ltd., 1990
[9] In book "Nonlinear spectroscopy", Ed. Bloembergen H., 1977, North-Holland
[10] *K.K. Shartz*, Izv.AN SSSR, ser. phys., 1977, т.41, №4, c.788-791 (in Russian)
[11] *D. Berben, K.Buse, S.Wevering, P.Herth, M.Imlau, Th. Woike,* J. Appl. Phys., 2000, v.87, n.3, p.1034-1041
[12] *S.M.Kostritski, O.G. Sevostyanov*, Appl. Phys. B65, 1997, p.527-533
[13] In book "Handbook of mathematical functions", Edited by M.Abramowitz and I.A.Stegun, 1979, National Bureau of standarts, Applied mathematics, Series-53
[14] *T.R.Volk,A.V.Ginzburg,V.I.Covalevich,L.A.Shuvalov* Izv. AN SSSR, ser. phys.., 1977, т.41, №4, c.783-787 (in Russian)
[15] *F.Jermann, J.Osten* J.Opt.Soc.Am., 1993, B10, 2085
[16] *N.Zotov, H.Boysen, J.Schneider,F.Frey* Mater. Sci. Forum, 1994, 166-169,631(in Russian)
[17] *R.Iyi, K.Kitamura, F.Izumi, J.K.Yamamoto, T.Hayashi, H.Asano, S.Kimura* J.Solid St. Chem., 1992, 101, 340.
[18] *A.Adibi, K.Buse, D.Psaltis* Phys. Rev, A63, 2001, p.023813
[19] *I.Sh.Akhmadulin, V.A.Golenishchev-Kutuzov, S.A.Migachev* FTT, 1998,Vol.40, N6, p.1109-1116 (in Russian)
[20] *J.M.Cabrera, J.Olivarest, M.Carrascosa, J.Rams, R.Muller, E.Dieguez* Advances in Physics, 1996, Vol.45, N5, p.349-392
[21] *F.S. Chen* J.Appl. Phys., 1969, 38, 3418
[22] *V.M.Fridkin* Pisma v JETF, 1966, 3, 252 (in Russian)
[23] *A.P.Levannuk, V.V.Osipov* Izv. AN SSSR, ser. phys., 1977, т.41, N4 (in Russian)
[24] *A.P.Levannuk, V.V.Osipov* Izv. AN SSSR, ser. phys., 1975, т.39, 686 (in Russian)
[25] *A.A. Ashkin, G.D.Boyd, et.al.* Appl. Phys.Lett.s, 1966, 9, 72
[26] *I.F.Kanayev, V.K.Malinovsii* FTT, 1974, 16, 3694 (in Russian)
[27] *H.B.Serreze, R.B.Golduer* Appl. Phys. Letts. 1973, 22, 626
[28] *D.Emin* Adv.Phys., 1975, 24, 305
[29] *D. Emin* Phys.Rev., 1993-II, v.48,N18,13691

Tələt R. Mehdiyev

$LiNbO_3$ OPTİK XÜSUSİYYƏTLƏRİ. BİRİNCİ HİSSƏ

YAG:Nd lazerin (532 nm) HeNe lazerindən (632.8 nm) arasıkəsilməyən şüalandırmayla ikinci şüalanma harmonikası ilə impuls oyanması şəraitində 0.03% Fe aşqarı ilə aşqarlanmış litium niobatın optik və yayılma spektrləri eksperimental araşdırılmışdır. Alınan eksperimental nəticələrin ehtimal ediləcək nəzəri interpretasiyası verilmişdir.

Талат Р. Мехтиев

ОПТИЧЕСКИЕ СВОЙСТВА $LiNbO_3$. ЧАСТЬ ПЕРВАЯ

Экспериментально исследованы оптические спектр и спектр рассеяния ниобата лития легированного 0.03% примесью Fe в условиях импульсного возбуждения второй гармоникой излучения (532 nm) лазера YAG:Nd с непрерывной подсветкой от He-Ne лазера (632.8 nm). Дана предположительная теоретическая интерпретация полученных экспериментальных результатов.

Received: 04.09.03

RECURRENCE RELATIONS TECHNIQUE IN AN ANTIFERROMAGNETIC SUPERLATTICE

V.A. TANRIVERDIYEV, V.S. TAGIYEV, S.M. SEYID-RZAEVA
Institute of Physics of the National Academy of Sciences of Azerbaijan
370143, Baku, H. Javid ave.33, ***E-mail : Physic @Physics ab.az.***

General dispersion equation of exchange spin waves propagating in a general direction in an antiferromagnetic superlattice is derived by the recurrence relations technique. The elementary unit cell of the superlattice under consideration consists of N different antiferromagnetic layers. The results are illustrated numerically for a particular choice of parameters

Rapid development of modern technologies leads to superlattices (*SLs*) wide application, and this causes an increased interest to their experimental [1-3] and theoretical investigation [4-6]. The study of spin waves is very useful in determining the fundamental parameters which characterize the magnetic systems — anisotropy, exchange coupling, magnetization, surface effects, impurities, dipolar interactions, and magnetic structure. [7]. Therefore theoretical studies of spin-wave excitations in magnetic multilayers, thin films, metamagnets and *SLs* have been the focus of considerable interest for many years, and Green's function method, interface rescaling technique, transfer matrix formalism or recurrence relations technique are used for their studies [8-12]. There have been numerous investigations of the spin waves propagating in the *SLs* composed of two different ferromagnetic or antiferromagnetic materials [13-15]. Comparatively fewer properties of antiferromagnetic SLs have been studied. Existing works on antiferromagnetic multilayers have primarily considered long- wavelength approximations [9,16] or microscopic periodic SL [17,18]. Some general expressions for excitations in discrete N – layered ferromagnetic *SLs* are derived in ref. [19].

In this paper the general dispersion equation of exchange spin waves (short- wavelength limit, where the exchange coupling is dominant) for *SL* with the elementary unit cell consisting of N (=2,3,…) different simple-cubic Heisenberg antiferromagnetic materials is derived by the recurrence relations technique. Recurrence relations technique leads to a compact expression for the spin-wave dispersion relation of the *SL*. The material j (=1,2,…,N) can be characterized by the following bulk parameters: the exchange integral J_j , Lande factors g_j and spin S_j . As indicated in fig.1 the j-th layer consists of n_j atomic layers. The exchange interaction between atoms of two atomic layers at each interface is assumed to be antiferromagnetic, but different from the corresponding bulk couplings. We assume the same lattice parameter α for all the N materials.

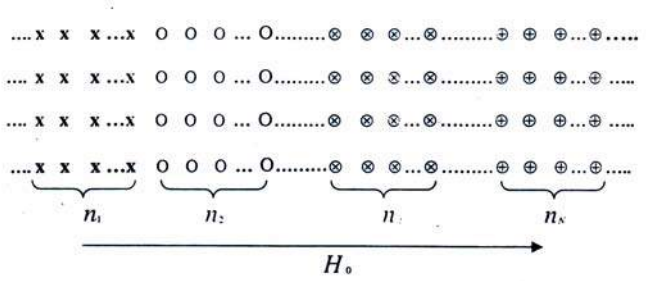

Fig.1. The elementary unit cell of *SL* consisting N different simple-cubic Heisenberg antiferrromagnetic materials. The same lattice parameter a is assumed for all the materials. The antiferromagnetic layers consist of n_j (j=1,2,…,N) atomic layers. The layers are infinite in the direction perpendicular to the axes z.

The Hamiltonian of the system can be written in the form

$$H = \sum_{n,\nu,\delta_{II}} J_{n,n}(\vec{S}_{n,\nu}\vec{S}_{n,\nu+\delta_{II}}) + \sum_{n,\nu} J_{n,n+1}(\vec{S}_{n,\nu}\vec{S}_{n+1,\nu}) - \sum_{n,\nu} g_n \mu_B H_n^{(A)}(S^z_{n,\nu a} - S^z_{n,\nu b}) - g_n \mu_B H_0 \sum_{n,\nu}(S^z_{n,\nu a} + S^z_{n,\nu b}) \quad , \tag{1}$$

where the first term describes exchange interactions inside atomic layer, the second term describes exchange interactions between neighbouring atomic layers and the last two terms include the Zeeman's energy and magnetic anisotropy energy. Here, n is the index of atomic layer, ν describes the position of a lattice site in this layer and $\delta_{||}$ is the vector of location of the nearest neighbours in the plane. The axis z of the coordinate system is normal to the film interfaces [001] and external field H_0 is assumed to be parallel to the z axis.

Using the equation of motion for the spin operators $S^+_{n,a}(\omega,k_{||})$ and $S^+_{n,b}(\omega,k_{||})$ corresponding to sublattices a and b one finds the following system of equations

$$\begin{cases} \lambda^a_n J_{n,n} S^+_{n,a} - J_{n,n}\gamma(k_{||}) S^+_{n,b} - J_{n,n+1} S^+_{n+1,b} - J_{n,n-1} S^+_{n-1,b} = 0 \quad , \\ \lambda^b_n J_{n,n} S^+_{n,b} - J_{n,n}\gamma(k_{||}) S^+_{n,a} - J_{n,n+1} S^+_{n+1,a} - J_{n,n-1} S^+_{n-1,a} = 0 \quad , \end{cases} \tag{2}$$

where λ_n^a , λ_n^b and $\gamma(k_{||})$ are defined as follows $\gamma(k_{||}) = 2(\cos k_x a + \cos k_y a)$,

$$\lambda_n^{a,b} = \left[\pm\left(\omega - g_n \mu_B \left(H_0 \pm H_n^{(A)}\right)\right) - 4J_{n,n}\langle S_n^z\rangle - J_{n,n+1}\langle S_{n+1}^z\rangle - J_{n,n-1}\langle S_{n-1}^z\rangle\right] \Big/ J_{n,n}\langle S_n^z\rangle \ ,$$

the upper sign refers to λ_n^a and the lower one to λ_n^b, respectively. Equation (2) are valid in the low-temperature limit and random-phase-approximation (RPA) $\langle S_{n,a}^z\rangle = -\langle S_{n,b}^z\rangle = \langle S_n^z\rangle$ has already been done.

The system of equations (2) can be solved by recurrence relations technique [13] to relate the spins at the first and second atomic layer of *j*-th and (*j+1*)-th layer of *m*-th elementary unit cell

$$\begin{pmatrix} S^+_{1,(j+1),m,a} \\ S^+_{1,(j+1),m,b} \\ S^+_{2,(j+1),m,a} \\ S^+_{2,(j+1),m,b} \end{pmatrix} = R^{(j,j+1)}(R^{(j)})^{n_j-2} \begin{pmatrix} S^+_{1,j,m,a} \\ S^+_{1,j,m,b} \\ S^+_{2,j,m,a} \\ S^+_{2,j,m,b} \end{pmatrix} = T^{(j)} \begin{pmatrix} S^+_{1,j,m,a} \\ S^+_{1,j,m,b} \\ S^+_{2,j,m,a} \\ S^+_{2,j,m,b} \end{pmatrix} \ . \qquad (3)$$

the matrices $R^{(j)}$ and $R^{(j,j+1)}$ have the form:

$$R^{(j)} = \begin{pmatrix} 0 & E \\ -E & r^{(j)} \end{pmatrix} , \qquad R^{(j,j+1)} = \frac{J_j}{J_{j,j+1}} \begin{pmatrix} -E & r_{12}^{(j,j+1)} \\ r_{21}^{(j,j+1)} & r_{22}^{(j,j+1)} \end{pmatrix} ,$$

$$r^{(j)} = \begin{pmatrix} -\gamma(k_{||}) & \lambda_j^b \\ \lambda_j^a & -\gamma(k_{||}) \end{pmatrix} , \quad r_{21}^{(j,j+1)} = \begin{pmatrix} \gamma(k_{||}) & -\lambda_{j+1}^b - \varepsilon_{j+1} \\ -\lambda_{j+1}^a - \varepsilon_{j+1} & \gamma(k_{||}) \end{pmatrix} , \quad r_{12}^{(j,j+1)} = \begin{pmatrix} -\gamma(k_{||}) & \lambda_j^b + \varepsilon_j \\ \lambda_j^a + \varepsilon_j & -\gamma(k_{||}) \end{pmatrix} ,$$

$$r_{22}^{(j,j+1)} = \begin{pmatrix} \left(\lambda_{j+1}^b + \varepsilon_{j+1}\right)\left(\lambda_j^a + \varepsilon_j\right) + \gamma^2(k_{||}) - J_{j,j+1}^2 / J_j J_{j+1} & -\gamma(k_{||})(\lambda_{j+1}^b + \lambda_j^b + \varepsilon_{j+1} + \varepsilon_j) \\ -\gamma(k_{||})(\lambda_{j+1}^a + \lambda_j^a + \varepsilon_{j+1} + \varepsilon_j) & \left(\lambda_{j+1}^a + \varepsilon_{j+1}\right)\left(\lambda_j^b + \varepsilon_j\right) + \gamma^2(k_{||}) - J_{j,j+1}^2 / J_j J_{j+1} \end{pmatrix} ,$$

$$\lambda_j^{a,b} = \left[\pm\left(\omega - g_j \mu_B (H_0 \pm H_j^{(A)})\right) - 6J_j\langle S_j^z\rangle\right] \Big/ J_j\langle S_j^z\rangle ,$$

$$\varepsilon_j = 1 - J_{j,j+1}\langle S_{j+1}^z\rangle / J_j\langle S_j^z\rangle , \quad \varepsilon_{j+1} = 1 - J_{j+1}\langle S_j^z\rangle / J_{j,j+1}\langle S_{j+1}^z\rangle ,$$

and E is twodimensional unit matrix.

The matrix $(R^{(j)})^{n_j-2}$ can be expressed through $R^{(j)}$ using similarity transformation [21].

$$(R^{(j)})^{n_j-2} = \begin{pmatrix} C_{n_j-2} & 0 \\ 0 & C_{n_j-2} \end{pmatrix} R^{(j)} - \begin{pmatrix} C_{n_j-3} & 0 \\ 0 & C_{n_j-3} \end{pmatrix} = \begin{pmatrix} -C_{n_j-3} & C_{n_j-2} \\ -C_{n_j-2} & C_{n_j-1} \end{pmatrix} ,$$

$$C_{n_j} = U_j \begin{pmatrix} \sin(n_j\theta_2^{(j)}) / \sin(\theta_2^{(j)}) & 0 \\ 0 & \sin(n_j\theta_1^{(j)}) / \sin(\theta_1^{(j)}) \end{pmatrix} U_j^{-1} , \qquad U_j = \begin{pmatrix} \sqrt{\lambda_j^b} & \sqrt{\lambda_j^b} \\ \sqrt{\lambda_j^a} & -\sqrt{\lambda_j^a} \end{pmatrix} . \qquad (4)$$

Here, $\theta_1^{(j)}$ and $\theta_2^{(j)}$ are defined by the expression $2\cos(\theta_{1;2}^{(j)}) = -\gamma(k_{\|}) \pm \sqrt{\lambda_j^a \lambda_j^b}$ with the minus and plus sign, respectively. $\theta_1^{(j)}$ and $\theta_2^{(j)}$ are discussed in ref. [20,21].

The 4x4 matrices $T^{(j)}$ are given by the following expressions

$$T_{11}^{(j)} = \frac{J_j}{J_{j,j+1}}\left[-\alpha_{n_j-1} - \beta_{n_j-2}\varepsilon_j\sqrt{\frac{\lambda_j^a}{\lambda_j^b}}\right], \qquad T_{12}^{(j)} = \frac{J_j}{J_{j,j+1}}\left[-\varepsilon_j\alpha_{n_j-2} - \beta_{n_j-1}\sqrt{\frac{\lambda_j^b}{\lambda_j^a}}\right],$$

$$T_{13}^{(j)} = \frac{J_j}{J_{j,j+1}}\left[\alpha_{n_j} + \beta_{n_j-1}\varepsilon_j\sqrt{\frac{\lambda_j^a}{\lambda_j^b}}\right], \qquad T_{14}^{(j)} = \frac{J_j}{J_{j,j+1}}\left[\varepsilon_j\alpha_{n_j-1} + \beta_{n_j}\sqrt{\frac{\lambda_j^b}{\lambda_j^a}}\right],$$

$$T_{31}^{(j)} = \frac{J_j}{J_{j,j+1}}\left[\gamma(k_{\|})\alpha_{n_{j-1}} - \left(\lambda_{j+1}^b + \varepsilon_{j+1}\right)\cdot\left(\beta_{n_j-1}\sqrt{\frac{\lambda_j^a}{\lambda_j^b}} + \varepsilon_j\alpha_{n_j-2}\right) + \varepsilon_j\gamma(k_{\|})\beta_{n_j-2}\sqrt{\frac{\lambda_j^a}{\lambda_j^b}} + \frac{J_{j,j+1}^2}{J_jJ_{j+1}}\alpha_{n_j-2}\right],$$

$$T_{32}^{(j)} = \frac{J_j}{J_{j,j+1}}\left[\varepsilon_j\gamma(k_{\|})\alpha_{n_{j-2}} - \left(\lambda_{j+1}^b + \varepsilon_{j+1}\right)\cdot\left(\varepsilon_j\beta_{n_j-2}\sqrt{\frac{\lambda_j^b}{\lambda_j^a}} + \alpha_{n_j-1}\right) + \sqrt{\frac{\lambda_j^b}{\lambda_j^a}}\left(\gamma(k_{\|})\beta_{n_j-1} + \beta_{n_j-2}\frac{J_{j,j+1}^2}{J_jJ_{j+1}}\right)\right]$$

,

$$T_{33}^{(j)} = \frac{J_j}{J_{j,j+1}}\left[-\gamma(k_{\|})\alpha_{n_j} + \left(\lambda_{j+1}^b + \varepsilon_{j+1}\right)\cdot\left(\beta_{n_j}\sqrt{\frac{\lambda_j^a}{\lambda_j^b}} + \varepsilon_j\alpha_{n_j-1}\right) - \varepsilon_j\gamma(k_{\|})\beta_{n_j-1}\sqrt{\frac{\lambda_j^a}{\lambda_j^b}} - \frac{J_{j,j+1}^2}{J_jJ_{j+1}}\alpha_{n_j-1}\right],$$

$$T_{34}^{(j)} = \frac{J_j}{J_{j,j+1}}\left[-\varepsilon_j\gamma(k_{\|})\alpha_{n_{j-1}} + \left(\lambda_{j+1}^b + \varepsilon_{j+1}\right)\cdot\left(\varepsilon_j\beta_{n_j-1}\sqrt{\frac{\lambda_j^b}{\lambda_j^a}} + \alpha_{n_j}\right) - \sqrt{\frac{\lambda_j^b}{\lambda_j^a}}\left(\gamma(k_{\|})\beta_{n_j} + \beta_{n_j-1}\frac{J_{j,j+1}^2}{J_jJ_{j+1}}\right)\right],$$

$$T_{21}^{(j)} = T_{12}^{(j)}\{a\to b; b\to a\}, \qquad T_{22}^{(j)} = T_{11}^{(j)}\{a\to b; b\to a\}, \qquad T_{23}^{(j)} = T_{14}^{(j)}\{a\to b; b\to a\}, \tag{5}$$

$$T_{24}^{(j)} = T_{13}^{(j)}\{a\to b; b\to a\}, \qquad T_{41}^{(j)} = T_{32}^{(j)}\{a\to b; b\to a\}, \qquad T_{42}^{(j)} = T_{31}^{(j)}\{a\to b; b\to a\},$$

$$T_{43}^{(j)} = T_{34}^{(j)}\{a\to b; b\to a\}, \qquad T_{44}^{(j)} = T_{33}^{(j)}\{a\to b; b\to a\},$$

where

$$\alpha_{n_j} = 0.5\left(\frac{\sin(n_j\theta_1^{(j)})}{\sin(\theta_1^{(j)})} + \frac{\sin(n_j\theta_2^{(j)})}{\sin(\theta_2^{(j)})}\right), \qquad \beta_{n_j} = 0.5\left(\frac{\sin(n_j\theta_2^{(j)})}{\sin(\theta_2^{(j)})} - \frac{\sin(n_j\theta_1^{(j)})}{\sin(\theta_1^{(j)})}\right). \tag{6}$$

The matrices $T^{(j)}$ (j=1,2…N) combine to yield transfer matrix $T = T^{(N)}T^{(N-1)}\cdots T^{(1)}$. The matrix elements of $T^{(N)}$ are obtained from the elements of $T^{(j)}$ when $j \to N$ and $j+1 \to 1$. The matrices $T^{(j)}$ (j=1,2…N) and T fulfill the following conditions

$$det(T^{(j)}) = J_j^2 / J_{j+1}^2, \quad detT=1, \; Tr(T)=Tr(T^{-1}), \tag{7}$$

where $Tr(T)$ and $Tr(T^{-1})$ are the sum of diagonal elements of T and its inverse matrix, respectively.

The eigenvalue problem for the matrix T has the form $T\Psi_{1;2}^{\pm} = \eta_{1;2}^{\pm}\Psi_{1;2}^{\pm}$, and the characteristic equation has the following form

$$\eta^4 - Tr(T)\eta^3 + t\eta^2 - Tr(T)\eta + 1 = 0, \tag{8}$$

where

$$t = T_{11}T_{22} - T_{12}T_{21} + T_{11}T_{33} - T_{13}T_{31} + T_{22}T_{33} - T_{23}T_{32} + T_{11}T_{44} - T_{14}T_{41} + T_{22}T_{44} - T_{24}T_{42} + T_{33}T_{44} - T_{34}T_{43},$$

$\eta_{1;2}^{\pm} = exp(\pm iLQ_{1;2})$ are four eigenvalues and $\Psi_{1;2}^{\pm}$ are the corresponding eigenvectors.

Here, $L = \sum_{\sigma=1}^{N} n_{\sigma}$, La is the periodic distance for the superlattice under consideration.

In general case three different situations are possible:

(i) Either the eigenvalues $\eta_1^{\pm}$ or $\eta_2^{\pm}$ is complex ,

(ii) Both the eigenvalues $\eta_1^{\pm}$ and $\eta_2^{\pm}$ are complex ,

(iii) Both the eigenvalues $\eta_1^{\pm}$ and $\eta_2^{\pm}$ are real.

In every case the following relations are fulfilled

$$\eta_1^{+} + \eta_1^{-} + \eta_2^{+} + \eta_2^{-} = Tr(T),$$
$$\eta_{1;2}^{+} + \eta_{1;2}^{-} = 2\cos\left(LQ_{1;2}\right) \quad . \qquad (9)$$

Using (8) and (9) one obtains the general dispersion equation for exchange spin waves in the superlattices under consideration

$$2\cos(LQ_{1;2}) = \frac{Tr(T)}{2} \pm \sqrt{\left(\frac{Tr(T)}{2}\right)^2 - t + 2} \quad . \qquad (10)$$

Equation (10) is the main result of this paper. It can be verified from equation (10) that when all media are identical,

$$J_1 = J_2 = \cdots = J_N = J_{j,j+1} \equiv J_j;$$

$$g_1 = g_2 = \cdots = g_N \equiv g_j;$$

$$\langle S_1^z \rangle = \langle S_2^z \rangle = \cdots = \langle S_N^z \rangle \equiv \langle S_j^z \rangle;$$

$$H_1^{(A)} = H_2^{(A)} = \cdots = H_N^{(A)} \equiv H_j^{(A)},$$

$Q_{1;2}$ reduces to $\theta_{1;2}^{)j)}$.

We note that bulk and surface spin waves in finite or semi-infinite system are described by the eigenvalues of the transfer matrix [19]. But in the case of antiferromagnetic structure surface spin waves can not be characterized by a single propagation constant [20,21]. Equation (10) shows that bulk, acoustic and optic spin waves in an antiferromagnetic SL are characterized by two propagation variables Q_1 and Q_2 as an antiferromagnetic constituent are characterized by $\theta_1^{(j)}$ and $\theta_2^{(j)}$. The number of these propagation variables does not depend on the number N of materials consisting of the elementary unit cell of SL and the number of atomic layer n_j of the material j $(j = 1,2...N)$.

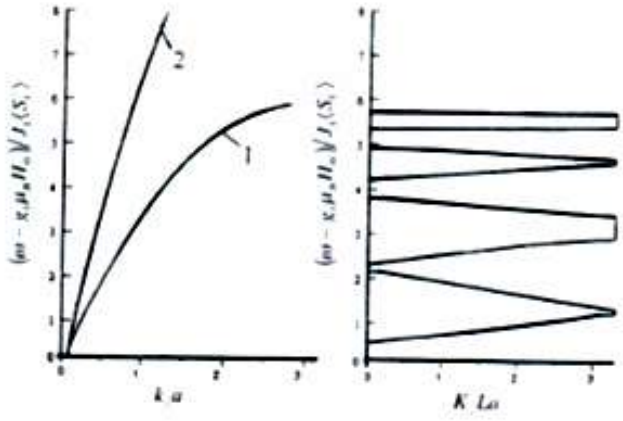

Fig.2. Bulk spin–wave dispersion graphs for [001] propagation with parameters $J_2/J_1 = 2$; $g_1 = g_2$; $g_1\mu_B H_1^{(A)}/J_1\langle S_1^z\rangle = 0.01$; $g_2\mu_B H_2^{(A)}/J_1\langle S_1^z\rangle = 0.03$;
a) bulk spin – wave dispersion curves for constituents 1 (lower curve) and 2 (upper curve);
b) bulk spin – wave dispersion curve for SL when $N=2$; $n_1 = n_2 = 6$; $J/J_1=0.5$.

Although the expression of $cos(Q_{1;2}L)$ is in a complex form one may find the energy range where they are real and $-1 \le cos(Q_{1;2}L) \le 1$. The bulk solution corresponds to the complex eigenvalues of the matrix T in the energy range where $\left|\eta_{1;2}^{\pm}\right| = 1$. We write these eigenvalues in the form $exp(\pm iK_z La)$, where K_z is the normal component of wavevector describing wave propagation in SL. For simple numerical illustration we choose the case of SL composed of two materials and $k_x = k_y = 0$. Fig.2,a shows the bulk spin-wave dispersion curves of component media 1 and 2 for a particular choice of parameters, while fig.2,b shows the bulk spin-wave dispersion curve of SL. The dispersion curves are drawn in the energy range $0 < \left(\omega - g_1\mu_B H_0\right)/J_1\langle S_1^z\rangle < 8$. In the energy range $0 < \left(\omega - g_1\mu_B H_0\right)/J_1\langle S_1^z\rangle < 6$ both components media 1 and 2 have bulk spin-waves. In this energy range the dispersion curve for SL exhibits broad pass and narrow stop bands. SL spin–wave dispersion curves and the dispersion curves of the component media 1 and 2 move up with increasing anisotropy field.

[1] *J.J. Chen,G. Dresselhaus, M.S.Dresselhaus, G.Sprinhoulz, C.Picher,G.Bauer*. Phys. Rev., 1996, B54, p. 4020.

[2] *C. A. Ramos,D. Lederman, A.R.King,V. Jaccarino*. Phys. Rev. Lett., 1990, 65, p. 2913.

[3] *T. M. Giebultowicz, P.Klosovski, N. Samarth, H. Lou, J.K. Furdyna, J.J. Rhyne*. Phys. Rev., 1993, B48, 12817.
[4] Ed. by *M. Cottam*. " Linear and Nonlinear Spin Waves in Magnetic Films and Superlattices", World Scientific, 1994.
[5] *A.S. Carrico and R.E. Camley*. Phys. Rev., 1992, B45, 13117.
[6] *R.L. Stamps, R.E. Camley, R.J. Hicken*. Phys. Rev., 1996, B54, 4159.
[7] *R.E. Camley*. J. Magn., Magn. Matter., 1990, 200, 583.
[8] *R.E. Camley and R.L.Stamps*. J.Phys. Condens. Matter., 1993, 3727.
[9] R.L. Stamps and R.E. Camley. Phys. Rev., 1996, B54, 15200.
[10] *L. Trallori, P. Politi, A. Rerrori, M.G. Pini*. J. Phys. Condens. Matter., 1995, 7, 7561.
[11] *E.L. Albuquerque, R.N. Costa Filho, M.G. Cottam*. J. Appl. Phys., 2000, 87, 5938.
[12] *D.H.A.L. Anselmo, E.L. Albuquerque, M.G. Cottam*. J. Appl. Phys., 1998, 83, 6955.
[13] *Feng Chen and H.K.Sy*. J. Phys. Condens. Matter., 1995, 7, 6591.
[14] *L.L.Hinchey and D.L.Mills*. Phys.Rev., 1986, B33, 3329.
[15] *E.L.Albuquerque, P.Fulko, E.F.Sarmento, D.R.Tilley*. Solid State Commun., 1986, 58, 41.
[16] *R.L. Stamps and R.E. Camley*. J.Magn. Magn. Mat., 1986, 54-57, 803-804.
[17] *H. T. Diep*. Physics Lett. A138, 1989, 69.
[18] *V.A.Tanriverdiyev, V.S.Tagiyev, M.B.Guseynov*. Transactions, Azerbaijan Academy of Sciences, 2000, 20, 2.
[19] *J.Barnas*. J.Phys. C: Solid State Phys., 1988, 21, 1021-1036.
[20] *T. Wolfram and R.E.DeWames*. Prog. Surf. Sci. 1972, 2, 233.
[21] *R.E.DeWames and T. Wolfram*. Phys. Rev., 1969, 185, 720.

V.Ə. Tanrıverdiyev, V.S. Tağıyev, S.M. Seyid-Rzayeva

ANTİFERROMAQNİT İFRAT QƏFƏSDƏ REKURRENT ƏLAQƏLƏR METODU

Rekurrent əlaqələr metodu ilə antiferromaqnit ifrat qəfəsin oxu boyunca yayılan spin dalğaları üçün ümumi dispersiya tənliyi tapılıb. Baxılan ifrat qəfəsin elementar özəyi N sayda müxtəlif antiferromaqnit laydan təşkil olunub. Alınan nəticələr parametrin seçilmiş qiymətləri üçün kəmiyyətcə təsvir olunub.

В.А. Танрывердиев, В.С. Тагиев, С.М. Сеид-Рзаева

ТЕХНИКА РЕКУРРЕНТНЫХ СООТНОШЕНИЙ В АНТИФЕРРОМАГНИТНОЙ СВЕРХРЕШЕТКЕ

Используя технику рекуррентных соотношений, получены общие дисперсионные уравнения для обменных спиновых волн, распространяющихся вдоль оси антиферромагнитной сверхрешетки. Элементарная ячейка рассматриваемой сверхрешетки состоит из N различных антиферромагнитных слоев. Приведены численные результаты для выбранных значений параметров.

Received: 14.01.03

CLASSICAL FACTORIZATION METHOD FOR THE NON-STATIONARY SYSTEM

R.G. AGAYEVA
Institute of Physics of the National Academy of Sciences of Azerbaijan
370143, Baku, H.Javid ave.33.

The classical factorization method is constructed for the non-stationary system with the use of quantum integrals of motion.

The classical factorization method (CFM) developed by Schrödinger [l] and extended by Infeld and his collaborators [2] allows the eigenfunctions (EF) and eigenvalues (EV) to be constructed for the stationary problems.

Within the framework of CFM the Hamiltonian for the harmonic oscillator is known to be represented as $\hbar\omega\left(\hat{a}^{+}\hat{a}^{-}+\frac{1}{2}\right)$, where ω is a frequency, $\hat{a}^{+}$, $\hat{a}^{-}$ are the Bose rising and lowering operators, respectively. Then the EV_s and the EF_s of the Hamiltonian are defined by the algebraic way provided the energy EV have a lower limit.

To solve the non-stationary problem means to determine the wavefunctlon ψ. satisfying the wave equation $i\hbar\frac{\partial\psi}{\partial t}=\hat{H}\psi$, where $\hat{H}$ is the Hamiltonian of the problem under consideration. However, the wave function of the non-stationary problem is not EF of $\hat{H}$ and, there fore, it is impossible for the CFM to be extended to the non-stationary case directly.

The wave function of the non-stationary system might be determined if this wave function obeys not only the wave equation but simultaneously is the EF of a certain operator

$$\hat{K}=\hat{A}^{+}\hat{A}^{-}+\frac{1}{2} \tag{1}$$

where $\hat{A}^{\pm}$ are the Bose rising and lowering operators for the given non-stationary system and the EV of $\hat{K}$ have the lower limit. Such a situation is realized provided

$$\left[\hat{K},i\hbar\frac{\partial}{\partial t}-\hat{H}\right]=0 \tag{2}$$

i.e. only on condition that $\hat{K}$ is the quantum integral of motion.

The aim of the present work is to show, with a harmonic oscillator with a time-dependent frequency being used as an example, that the CFM may be developed for the non-stationary system provided the method of the quantum motion integrals is used.

There is a further point to be made, in the case of the non-stationary problem one can solve the EV problem for the operator $\hat{K}$ instead of the corresponding wave equation. In the stationary case this operator transform to the energy operator.

Let us consider a non-stationary harmonic oscillator described by the Hamiltonian

$$\hat{H}=\frac{\hat{p}^{2}}{2m}+\frac{m\omega^{2}(t)\hat{x}^{2}}{2} \tag{3}$$

where x is a usual canonical coordinate, p is its conjugate momentum, and m is a mass.

It is known that lowering and rising operators for such system [3] are:

$$\hat{A}^{-}=\frac{i}{\sqrt{2\hbar}}\left(\frac{\varepsilon\hat{p}}{\sqrt{m}}-\dot{\varepsilon}\sqrt{m}\hat{x}\right),$$
$$\hat{A}^{+}=-\frac{i}{\sqrt{2\hbar}}\left(\frac{\varepsilon^{*}\hat{p}}{\sqrt{m}}-\dot{\varepsilon}^{*}\sqrt{m}\hat{x}\right) \tag{4}$$

where the function $\varepsilon(t)$ is a definite solution of the classical harmonic oscillator equation

$$\ddot{\varepsilon}+\omega^{2}(t)\varepsilon=0\,. \tag{5}$$

The following commutation relationship holds

$$\left[\hat{A}^{-},\hat{A}^{+}\right]=1 \tag{6}$$

It is easy to check that

$$\left[i\hbar\frac{\partial}{\partial t}-\hat{H},\hat{A}^{\pm}\right]=0 \tag{7}$$

i.e. the operators (4) are invariants.

Formulae (5) and (6) give the following equality,

$$\dot{\varepsilon}\varepsilon^{*}-\dot{\varepsilon}^{*}\varepsilon=2i \tag{8}$$

which is valid for any moment of the t .

Let us introduce an operator $\hat{K}$ according to (1) where $\hat{A}^{\pm}$ are given by the expressions (4). If $\hat{H}$ has the form (3) it is easy in compliance with (2) to be convinced that $\hat{K}$ is the motion integral. This means that $\hat{K}$ commutes with the operator $\left(i\hbar\frac{\partial}{\partial t}-\hat{H}\right)$. Hence, these operators have exactly the same set of EF_s. Consequently, the wave function of non-

stationary harmonic oscillator can if be found if the EV problem for operator $\hat{K}$ is solved:

$$\hat{K}\psi = k\psi \tag{9}$$

Construct the following motion integrals

$$\hat{X}_0 = \left(\hat{A}^- + \hat{A}^+\right)/\sqrt{2} \tag{10}$$

and

$$\hat{P}_0 = \left(\hat{A}^- - \hat{A}^+\right)/i\sqrt{2} \tag{11}$$

They are referred to as the operator of the initial coordinate and the operator of initial impulse, respectively [4]. Let us express $\hat{K}$ from (l) in terms of these operators:

$$\hat{K} = \left(\hat{X}_0^2 + \hat{P}_0^2\right)/\sqrt{2} \tag{12}$$

$\hat{X}_0$ and $\hat{P}_0$ are the Hermitian operators. Then these operators have the real EV that places the lower limit of EV of the expression (12): $k \geq 0$ This enables to apply CFM to solving the problem (9).

Denote the quantities belonged to the ground state, i. e. to the lowest EV of the operator $\hat{K}$, by subscript "0".Then

$$\hat{K}\psi_0 = k_0\psi_0 \tag{13}$$

Let us multiply the equation (13) on the left-hand side by and make use of the commutation relationship (6) taking into account (1). Finally, instead of equation (13) we obtain $\hat{K}\hat{A}^-\psi_0 = (k_0 - 1)\psi_0$. Since k_0 is the lowest EV of the operator $\hat{K}$ it follows that

$$\hat{A}^-\psi_0 = 0 \tag{14}$$

whence

$$\psi_0 = C_0 exp\left(im\dot{\varepsilon}x^2 / 2\hbar\varepsilon\right) \tag{15}$$

and

$$C_0 = \sqrt[4]{\frac{m}{\pi\hbar\varepsilon^2}} \tag{16}$$

is calculated from the normalization for ψ_0 . By means of (14) we get from the expression (13) $k_0 = 1/2$.

Let us multiply the equality (13) on the left-hand side by $\hat{A}^+$ and make use of the expressions (6) and (1). We obtain $\hat{K}\hat{A}^+\psi_0 = \left(k_0 + 1\right)\hat{A}^+\psi_0$, whence $\psi_1 = C_1\hat{A}^+\psi_0$, $k_1 = k_0 + 1$. Using the mathematical induction method one can prove that $\psi_n = C_1\hat{A}^+\psi_{n-1}$, $k_n = n + \frac{1}{2}$. The value of C_n is given by the normalization conduction. On the whole we get the wave function of the non-stationary harmonic oscillator in the form

$$\psi_n = (n!)^{-1/2}\left(\hat{A}^+\right)^n\psi \tag{17}$$

that exactly coincides with the well known result for the system under consideration [4].

The author thanks Prof. Gashimzade F.M. for helpful discussions.

[1] *E. Schrödinger*. Proc. R. Irish. Acad. 1940, A46, p. 9; 1940, A46, p.183; 1941, A47, p. 53
[2] *L.Infeld, T.E. Hull*. Rev. Mod. Phys. 1951, 23, p. 21-63.
[3] *R.G. Agayeva*. J. Phys. **A:** Math. Gen. 1980, 13, p.1685-1699.
[4] *I.A. Malkin and V.I. Man'ko* . Dynamic Symmetries and Coherent State of Quantum System. M., «Nauka». 1979.

R.Q. Ağayeva

QEYRİ STASİONAR SİSTEMLƏR ÜÇÜN KLASSİK FAKTORİZASİYA METODU

Hərəkətin kvant inteqrallarının köməyi ilə qeyri stasionar sistemlər üçün klassik faktorizasiya metodu işlənib.

Р.Г.Агаева

КЛАССИЧЕСКИЙ МЕТОД ФАКТОРИЗАЦИИ ДЛЯ НЕСТАЦИОНАРНЫХ СИСТЕМ

С помощью квантовых интегралов движения развит классический метод факторизации для нестационарных систем.

Received: 31.01.03

REALIZATION OF THE TOMOGRAPHIC PRINCIPLE IN QUANTUM STATE OF DAMPED OSCILLATOR

E.A. AKHUNDOVA
Institute of Physics of the Azerbaijan National Academy of Sciences
H. Javid av. 33, Baku, 370143

The general principle for the tomographic approach to quantum state reconstruction, which until new has been based on a simple rotation transformation in the phase space is considered. The realization of the principle in specific example is presented.

1. Introduction

In 1932 Wigner [1] introduced a real function *W(q,p)* which is related by Fourier transform with complex density matrix $\rho(x,x')$. The Wigner function has the specific properties which are similar to properties of a probability distribution function of classical statistical mechanics. The motivation to introduce such function was to make the description of quantum state closer to intuitively more familiar description of classical state by means of probability distribution on the phase space. Moyal [2] has formulated evolution equation of quantum state in terms of Wigner function. The Moyal formulation of quantum mechanics showed very clearly what is similarities and differences of the classical and quantum fluctuations.

Nevertheless the Wigner function can not be considered as joint probability distribution on phase space. The obvious reason for this is the fact that the Wigner function can take negative values for quantum states [3-5]. The Wigner function is used to study the evolution of quantum systems [5-8] since it provides a convenient representation similar to classical picture of the evolution.

Recently, in [9-11] the probability representation of quantum mechanics was introduced and the new evolution equation was derived, which was a generalization of the result obtained in [12], where the role of the Wigner function was played by the particles position in an ensemble of rotated and scaled reference frames in the system's classical phase space (the classical representation of quantum mechanics uses the symplectic tomography procedure suggested for measuring quantum states [13,14]. Tomography is well known in the field of medicine where it is extensively used for image reconstruction in diagnostic systems. It is based on the possibility of recording transmission profiles of the radiation which has penetrated a living body from various directions. In quantum optics, one has the opportunity of measuring all possible, so that tomography can be easily implemented. In fact Vogel and Risken [ ] pointed out that the marginal distribution is just the Rodon transform (or "tomography") of the Wigner function.

By inverting the Radon transform, one can obtain the Wigner function and then recover the state, this is the basis of the method proposed by Smithey et al [15].

The aim of this paper is to consider the tomographic principle and investigate in a frame of this principle the quantum system described by the quadratic non-stationary Hamiltonian.

2. Symplectic tomography

In the usual optic homodyne tomography the observed quantities are the quadratures $\hat{x}_\varphi = \hat{q}cos\varphi + \hat{p}sin\varphi$ obtained as mixtures of position $\hat{q}$ and momentum $\hat{p}$ by means of a rotation *g* in phase space

$$\begin{bmatrix} q \\ p \end{bmatrix} \to g \begin{bmatrix} q \\ p \end{bmatrix}, g = \begin{bmatrix} cos\varphi & sin\varphi \\ -sin\varphi & cos\varphi \end{bmatrix} \qquad (2.1)$$

The quadrature histograms $w(x,\varphi)$ also called marginal distributions are projections (Rodon transformation) of Wigner function [1]

$$w(x,\varphi) = \int W(qcos\varphi - psin\varphi, qsin\varphi + pcos\varphi)dp \qquad (2.2)$$

On the other hand the resulting marginal distribution $w(x,\varphi)$ is [13]

$$w(x,\varphi) = < x_\varphi |\hat{\rho}| x\varphi > = < q|G(g)\hat{\rho}\ G^{-1}(g)|q >$$

where $|x_\varphi>$ are eigenkets of quadrature operators and *G(g)* is the unitary group representation for the transformation *g*. In this case

$$G(g) = exp\left[i\varphi \left(\frac{\hat{p}^2}{2} + \frac{q^2}{2} \right) \right] \qquad (2.4)$$

As was shown in [12] for the generic linear combination of the position *q* and momentum *p*, which a measurable observable in the phase space

$$\hat{x} = \mu\hat{q} + \nu\hat{p} + \delta \qquad (2.5)$$

where μ, ν, δ are real parameters, the marginal distribution $\omega(x,\mu,\nu)$ is related to the state of the quantum system expressed in terms of its Wigner function *W(q,p)* as follows:

$$\omega(x,\mu,\nu) = \int exp[-ik(x - \mu q - \nu p)W(q,p)\frac{dkdqdp}{(2\pi)^2} \qquad (2.6)$$

where $x=X-\delta$. By means of the Fourier transform of the function ω, one can then obtain the relation

$$W(q,p) = (2\pi)^2 z^2 \tilde{\omega}(z, -zq, -zp) \qquad (2.7)$$

where $-zq$, $-zp$ and z are the conjugate variables to μ, ν and x respectively and the Fourier transform $\tilde{\omega}$ has the property

$$\omega\, z, -zq, -zp) = \frac{1}{z^2}\omega\,(1, -q, -p) \tag{2.8}$$

It is worth remarking that in this case the connection between the Wigner function and the marginal distribution is simply guaranteed by means of the Fourier transform instead of the Rodon transform.

The procedure developed is called "symplectic tomography" [13], since in this case the marginal distribution is obtained by using a symplectic transformation g belonging to the symplectic group ISp(2,R)

$$\begin{bmatrix} q \\ p \end{bmatrix} \to g\begin{bmatrix} q \\ p \end{bmatrix}, g = \begin{bmatrix} cos\varphi & sin\varphi \\ -sin\varphi & cos\varphi \end{bmatrix}\begin{bmatrix} \lambda & 0 \\ 0 & \lambda^{-1} \end{bmatrix} \tag{2.9}$$

For this transformation, one has

$$\mu = \lambda cos\varphi, \quad \nu = \lambda^{-1} sin\varphi, \delta = 0 \tag{2.10}$$

This, for the realization of the scheme, the element g is the product of squeezing and rotation operators. This means that for our scheme the representation operator is

$$G(g) = exp\left[i\varphi\left(\frac{\hat{p}^2}{2} + \frac{q^2}{2} \right)\right] exp\left[\frac{i\lambda}{2}\left(\hat{q}\,\hat{p} + \hat{p}\,\hat{q}\right)\right] \tag{2.11}$$

3. Marginal distribution for quantum dumped oscillator.

Let us consider a quantum system described by Hermitian non-stationary Hamiltonian [16]

$$\hat{H} = \frac{1}{2}\left(\hat{p}^2 e^{2\Gamma(t)} + \omega_0^e(t) e^{2\Gamma(t)}\hat{x}^2\right) - f(t)e^{2\Gamma(t)}\hat{x} \tag{3.1}$$

The wave functions for the Fock states of this system ψ_n have the form

$$\psi_n(x,t) = (n!)^{-1/2}\left(\frac{\varepsilon^*}{2\varepsilon}\right)^{n/2}(\pi\varepsilon^2)^{-1/4}\, exp\left[\frac{i\dot{\varepsilon}}{2\varepsilon}e^{2\Gamma(t)}x^2 - \frac{x\delta}{\varepsilon} - \frac{\varepsilon^*}{4\varepsilon}\delta^* - \frac{1}{4}|\delta|2 - \right.$$
$$\left. - \frac{i}{2}\int Im(\delta\,\delta^*)\right] H_n\left[\frac{x + Re(\varepsilon^*\delta)}{|\varepsilon|}\right] \tag{3.2}$$

where the $H_n(x)$ are Hermite polynomials and $\varepsilon(t)$ is a complex function satisfying the equation

$$\ddot{\varepsilon} + 2\dot{\Gamma}(t)\dot{\varepsilon} + \omega_0^2(t)\varepsilon = 0 \tag{3.3}$$

and the additional relation

$$e^{2\Gamma(t)}(\varepsilon^*\dot{\varepsilon} - \varepsilon\,\dot{\varepsilon}^* = 2i \tag{3.4}$$

and

$$\delta(t) = -i\int \varepsilon(\tau)e^{2\Gamma(t)} f(t)d\tau$$

The corresponding Wigner function is as follows:

$$W_n(p,q) = 2(-1)^n e^{-2z(t)} Ln(4z(t) \tag{3.5}$$

$$z(t) = \frac{1}{2}\left[|\varepsilon|^2 p^2 + |\dot{\varepsilon}|^2 e^{4\Gamma} q^2 - 2e^{2\Gamma} Re\dot{\varepsilon}\,\varepsilon^*)qp + I_m(\varepsilon^*\delta)p - e^{2\Gamma} Im(\varepsilon^*\delta)q + |\delta|^2 + ie^{2\Gamma} Re(\varepsilon\dot{\varepsilon}^*)\right.$$

The marginal distribution (2.6) as it was shown above is expressed in terms of its Wigner function. Then the marginal distribution $\omega_m(x,\mu,\nu)$ for the Fock states of our system is as follows

$$\omega_n(x,\mu,\nu,t) = \int exp\left[-ik(x - \mu q - \nu p)\right] W_n(q,p,t)\frac{d\,k\,d\,q\,d\,p}{(2\pi)^2} \tag{3.6}$$

Substituting (3.5) in (3.6) and taking for simplicity $f(t)=0$ we obtained the exact expression for marginal distribution in the following form:

$$\omega_n(x,\mu,\nu,t) = \frac{1}{2^n n!\sqrt{\pi\varepsilon\varepsilon^*(a^2+b^2)}}\, exp\left(-\frac{x^2}{\varepsilon\varepsilon^*(a^2+b^2)}\right) H_n^2\left(\frac{x}{\sqrt{\varepsilon\,\varepsilon^*(a^2+b^2)}}\right) \tag{3.7}$$

where

$$a = \frac{1}{\varepsilon\,\varepsilon^*} \cdot exp\left[\Gamma(t)\right] \nu\,(\varepsilon^* \varepsilon + \varepsilon\,\dot{\varepsilon}^*) + \mu \quad ,$$

$$b = \nu \Big/ \varepsilon\,\varepsilon^* \,.$$

In the following paper we will obtain the smoothed Wigner function of our system and its smoothed marginal distribution and compare both expressions.

I am very grateful to professor V.I. Man'ko for numerous discussions and suggestions.

[1] *E.P. Wigner*. 1932, Phys. Rev., v.40, p. 749

[2] *J.E. Moyal*. Proc. Cambrige Philos. Soc., 1949, v. 45, №9.

[3] *Y.S. Kim and H.E. Noz*. "Phase space picture of quantum mechanics" Word Scientific, Singapore, 1991.

[4] *M.Hillery, R.F. O'Connel, M.O. Scully and E.P. Wigner*. Phys. Rep., 1984, v. 106, p.121.

[5] *V. Tatarski*. Usp. Fiz. Nauk, 1983, v. 139, p.587.

[6] *E.A. Akhundova, V.I. Dodonov, V.I. Man'ko*. Physica, 1982, v.115 A, p.215.

[7] *E.A. Akhundova, V.I. Dodonov, V.I. Man'ko.* Soc. J. Theor. Phys., 1985, v. 60, p.413.

[8] *E.A. Akhundova and M.A.Mmukhtarov.* J. Phys. A: Math.Gen., 1995, v.28, p.5287.

[9] *S. Mancini, V.I. Man'ko and P. Tombesi*. Found. Phys., 1997, v. 27, p.801.

[10] *S. Mancini, V.I. Man'ko and P. Tombesi*. Phys. Lett. A, 1996, v.213, p.1.

[11] V.I. Man'ko. "Quantum mechanics and classical probability theory", in *B. Cruber and M. Ramek* (eds), Symmetries in science IX, Plenum Press, New York, 1997, p.225.

[12] *S. Mancini, V.I. Man'ko and P. Tombesi*. Quantum semiclass. Opt., 1995, v.7, p.615.

[13] *G.M. D'Ariano, S. Mancini, V.I. Man'ko and P. Tombesi*. Quantum Semiclass. Opt., 1996, v.8, p.1017.

[14] *K Vogel and H. Risken*. Phys. Rev. A, 1989, v.40, p.2847.

[15] *D.*T. Smithey, M.Beck, M.G. Raymer and A. Faridani. Phys.Rev.Lett., 1993, v.70, p.1244.

[16] *V.*V. Dodonov and V.I. Man'ko. Phys.Rev.A, 1979, v.20, p.550.

E.A. Axundova

SÖNMƏDƏ OLAN OSSİLYATORUN KVANT HALLARI ÜÇÜN TOMOQRAFİK PRİNSİPLƏRİN HƏYATA KEÇİRİLMƏSİ

Fırlanmanın faza fəzasında sadə çeviricisiyə əsaslanan kvant hallarının təsviri üçün tomoqrafik yanaşma sisteminin ümumi prinsipləri nəzərdən keçirilib. Bu prinsipin həyata keçirilməsi xüsusi misalda təqdim olunmuşdur.

Э.А. Ахундова

РЕАЛИЗАЦИЯ ТОМОГРАФИЧЕСКОГО ПРИНЦИПА ДЛЯ КВАНТОВЫХ СОСТОЯНИЙ ЗАТУХАЮЩЕГО ОСЦИЛЛЯТОРА

Рассмотрен общий принцип томографического подхода для описания квантовых состояний системы, который основан на простом преобразовании вращения в фазовом пространстве. Представлена реализация этого принципа на особом примере.

Received: 24.10.02

ELASTIC AND INELASTIC SCATTERING OF PROTONS ON ATOMIC NUCLEI

M. M. MIRABUTALYBOV, S.G. ABDINOVA
Azerbaijan State Oil Academy, Physics Department.

In the frameworks of distorted wave HEA, on the base of three-dimensional formulation the expression for scattering amplitude of protons of high energies on atomic nuclei was obtained in the analytical form. As a consequence of short range character of a proton-nucleon interaction, the scattering of protons on nuclei was presented as a sequence of unitary scattering. With a help of the developed mathematical method the recurrent formula was received what allowed to express the form-factor in the distorted wave in Born,s ones and its derivatives .As a result of the analysis of experimental cross sections of elastic scattering of protons with energy 1 GeV, the parameters of distribution of protons and neutrons in spherical nuclei ^{40}Ca, ^{48}Ca, ^{90}Zr, ^{208}Pb as well as a width of a surface layer of nucleons, root-mean-square radii of protons and neutrons were determined. Fermi-function was used for the distribution of nucleons density.

Development of experimental engineering last decade allowed tocarry out numerous experiments on scattering of protons on nuclei in the range of intermediate energies of striking particles. This area of energies is of a particular interest, because checking behavior of amplitude of particles scattering on nuclei becomes possible. Different methods for getting obvious expressions of the amplitude for electrons scattering on nuclei are listed in [1]. The most successful expression of the amplitude was presented in[2]. Further, this theory was developed in [1], where opportunities and good accuracy for performance of quantitative studies were shown. Later in [3,4] this method was advanced for elastic and inelastic scattering of electrons on spherical nuclei and the good results were received. What concerns proton scattering, it appears possible to receive the amplitudes [5] fair in the range of small angles. Recently, in [6] on the base of three-dimensional quasiclassics within the limits of high-energy approach (HEA), the amplitude of protons scattering on nuclei was obtained in the range of small angles of scattering as well as of large ones. Obviously, this method will find it's wide application.

The purpose of the present study is to receive the amplitude of scattering in an analytical form to connect it with the theory of multy-scattering and to develop a method of it's calculation. Let's write down a differential section of the process in general form:

$$\frac{d\sigma}{d\Omega} = \frac{1}{2}\left(\frac{k}{E}\right)^2 \frac{2J_f+1}{2J_i+1} \sum_{\sigma_i\sigma_f} \sum_{M_i M_f} \left| f_{if}\left(k_i, k_f\right) \right|^2 \tag{1}$$

Wave functions of relative motion of the striking and scattered nucleons as the solutions of Schredinger equation produce the following form:

$$\psi^{(\pm)}(\mathbf{k},\mathbf{r}) = \exp\left\{ i \left[\mathbf{kr} \mp \Phi^{(\pm)}(\mathbf{k},\mathbf{r}) \right\} \right. \tag{2}$$

where the distorted member is

$$\Phi^{(\pm)}(\mathbf{k},\mathbf{r}) = \frac{m}{\hbar^2 k} \int_0^\infty V\left(\mathbf{r} \mp \hat{k}s\right) ds \tag{3}$$

Using property of spherical symmetry of nuclear potential from the static equation we get:

$$\nabla^2 V(r) - k_0^2 V(r) = 4\pi\gamma\rho(r) \tag{4}$$

The coefficient of expansion of potential is received in form

$$a = \left(\frac{4\pi}{3k^3}\right) \gamma\rho\ (0) + \frac{k_0^2\, V(0)}{3k^3}, \tag{5}$$

where γ=0,08.

Here γ corresponds to the irrationalized constant of connection, defined from the experiment on nucleon-nucleon scattering [7].

It is possible to neglect the change of nucleons location in the nucleus during a flight of a fast proton through it. The scattering occurs basically forward on small angles. Scattered nucleon consistently interacts with several nucleons of a nucleus,

which are met on it's way. Therefore, as a consequence of short-range nucleon-nucleon interaction, the scattering of nucleon may be written as a sequence of unitary scattering. Taking it into account, nuclear potential may be represented as the sum of component interactions of the striking particle with the nucleons of the target nucleus:

$$V(\mathbf{r}\xi) = \int \upsilon(|\mathbf{r} - \mathbf{x}|)\rho(\mathbf{x}\xi)d\mathbf{x} \tag{6}$$

As the binding energy of a nucleus is small in comparison with the energy of a striking proton, the nucleons binding may be neglected and hence, the potential of nucleon-nucleon interaction can be expressed in the amplitudes of scattering on free nucleons defined from the solution of Schredinger equation

$$f_{NN}(\mathbf{k}',\mathbf{k}) = -\frac{\mu_0}{2\pi\ \hbar^2}\int e^{-i\mathbf{k}'\mathbf{r}'}\upsilon(\mathbf{r}')\ \psi_{\mathbf{k}}(\mathbf{r}')\ d\mathbf{r}', \tag{7}$$

where $\upsilon^{иск}(\mathrm{r}) = \upsilon(r)\exp\left\{-\frac{im}{\hbar^2 k}\int_{-\infty}^{z}\upsilon dz'\right\}$ is a distorted nucleon-nucleon potential, μ_0 - equivalent mass, q´- momentum of the particle striking on a nucleon target. Taking into account Fourier transformation in (6), the nuclear potential is received :

$$V(\mathbf{r}\xi) = -\frac{\hbar^2}{(2\pi)^2\mu_0}\int e^{i\mathbf{q}'(\mathbf{r}-\mathbf{x})}f_{NN}(\mathbf{q}')\rho(\mathbf{x}\xi)d\mathbf{q}'d\mathbf{x} \tag{8}$$

.

Here for nucleon-nucleon amplitude a following parameterization is chosen:

$$f_{NN}(q') = \frac{ik\sigma}{4\pi}(1 - i\varepsilon_0)\ e^{-\beta^2 q'^2}/2 \tag{9}$$

After integration the following expression for differential section is received:

$$\frac{d\sigma}{d\Omega} = \left(\frac{k^2}{4\pi\mathrm{E}}\right)^2 \frac{1}{2}\frac{2J_f+1}{2J_i+1}\sum_{LM}\frac{1}{2L+1}\left|\ F_{LM}(q)\ \right|^2, \tag{10}$$

where the form-factor is

$$F_{LM}(q) = \int e^{i[\mathbf{q}\mathbf{x}+\Phi(x)]}f_{NN}(\mathbf{q}_{эф})\rho_L(x)\ Y^*_{LM}(\hat{x})\ dx \tag{11}$$

For derivation of this form-factor we obtained the following recurrent formula:

$$(m+1)\ F_{L,m+1}(q) = \sum_{n=0}^{6}\alpha_n F_{L,m}^{(n)}(q) + \sum_{n=1}^{6}\beta_m F_{L,m-1}^{(n)}(q), \quad m=1,2,3,\ldots.. \tag{12}$$

$$F_{L,1}(q) = \sum_{n=0}^{4}\alpha_n F_{L,0}^{(n)}(q), \qquad F_{L,m}^{(n)}(q) = \frac{\partial^n F_{L,m}(q)}{\partial q^n} \tag{13}$$

This recurrent formula allows to express the form factor $F_L(q,\gamma)$ (11)Born's form-factor and it's derivatives.

ELASTIC SCATTERING OF PROTONS ON SPHERICAL NUCLEI.

Analysis of the cross-sections with a help of multy scattering theory of protons of intermediate energies allows to obtain a quiet exact information about nucleon distribution in nuclei. It is known, that the fast protons have the same sensitivity as protons and neutrons of a nucleus. Therefore, the data on scattering of protons on nuclei makes it possible to get the information about izoscalar density, i.e. about the sum of neutron and proton densities.

$$\rho(r) = \rho_p(r) + \rho_n(r) \tag{14}$$

Distribution of protons and neutrons densities is chosen as Fermi-function

$$\rho_i(r) = \rho_{oi}\left(1 + e^{\frac{r-c}{b_i}}\right)^{-1} = \rho_{oi}\tilde{\rho}\left(r|b_i\right), \quad i = p;n \tag{15}$$

Experimental data on elastic scattering of protons with energy ~ 1GeV on nuclei ^{40} Ca, ^{48}Ca, ^{90} Zr and ^{208} Pb [6] are analyzed within the framework HEA with a use of probe function (14). The best consent with the theoretical cross sections is achieved at the certain sets of protons and neutrons as it is shown on fig. 1 and 2. The parameters itself are presented in the table.

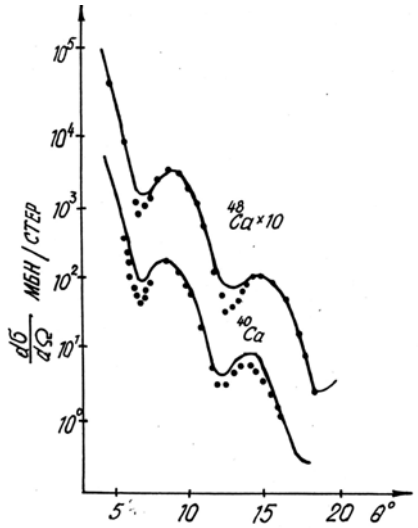

Fig.1. Differential sections of elastic scattering of protons with energy 1 GeV on ^{40} Ca and ^{48} Ca. Points- experimental data, solid lines- cross sections, derived by a method of distorted waves.

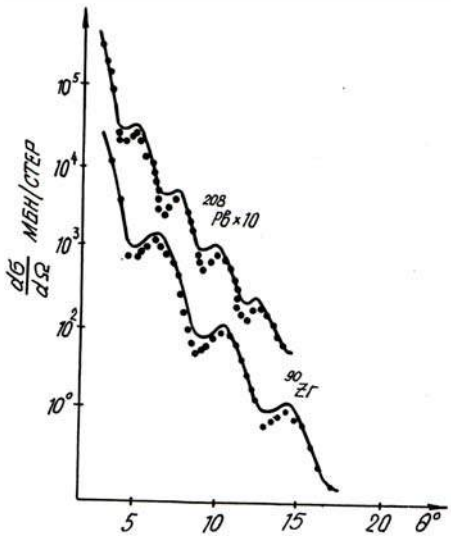

Fig.2. Differential sections of elastic scattering of protons with energy 1 GeV on nuclei ^{90} Zr and ^{208} Pb. Points- experimental data. Solid lines- cross sections derived by the method of distorted waves.

As it is seen from the table, the good agreement of the cross sections is received at $\alpha = \alpha = \alpha$, i.e., thickness of a surface layer of protons and neutrons in the spherical nuclei are not different. It proves once again that the fast protons on the sur`faces of spherical nuclei are not sensitive to a thin structure. As it is known, the fine structure in distributions of protons density appears at the account of three-parameter Fermi –functions in elastic scattering of electrons on nuclei.

TABLE.

Parameters describing distribution of density of protons, neutrons and nucleons.

^{40} Ca	0.60	0.6	2.260	3.920	2.662	3.70	1
^{48} Ca	0.64	0.4	2.480	3.590	2.754	3.18	1.023
^{90} Zr	0.40	0.30	2.306	4.308	4.207	4.22	1.040
^{208} Pb	o.60	0.3	1.710	5.482	4.982	5.26	1.048

To satisfy condition (14) we chose distribution of proton and neutron density in the following general form:

$$\rho_{p(n)}(r) = \frac{1}{2}\left[1 \mp \beta(r)\right]\ \tilde{\rho}(r),\ \ \beta(r) = \alpha_0 - \alpha_1 \frac{r^2}{c^2}, \tag{16}$$

Thus the distribution of protons and neutrons density in nuclei accept the following form:

$$\rho_{p(n)}(r) = \rho^0_{0p(n)}\left(1 \pm W_{p(n)} \frac{r^2}{2c^2}\right)\tilde{\rho}(r)\ , \tag{17}$$

where $W_{p(n)}$ - parameters, describing the fine structure in distribution of protons and neutrons density, are connected with each others.

All calculations were carried out using the parameters of elementary amplitudes, according to the data on elastic nucleon-nucleon scattering [10,11].

Comparing the derived cross sections with experimental ones it can be seen that on the right slopes of diffractional peaks the consent is good, while on the left slopes and in the area of diffractional minimum some excess of the derived values is observed.

On fig.3. the diagrams of distribution of protons and neutrons density are presented. Parameters of these distributions are obtained from the combined analysis of experimental cross sections in the distorted wave HEA of proton and electron scattering on the appropriate nuclei [9].

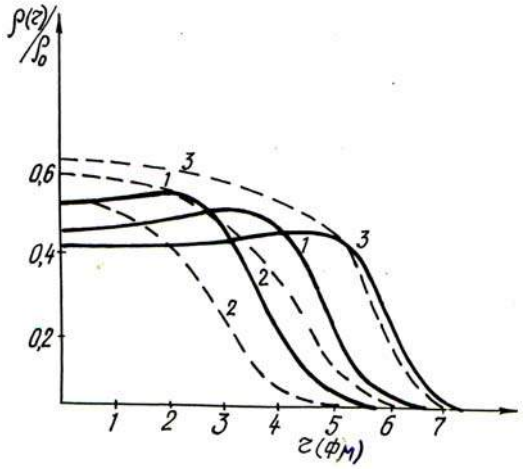

Fig. 3. Distributions of density of protons (solid lines), neutrons (dotted): 1- ^{90}Zr, 2- ^{48}Ca, 3- ^{208}Pb

REFERENCES

1.Lukianov V.K., Paul U.S.E. 1974, 5, 955
2.Jennie D.R., Boss F.L., Ravenhall D.G. Phys. Rev. B. 1965, v. 137, p.882.
3.Javadov A.V., Mirabutalibov M.M.. News of SA USSR, ph. series, 1976, 40, 2156.
4.Mirabutalibov M.M. The scientists of a slip ASU of sulfurs. Phys. and math. 1979,4, 92.
5.Glauber R.J. Lec.in Theor. Phys. N.Y. 1959,1,315.
6.LukianovV.K. In.To. News of SA of Dews. Sulfurs. v.58. 8.
7.Delvin E.T. Phys. Rev. Letters. 1960, 4, 242.
8.Alkhasov G.D., Belostotsky S.L. Nucl. Phys. 1982, A381, 430.
9.Javadov A.V., Mirabutalibov M.M.. News of SA USSR. Phys. series. 1978, 42, 1869.
10.Marcus Sim. Phys. Rev. Lett.78, 1997, p.4161-4164.
11.Arellano H.F. Brieva F.A. Phys. Rev. 1996. C.54, p. 2570.

PREDICATION OF ACTIVITY COEFFICIENTS FOR KI IN METHANOL SOLUTIONS USING CHEMICAL MODEL (CM) AT 25°C

KARAMAT NASIRZADEH

Department of Chemistry, Azerbaijan University of Tarbiat Moallem, Tabriz, IRAN

E-mail: kn@chemist.com

The osmotic coefficients of potassium iodide in methanol have been measured by the isopiestic method at 25 °C. Sodium Iodide was used as isopiestic standard for the calculation of osmotic coefficients. The molality ranges covered in this study correspond to about 0.1-1 $mol \cdot kg^{-1}$. Experimental osmotic coefficient data are reliably represented by the chemical model of Barthel et al. in two forms. The parameters from the fit were used to calculate the osmotic coefficients.

Keywords: osmotic coefficient, potassium Iodide, Barthel model, isopiestic, methanol, electrolyte solutions.

1. Introduction:

The systematic investigation of non-aqueous solutions is guided by the progress of our knowledge on solute- solute and solute-solvent interactions. By combination with chemical models of the solution, valuable results can be obtained which assist the understanding of the properties of these solutions. For dilute electrolyte solutions consistent and reliable equations are based on the modern conception of electrochemistry which takes into account both long and short-range forces between the solute and solvent particles. Solution chemists usually think of short-range interactions in terms of ion pair formation.

In our previous works the Pitzer and Mayorga model were used for the predication of activity coefficients and osmotic coefficients of methanol + LiCl, LiBr and $+LiCH_3COO$ at 25°C [1]. In this research osmotic coefficients of KI were determined by an improved isopiestic technique at 25°C. The Sodium Iodide solutions were applied as a reference. While there is limited information for the osmotic coefficient of KI in methanol in the literature, osmotic coefficients from vapor pressure measurements can be found in the literature for methanol solutions of KI at 25°C [2]. For the purpose of establishment of correlation between osmotic coefficient data and salt molality, the chemical model of Barthel et al [3,4] were used. It allows the use of the classical association concept initially introduced by Bjerrm after some

refinements concerning the spatial extension and structure of ion pairs and mean force potentials. The ions in an ion pair retain their individual ionic characters and are liked only by columbic and short-range forces. The distribution of the ions in the solution depends on the forces acting between all the particles, ions and solvent molecules.

2. Experimental:

2.1. Apprattus and procedure:

The isopiestic apparatus used in this work is essentially similar to the one used previously [5,6]. Recently this technique has been used for the measurement of osmotic coefficient of some lithium salts in methanol and ethanol solutions [1,7]. This apparatus consisted of a five-leg manifold attached to round-bottom flasks. The five flasks were typically used as follows. Two flasks contained the standard NaI solutions, two flasks contained the KI solutions, and the central flask was used as a methanol reservoir. At the beginning of each experiment, several drops of methanol were placed on the central flask to help sweep out the air in the vessel during evacuation and to reduce evaporation from the solutions. The apparatus was held in constant temperature bath for at least 120 h for equilibration at (25.0±0.01)°C.

2.2. Chemicals:

The salts and methanol obtained from Merck. They were all suprapure reagents (NaI, GR min 99.5%, KI, GR, and min 99%). The salts were used without further purification and were dried in an electrical oven at about 120°C for 24 h prior to use.

3. Results and discussion:

3-1. Experimental results

Isopiestic equilibrium molalities with reference standard solutions of NaI in methanol as reported in Table 1 enabled the calculation of the osmotic coefficient, ϕ, of the solutions of potassium iodide in methanol from

$$\phi = \frac{\nu^* \phi^* m^*}{\nu m} \qquad (1)$$

where ν^* and ν are the sum of stoichiometric numbers of anion and cation, ($\nu_+ + \nu_-$), in the reference solution and the solution of potassium iodide, respectively, m^* is the molality of the reference standard in isopiestic equilibrium with these solutions, and ϕ^* is the osmotic coefficient of the isopiestic reference standard, calculated at m^*. The necessary ϕ^* values at any m^* were obtained from the fitted Pitzer and Mayorga equation, including the $\beta^{(2)}$ term, as

described by Zafarani-Moattar and Nasirzadeh.[1] It was shown that,[1] using $\alpha(1)=2$, $\alpha(2)=1.4$, $\beta^{(0)}=0.40830$, $\beta^{(1)}=1.04430$, $\beta^{(2)}=-0.875$ and $C^{\phi}=-0.02224$, the osmotic coefficients of the isopiestic reference standard solutions, ϕ^*, are reproducible with standard deviation of 0.005 for NaI in methanol solutions in the range (0.02 to 4.33) mol·kg^{-1} at 25ºC. From the calculated osmotic coefficient data, the activity of methanol in potassium iodide solutions and the vapor pressure of methanol over these solutions were determined at isopiestic equilibrium molalities, with the help of the following thermodynamic relations:

$$\phi = -\frac{ln\, a_s}{\nu m M_s} \qquad (2)$$

$$ln\, a_s = ln\left(\frac{p}{p^*}\right) + \frac{\left(B - V_s^*\right)\left(p - p^*\right)}{RT} \qquad (3)$$

In these equations, a_s is the activity of solvent, B, V^*_s and p^* are second virial coefficient, molar volume and vapor pressure of pure methanol, respectively. The values of M_s=0.032042, B=-2.075×10^{-3} m^3·mol^{-1}, V_s^*= 4.073×10^{-5} m^3·mol^{-1} and p^*= 16957.7 Pa (taken from ref. [2]) were used at 298.15 K.

A comparison of our vapor pressure data to that of Barthel et al.[4], and Bixon et al.[8] is shown in Figure 1 for KI in methanol solutions. Figure 1 shows that our data agree well with vapor pressure data of Barthel et al.[4]. However, the data obtained by Bixon et al.[8] are for 24.9 °C and are somewhat scattered.

Table 1. Experimental isopiestic molalities and osmotic coefficients for KI in methanol at 25 °C

m_{NaI} / (mol· kg^{-1})	m_{KI} / (mol· kg^{-1})	Φ_{exp}	Φ_{Pitzer}	Φ_{CM1}	Φ_{CM2}
0.0000	0.0000	1.000	1.000	1.000	1.000
0.1295	0.1322	0.816	0.819	0.815	0.814
0.1806	0.1841	0.817	0.816	0.812	0.812
0.2799	0.2884	0.818	0.817	0.811	0.814
0.3128	0.3240	0.818	0.818	0.814	0.814
0.3484	0.3630	0.819	0.819	0.811	0.816
0.3971	0.4174	0.820	0.821	0.818	0.816
0.4532	0.4813	0.822	0.823	0.820	0.818
0.4662	0.4964	0.822	0.823	0.821	0.819
0.5144	0.5527	0.824	0.825	0.824	0.819
0.5690	0.6179	0.826	0.827		0.822
0.5915	0.6451	0.827	0.828		0.825
0.6194	0.6792	0.829	0.829		0.826
0.6558	0.7243	0.830	0.830		0.829
0.6896	0.7666	0.832	0.832		0.830
0.7265	0.8135	0.834	0.834		0.832
0.7382	0.8284	0.835	0.834		0.833
0.7658	0.8640	0.836	0.836		0.834
0.7819	0.8850	0.837	0.837		0.835
0.8532	0.9790	0.841	0.843		0.839

Figure 1. Comparison of vapor pressure for KI in methanol solutions at 25 °C. (O) present work; (×) Barthel et al.[1], (Δ) Bixon et al.[2]

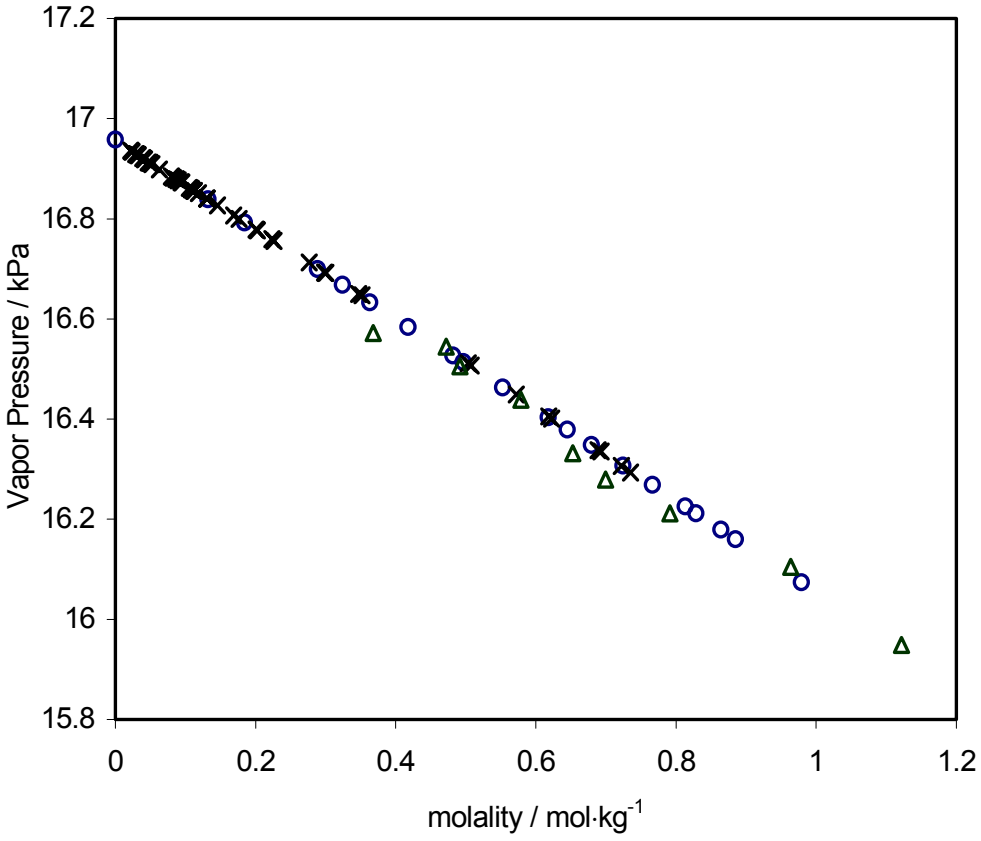

3.2. Correlation of data

Several models are available in the literature for the correlation of osmotic coefficients as a function of molalities. The Chemical model of Barthel et al. has been successfully used for non-aqueous electrolytes in two forms. In low concentrations, m≤0.15 mol·kg^{-1} the osmotic coefficients were fitted to the chemical model using

$$\phi = 1 + \frac{1}{m}\int_0^m m\, d\, \ln(\alpha\gamma_{\pm}') \tag{4}$$

In connection with the association constants $K_A^{(m)}$ in the molal scale

$$K_A^{(m)} = \frac{1-\alpha}{\alpha^2 m}\frac{\gamma^{\circ}}{\gamma_{\pm}^2} \tag{5}$$

In equation(4) and (5),1-α is the fraction of oppositely charged ions acting as ion pairs,$\gamma_\circ$ and $\gamma_\pm$ are the activity coefficients (molal scale) of ion pairs and free ions. The activity coefficients$\gamma_\pm$' and $\gamma_\circ$ are given by the relationships (dilute solutions):

$$\ln \gamma \pm' = -\frac{kq}{1+kR} + \ln \frac{\frac{\rho}{\rho_\circ}}{1+mM_E}; \ln \gamma_\circ = B_\circ . \alpha . m \qquad (6a,b)$$

$$q = \frac{e^2}{8\Pi \varepsilon_\circ \varepsilon kT}; k^2 = 1600\Pi q N_A (\alpha c) \qquad (6c,d)$$

$$c = \frac{0.001 m \rho}{1+mM_E} \qquad (6e)$$

In this equations, R is the distance parameter of the chemical model up to which oppositely charged ions are counted as ion-pairs, ρ and ρ° are densities of solution and pure solvent in kg·m^{-3}, e is the elementary charge, ε is the relative permitivity of the solvent, N_A is the avogadro's number, k is the Boltzman constant, T is the temperature in K, C is the electrolyte concentration in mol·dm^{-3}, and M_E is the molecular weight of the salt in kg·mol^{-1}.The necessary densities for KI in methanol solution that taken from Barthel et al.[2] and used for correlation of chemical model.

The association constant of the CM on the molality scale is given by

$$K_A^{(m)} = 4\Pi N_A \rho_\circ \exp[\frac{-\Delta G_A^*}{RT}] \int_a^R r^2 \exp[\frac{2q}{r}] dr \qquad (7)$$

In equation (7), ΔG_A^* is the non-columbic part of the Gibbs energy of ion pair formation.

The use of activity coefficients, both for free ions and ion pairs in the calculation of the association constant, is an extension of the original(low concentration) chemical model(CM1) where the ion pairs in the solution are considered with ideal behavior, lnγ°=0, in contrast to CM2, where lnγ°≠0. The extended model CM2 allows the application of the chemical model to a significantly wider concentration range. The linear form of lnγ° is theoretically well understood. Here we use the coefficient B° as an adjustable parameter of the chemical model.

The CM2 model increases the concentration limit of the CM1 model, which is about 0.15 to approximately 0.6 mol·kg^{-1}[9]. Figure 2 shows the experimental and theoretical osmotic coefficients for KI in methanol solutions.

Figure 2: experimental and theoretical osmotic coefficients for KI in methanol solutions.

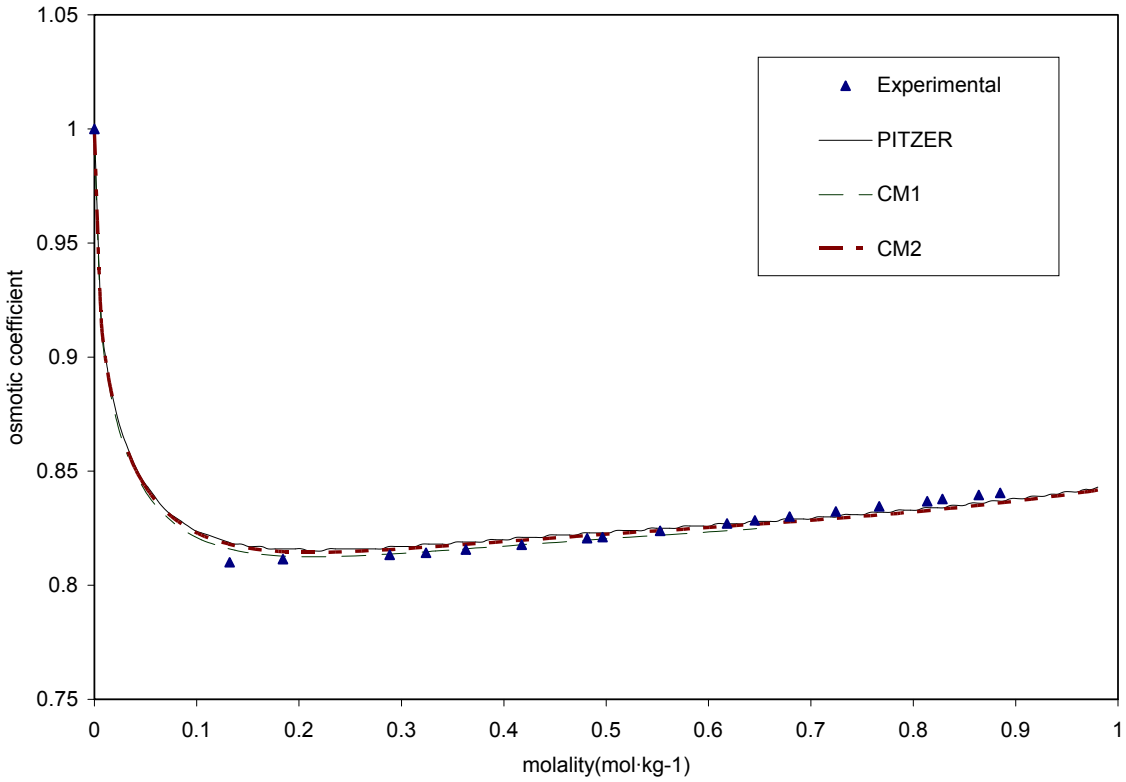

The association constants (Barthel model parameters) of KI in methanol solution are reported in table 2.

Table 2: Association constants of KI in methanol solutions at 25°C.

Salt	a^{nm}	$K_A{}^m$	B0
KI	0.35	10.55	3.19

4. Conclusions

Experimental data show that the osmotic and activity coefficients of KI/methanol and NaI/methanol solutions decrease rapidly at increasing salt concentration. These effects have several reasons: small ion sizes yielding small volume effects, high association constant or

weak ion solvation. The advantage of the CM calculation is the use only two parameters which, furthermore, can be understood from chemical evidence and this parameters have the physically significant.

References:

[1] M. T. Zafarani-Moattar, K. Nasirzadeh; J. Chem. Eng. Data, 43(2), (1998) 215- 219

[2] J.Barthel, R. Neueder; G.Lauermann; J. Solution Chem, 14(9), (1985) 621-633

[3] W.Kuns, J.Barthel, L.Klein, T.Cartailler, P.Turq, and B.Reindl; J. Solution Chem, 20(9), (1991) 875-891

[4] J. Barthel, H.J.Gores, G.Schmeer, and R.Wachter; In Topics in current chemistry, Vol. 111(Springer, Heidlberg), (1983).

[5]M. Kabiri-Badr; M.T. Zafarani-Moattar; J. Chem. Eng. Data, 40, 412-414(1995).

[6] L.R Oches.; M. Kabiri-Badr; H. Cabczes.; AIChEJ.; 36, 1908-1912 (1990).

[7] M. T. Zafarani-Moattar, J.Jahanbin; Fluid Phase Equilibria;166(1999)207-223

[8] Bixon, E.; Gurry , R.;Tassios, D. , *J. Chem. Eng. Data*. 1979, 24, 9-11.

[9]J.Barthel, R. Neueder; H.Peopke, H.Wittmann; J. Solution Chem, 27(12), (1998) 1055-1066.